INSIGHTS INTO *KRAS* BIOLOGY THROUGH ITS NOVEL INTERACTIONS

by

Sunita Shankar

A dissertation submitted in partial fulfillment
of the requirements for the degree of Doctor of
Philosophy
(Molecular and Cellular Pathology)
in The University of Michigan
2015

Doctoral Committee:

Professor Arul M. Chinnaiyan, Chair
Professor Eric Fearon
Associate Professor David Ferguson
Associate Professor Judith Leopold
Assistant Professor Marina Pasca di Magliano
Assistant Professor Scott Arthur Tomlins

DEDICATION

For my Aai

ACKNOWLEDGEMENTS

I would like to sincerely thank my mentor Arul Chinnaiyan for the opportunity and training he provided during my doctoral research. His guidance through these years has helped shape critical scientific thinking, eventually converting me into an ardent RAS biologist. I also thank my thesis committee members Eric Fearon, Dave Ferguson, Marina Pasca di Magliano, Scott Tomlins and Judy Leopold for their suggestions, time and support during the course of these studies. I am grateful for the help of all the collaborators who contributed to these projects.

I have greatly benefited from the support I have received from Mohan, Xuhong and all my friends and colleagues in the Chinnaiyan lab. To my friends who helped bring cheer and care for me and my family, I will remain forever indebted.

Without the help and encouragement I received from Chandan, my companion of many expeditions, I may have never enrolled, worked through nor completed this work. He remains my relentless adviser sharing both his scientific acumen and personal wisdom to help me achieve this shared goal. I am grateful to our children Urja and Josh for their kindness, patience and support as I pursued goals, often times at their expense. Finally, I would like to express my gratitude for the tremendous backing I received from all my family members, whose unquestioned support has been pivotal for this work.

TABLE OF CONTENTS

LIST OF FIGURES

LIST OF TABLES

CHAPTER 1

INTRODUCTION

In the early 1980s mammalian homologues of oncogenic viral, Harvey and Kirsten RAS genes were identified in normal rat cells. These genes termed the *Ha-RAS* and *Ki-RAS* respectively, demonstrated the potential to transform normal mammalian cells. In 1983, an additional homolog, *N-RAS* was identified from neuroblastoma and leukemic cells. By 1984, oncogenic mutations in the *RAS* genes were discovered in many human cancer cells, establishing *RAS* as a pre-eminent family of oncogenes. Over the years there has been a concerted effort to understand RAS biology and its role in the oncogenic process.

The RAS-GTPase cycle

RAS genes encode a family of small GTPases [1] that transduce extracellular growth signals by cycling between a GTP-bound activated state and a GDP-bound basal state [2,3]. The cycling of RAS proteins between inactive and active states constitutes a molecular switch through which a number of cellular signaling pathways are regulated. Extracellular growth factor mediated membrane receptor activation (for example upon mitogenic stimulation) tethers RAS to the plasma membrane where proteins termed as Guanine nucleotide Exchange Factor (GEFs) like SOS (Son of Seveless), can activate RAS proteins by exchanging RAS bound GDP with GTP, thereby activating RAS (**Figure** 1.1). Activated RAS is then brought back to ground state through hydrolysis of GTP to GDP by intrinsic GTPase activity of RAS proteins, greatly

enhanced through interaction with GTPase activating proteins (GAPs) like Neurofibromatosis 1 (NF1).

RAS mutations in cancer

Approximately 30% of all human cancers harbor oncogenic mutations in RAS. Although *H/N/K-RAS* genes are highly homologous, the frequency and types of mutations observed in different human cancers is varied with *KRAS* being the most frequently mutated *RAS* gene, followed by *NRAS* and *HRAS*[4]. *KRAS* mutations are most frequently observed in pancreatic (90%), lung (30%) and colon cancers (50%); mutations in *NRAS* are frequently observed in the cancers of skin (30%) and hematopoietic and lymphoid malignancies (12%). *HRAS* mutations are more prevalent in bladder (15%) and head and neck cancers (8%)[4]. Mutations in *RAS* genes predominantly involve one of three highly conserved amino acid residues- *G12*, *G13* or *Q61* (**Figure 1.2**). A preference for one of the three amino acid substitutions is specific for each *RAS* family member and is also dependent on the cancer type (for example *NRAS Q61* mutations are frequently observed in melanoma while *NRAS G12/NRAS G13* mutations are more prevalent in leukemia). Further, the range of mutations in *KRAS* at a single amino acid have varied prognosis in lung and colon cancers. Together this suggests that the three RAS proteins have different etiologies in the development of cancer which is dependent on the position and type of alteration observed in a specific cell of origin[5,6].

Multiple studies have shown that mutations in the RAS genes increase cell proliferation rates and can initiate neoplastic transformation[7-9]. In addition, it has been shown in multiple cancer models using genetically engineered mice, that *RAS* mutations are also required for tumor maintenance, such that ablation of the defective *RAS* gene leads to tumor regression in these

models[10-12]. This establishes the "oncogenic driver" status of the mutated *RAS* genes and makes it one of the most highly validated targets for therapeutic intervention in cancers.

RAS mutations in developmental disorders and RASopathies

Besides somatic *RAS* mutations in cancer, germline mutations in the *RAS* genes or *RAS* regulators are known to be responsible for certain developmental disorders collectively referred as RASopathies [13,14]. These include Neurofibromatosis type I, Noonan Costello, and Cardio Facio Cutaneous syndromes amongst others. Aberrant RAS signaling due to *RAS* mutation or activation of RAS through loss of RAS regulation (like NF1/SOS1 mutations) or increased downstream signaling (for example, through BRAF mutations) have been shown to be responsible for several of these developmental abnormalities. Since all these aberrations ultimately result in increased RAS-GTP levels, these diseases are collectively referred to as RASopathies. A discussion of the various RASopathies allows understanding of RAS regulators in the developmental context which may have a bearing on some of the observations made in this thesis.

Neurofibromatosis type I is a familial cancer syndrome, caused due to dominantly transmitted loss of function mutations in the *NF1* gene. As alluded to earlier, NF1 is a tumor suppressor GTPase activating protein (GAP), that when mutated prevents the cycling of the RAS-GTP to inactive GDP bound form. Patients harboring germline mutations of NF1 gene are predisposed to a variety of cancers like neurofibromas, astrocytomas and juvenile myelomonocytic leukemia (JMML) [15,16]. Mutations in *PTPN11/SHP-2* phosphatases account for about 50% of Noonan syndrome cases[17], an autososmal dominant developmental disorder characterized by facial anomalies, heart and skeletal defects and hematological disorders.

PTPN11 is a non-receptor type 2 phosphatase that activates the RAS/MAPK signaling pathway downstream of several receptor tyrosine kinases. Study of the missense germline mutations of *PTPN11* suggests the residues that maintain the structurally inactive conformation are frequently mutated keeping PTPN11 in an active conformation, resulting in the neurological disease [18,19]. Somatic mutations in PTPN11, relatively less well characterized at present, have been reported in leukemia that are distinct from the germline mutations and show more pronounced RAS signaling through effector activation[20-22].

Germline KRAS mutations in residues other than frequently observed in cancers (namely, Val^{14}, Thr^{58}, Val^{152} and Asp^{153}) also account for 2% of cases with Noonan syndrome. HRAS mutations restricted to Gly^{12} and Gly^{13}, which are less frequent in cancers, account for the majority of cases with Costello syndrome[23], a disease of mental retardation, distinctive facial appearance and cardiovascular abnormalities. Distinct mutations in the *RAS/RAF* pathway genes (**Table 1**) in developmental disorders and their somatic counterparts in cancers point to a widespread requirement for cell/tissue and/or developmental specific roles for the different RAS genes in these distinct diseases.

RAS structure

The RAS family of proteins belong to a class of small GTPases, encompassing 39 different proteins characterized by a phosphate binding motif (P-loop) and multiple G domains (GTP binding domains), as shown in **Figure 1.3**. These proteins also share nucleotide sensitive Switch I and Switch II domains which interact with various effectors depending on the GDP/GTP bound state of the molecule. The small GTPases are known to play a key role in multiple cellular

processes, including growth, cytoskeletal rearrangements, motility, adhesion and cellular differentiation.

Sequence alignment of the three RAS proteins shows that the N-terminal 80 amino acids which encompass the P-loop, the Switch I and II domains are identical, between H/N and KRAS proteins. A high degree of homology exists until amino acids 166, after which the C-terminal 25 amino acids constitute the hypervariable regions of different RAS proteins effecting differential post translational modifications and membrane anchoring properties.

Crystallographic structures of HRAS [24] bound to GDP/GTP homologs [25] were determined in 1990,. RAS was described as a heart shaped structure with a hydrophobic core of six beta strands and five alpha helices interconnected by loops. GTP hydrolysis was found to be determined largely by five loops on one side of the protein with Q61 being the most critical residue for the GTPase catalytic activity [26]. In its GTP bound state, only small structural changes in the Switch I (amino acids 32-40) and Switch II (amino acids 62-70) are observed when compared to the GDP bound state. Oncogenic mutations at G12/G13 positions (with their large side groups) interfere directly with the GTPase 'active conformation' of the protein and also interfere with the nucleophilic attack of the gamma phosphate of GTP preventing GTP hydrolysis. These small structural aberrations resulting from the substitution of critical amino acids suffice to keep RAS locked in its GTP bound state and have proved to be challenging for therapeutic targeting.

RAS signaling

RAS in its active conformation is now known to activate a number of cellular pathways but it wasn't until 1993 that yeast two-hybrid and *in vitro* interaction analyses helped demonstrate a

direct interaction between RAF1 and activated RAS[13,27]. Subsequently, RAF1 was extensively characterized, and shown to activate the extracellular signal-regulated kinase (ERK) or the mitogen-activated protein kinase (MAPK) pathway which in turn phosphorylates and activates nuclear factors like the E26 transformation-specific (ETS transcription factors)[28] which associate with different nuclear factors to initiate transcription for cell proliferation/differentiation. This signaling from the GTP-bound RAS at the plasma membrane to the nucleus has been demonstrated to be sufficient and necessary for RAS induced transformation[29,30]. Detailed mapping of the RAS-RAF1 interaction that initiates the MAPK cascade[17] showed that the HRAS effector domain within the Switch I domain (amino acids 32-40) associates with RAS binding domains within the N terminal of RAF1/BRAF and are critical for RAS transformation. Although the crystal structure of full length RAF bound to RAS has not yet been determined, the critical role of RAS Switch I binding to RAF1 was demonstrated in a study involving the RAS related protein RAP1A and RAS binding domain (RBD) of RAF1[31]. Furthermore, the structure of HRAS Q61L mutant bound to RAF1-RBD[32], recently revealed that the switch II domain of Q61L is rigid compared to wild type RAS and acquires an anti-catalytic conformation, suggesting that at least for this mutant, RAF binding has allosteric effects on the Switch II domain.

The next class of RAS effectors were identified through experiments to delineate whether the Class I phosphoinositide 3-Kinase (PI3K) activity that co-immunoprecipitates with RAS[33] is a RAS regulator or effector of diverse RAS signaling[34]. The p110 catalytic unit of PI3K was found to associate with RAS only in its active GTP-bound form, qualifying it as an effector, however like the GTPase activating protein NF-1, PI3K binding required both the RAS Switch I and II domains. Specifically, the RAS-PI3K interface makes contact with the Switch I effector

domain (amino acid residues 32-40) as well as extensive contacts with the Switch II domain with Y64 being the critical residue[35]. Like RAF, PI3K binding to RAS-GTP activates PI3K activity and was required for NIH3T3 cellular transformation[26]. In a highly conserved signaling pathway, RAS activation of PI3K results in the conversion of phosphatidylinositol (3,4)-bisphosphate (PIP2) lipids to phosphatidylinositol (3,4,5)-trisphosphate (PIP3). At the plasma membrane PKB/Akt binds PIP3, where Akt phosphorylation activates the mammalian Target of Rapamycin C1 (mTORC1) and mTOR pathways which in turn phosphorylate the eukaryotic translation initiation factor 4E binding protein (4EBP1) and protein S6 (S6K1), directly promoting protein synthesis and cell proliferation. The prevalence of mutations in the RAF and PI3K genes in cancer further underscores the critical roles of these pathways in oncogenesis.

Additionally, the Ral-GDS effector pathway also plays a distinct role in regulating cell proliferation and apoptosis through the RalA and RalB GTPases [36]. As can be seen in **Figure 1.4** several RAS effectors that regulate diverse cellular functions have been described. Phospholipase Cε was identified as an effector that binds the Switch I domain of HRAS[35], its activation leading to hydrolysis of phosphatidylinositol 4,5-bisphosphate in a GTP-dependent manner [37]. With a guanine exchange factor (GEF) domain, PLCε also serves as a bifunctional phospholipase that activates the MAP kinase pathway[38]. The T-cell lymphoma invasion and metastasis-1 (TIAM1) is a Rac GTPase GEF that binds HRAS in a GTP dependent manner to mediate Rac activation by RAS [39]. TIAM1 was also shown to be required for RAS transformation in a mouse model of skin carcinogenesis[40]. The lesser characterized RAS effectors like the AF-6 [41] also bound HRAS in its GTP bound state.

Among the RAS regulators the RIN1 protein was shown to interact directly with HRAS-GTP and unlike RAF, interferes with RAS function in the yeast model[42]. RIN1 is a GEF for the

Rab 5 GTPase that was shown to stimulate the endocytosis of receptor tyrosine kinases upon its association with activated HRAS[43].

A non-catalytic adaptor protein, RASSF5 (Ras association (RalGDS/AF-6 domain family member 1) was identified as an effector that binds the Switch I domain of HRAS in a GTP dependent manner[44]. A more recent study showed that mutant KRAS engaged RASSF5/MST1 (mammalian sterile-20-like-protein kinase-1complex) to initiate apoptosis of HEK293 cells[45]. RASSF2, a member of the same family was shown to have preferential binding to KRAS-GTP compared to HRAS-GTP[46] and like RASSF1 was characterized as a tumor suppressor [47]. HRAS-GTP was more recently shown to bind an E3 ubiquitin ligase IMP (Impedes Mitogenic signal Propagation) and negatively regulate MAP kinase activity by limiting the engagement of RAF-MEK complex in the presence of activated RAS[48]. Lesser characterized effectors like Grb7[49], RAPH1 or PDZ-GEF[50], have been reported but their role in mammalian RAS signaling remains to be investigated.

As may be noted, most of the studies cited above have used mutant HRAS as a bait for the search of effectors and to demonstrate the role of these effectors in RAS signaling. With an increasing appreciation of distinct differences in oncogenic potential across the *RAS* family members, a search for mutant KRAS specific interactions using mass spectrometric approach, uncovered a novel RNA binding protein effector, HNRNPA2B1 which associates with mutant KRAS in a phosphorylation and GTP dependent manner and potentiates AKT/mTOR pathway signaling to promote pancreatic tumor growth in cell line and mouse models[51]. The search for new regulators and effectors through which the different RAS proteins, especially KRAS, exert their effects on signaling cascades in cancer is the core component of this thesis.

RAS regulation

Temporal regulation of RAS expression

Of the four *RAS* genes (*HRAS*, *NRAS* and the two *KRAS* splice variants, *KRAS4A* and *KRAS4B*) only *KRAS4B* is known to be essential for embryogenesis[52] with partial functional overlap with *NRAS*. In genetic ablation studies, knockout of HRAS or NRAS had no significant effects on mouse development and only *KRAS* was reported as essential and sufficient for normal growth and development[53]. However, expression of *HRAS* from the *KRAS* locus (to replace *KRAS* expression) led to normal development[54], suggesting that other RAS proteins can compensate for KRAS functions but distinct spatial/temporal expression program may define their role in embryogenesis (**Figure 1.5**).

Post Transcriptional Gene Regulation of RAS transcripts

Apart from temporal and context dependent regulation, RAS expression is also controlled post transcriptionally (**Figure 1.5**). MicroRNAs are small 21-22 nucleotide RNA molecules that bind target transcripts (in their 3'untranslated regions (UTR) or coding regions) and lead to repression or degradation by the RNA silencing machinery[55]. In 2005, conserved *let-7* microRNA binding sites were identified in the 3'UTR of RAS transcripts which were shown to regulate RAS protein levels. Although this study focused on the role of *let-7* in vulval development in C. elegans, *let-7a* regulation of *NRAS* and *KRAS* transcripts were clearly demonstrated using luciferase reporter assays [56]. Multiple studies have since shown that *let-7* family represents tumor suppressor microRNAS and their levels are reduced in lung cancers[57] [56].

Genetic evidence for *KRAS*/*let-7* regulation was established when a single nucleotide polymorphism (SNP) in the let-7 binding sites in the 3'UTR of *KRAS* (termed *KRAS-LCS6*) was

shown to elevate KRAS levels and was associated with increased risk for lung cancer [58] [59]. *KRAS-LCS6* also increased risk for triple negative breast cancers [60] and shown to have prognostic value in colon cancers[61].

Recently, a simple, elegant analysis of the coding sequences of the RAS genes has revealed an intriguing level of RAS regulation at the level of translation. Despite the similarity of the RAS proteins at the protein level, the nucleotide sequence coding for the proteins are highly divergent such that rare codons present in the *KRAS* transcript limit protein expression and reduce its oncogenic potential in a carcinogenic mouse model, known to be resistant to oncogene induced stress[62]. Paradoxically, the *KRAS* alleles encoding synonymous codons that optimize expression failed to generate tumors in a *de novo* lung carcinogenesis model[63], suggesting that codon bias determines protein expression levels, consequently affecting its oncogenic potential only in a context dependent manner.

Although the post transcriptional gene silencing of *RAS* transcripts through microRNA regulation is the least studied the recently discovered rare codons inherent to *KRAS* transcript is an emerging field.

This thesis provides insights into a novel mechanism by which mutant KRAS may control the expression of its transcript levels through direct interactions with a key component of the RNA silencing machinery.

Trafficking of RAS family of proteins

Nascent RAS proteins undergo differential post translation modifications for attachment to the plasma membrane [64]. The hypervariable region of RAS proteins consisting of 25/26 amino acids with the C-terminal CAAX motif (**Figure 1.2**) are critical for its association with the inner

membrane[65]. Both the C-terminal polylysine stretch and farnesylation of the KRAS4B protein are sufficient for membrane association, whereupon it undergoes proteolytic cleavage of the AAX sequence, catalyzed by RAS- converting enzyme (RCE1). The terminal cysteine residue is then subject to carboxymethylation by isoprenylcysteine carboxymethyltransferase-1 (ICMT). The HRAS, NRAS and KRAS4A proteins all lack the polylysine stretch and therefore require palmitoylation besides prenylation for efficient membrane association. Unlike KRAS4B, prenylated HRAS and NRAS proteins traffic to the Golgi compartment, but require additional modification prior to plasma membrane anchoring[66]. For HRAS, monopalmitoylation at residue 181 and 184 is sufficient while NRAS requires a second targeting sequence for its movement from the Golgi endomembrane to the plasm membrane[67]. More recent studies have identified PDEδ, a guanine nucleotide dissociation inhibitor-like (GDI like) solubilization factor that binds endomembrane associated farnesylated KRAS or depalmitoylated HRAS/NRAS in a nucleotide independent manner, solubilizes them and redirects these proteins to the plasma membrane[68].

EGFR mediated clathrin dependent localization of KRAS (but not HRAS/NRAS) to early and late endosomes has been reported[69], where it engages different effectors for signaling. A PKC dependent phosphorylation event targeting Serine 181 of KRAS leads to its translocation to the mitochondria, where it was shown to associate with Bcl-XL to induce apoptosis[70].

Ubiquitination of about 2% of plasma membrane bound HRAS/NRAS, but not KRAS proteins leads to increased targeting to the endosomal membranes where it limits ERK activation [71]. More recently mono-ubiquitination of KRAS[72] was shown to increase the stability of the proteins and activate signaling through its effector pathways. Recently, we[73] have also demonstrated that the SMURF2:UBCH5 complex, components of the ubiquitination pathway, may regulate the stability of KRAS[73].

Together these studies portray a picture of a highly complex interplay of compartmentalized signaling modules regulated by RAS family proteins' expression, post translational modifications, trafficking through different intracellular membranes, and turnover, with NRAS, HRAS and KRAS (isoform 4A, and 4B), playing distinct as well as shared roles.

Biochemical regulation of RAS activity

As discussed extensively in earlier sections, apart from intrinsic nucleotide binding and hydrolysis, RAS activation through SOS-GEFs and inactivation through GAPs further control the dynamic equilibrium of GDP/GTP bound states of RAS[2]. Modulation of the RAS GTPase cycle at the plasma membrane is probably the most studied aspect of RAS regulation (**Figure 1.1**).

Yet, while RAS activation through oncogenic mutations have been known to increase cell proliferation in many models, activated RAS also induces cell cycle arrest and senescence unless accompanied with collateral mutations in tumor suppressor genes in a cell context dependent manner[74]. This oncogene induced senescence is thought to be due to Reactive Oxygen Species (ROS) activation of p38 MAPK pathway which ultimately results in the repression of E2F target genes[75].

In this thesis, intersections of KRAS with novel pathways were identified at three different levels.

At the chromosomal level, using an integrative genomics approach called Amplification Breakpoint Ranking and Assembly (ABRA) analysis, we nominated *KRAS* as a gene fusion with the ubiquitin-conjugating enzyme *UBE2L3* **(CHAPTER 2)**. Although the *UBE2L3-KRAS* gene fusion was identified only in one prostate cancer cell line, DU145, and shown to promote cellular

transformation, in a larger context, it could represent genetic evidence for the close proximity of KRAS with the proteasome, which is a recurrent theme in various synthetic lethal screens of KRAS[73,76-78].

At the level of gene expression, we identified frequent 'outlier kinases', like *MET, MST1R, AKT2, EPHA2, AXL,* and *PLK2* in pancreatic cancer cell lines, which impart cell line specific dependency in both *in vitro* and *in vivo* models. Particularly, a subset of *KRAS*-dependent pancreatic cancer cell lines display outlier expression of polo-like kinases (PLKs) **(CHAPTER 3)** and show increased sensitivity to PLK inhibition using BI6727 in combination with KRAS knockdown. PLK1, a serine/threonine kinase is a key player in mitosis[79] and forms an integral part of both the anaphase-promoting complex (APC) and, incidentally, the proteasome pathway was identified as a synthetic lethal partner of *KRAS*[78].

At the level of the protein, an unbiased mass spectrometric analysis identified Argonaute 2 (AGO2) as a RAS interacting protein, which we characterized **(CHAPTER 4)**. Further, we provide evidence for the phenotypic consequence of the RAS-AGO2 interaction in cellular transformation, and delve into the mechanistic aspects of this interaction (**CHAPTER 5),** that portends a bearing on RAS biology in normal cell physiology as well. This most surprising intersection of the signaling networks of KRAS with the RNA silencing machinery through its interaction with its core component protein, AGO2, offers new insights into RAS biology.

REFERENCES

1. Sweet, R.W., *et al.* The product of ras is a GTPase and the T24 oncogenic mutant is deficient in this activity. *Nature* **311**, 273-275 (1984).
2. Schubbert, S., Shannon, K. & Bollag, G. Hyperactive Ras in developmental disorders and cancer. *Nat Rev Cancer* **7**, 295-308 (2007).
3. Karnoub, A.E. & Weinberg, R.A. Ras oncogenes: split personalities. *Nat Rev Mol Cell Biol* **9**, 517-531 (2008).
4. Stephen, A.G., Esposito, D., Bagni, R.K. & McCormick, F. Dragging ras back in the ring. *Cancer Cell* **25**, 272-281 (2014).
5. Ihle, N.T., *et al.* Effect of KRAS oncogene substitutions on protein behavior: implications for signaling and clinical outcome. *J Natl Cancer Inst* **104**, 228-239 (2012).
6. Fetics, S.K., *et al.* Allosteric Effects of the Oncogenic RasQ61L Mutant on Raf-RBD. *Structure* **23**, 505-516 (2015).
7. Rhim, J.S., *et al.* Neoplastic transformation of human epidermal keratinocytes by AD12-SV40 and Kirsten sarcoma viruses. *Science* **227**, 1250-1252 (1985).
8. Yoakum, G.H., *et al.* Transformation of human bronchial epithelial cells transfected by Harvey ras oncogene. *Science* **227**, 1174-1179 (1985).
9. Yancopoulos, G.D., *et al.* N-myc can cooperate with ras to transform normal cells in culture. *Proc Natl Acad Sci U S A* **82**, 5455-5459 (1985).
10. Fisher, G.H., *et al.* Induction and apoptotic regression of lung adenocarcinomas by regulation of a K-Ras transgene in the presence and absence of tumor suppressor genes. *Genes Dev* **15**, 3249-3262 (2001).
11. Ying, H., *et al.* Oncogenic Kras maintains pancreatic tumors through regulation of anabolic glucose metabolism. *Cell* **149**, 656-670 (2012).
12. Chin, L., *et al.* Essential role for oncogenic Ras in tumour maintenance. *Nature* **400**, 468-472 (1999).
13. Kratz, C.P., *et al.* Cancer spectrum and frequency among children with Noonan, Costello, and cardio-facio-cutaneous syndromes. *Br J Cancer* (2015).
14. Tidyman, W.E. & Rauen, K.A. The RASopathies: developmental syndromes of Ras/MAPK pathway dysregulation. *Curr Opin Genet Dev* **19**, 230-236 (2009).
15. Chan, G., *et al.* Essential role for Ptpn11 in survival of hematopoietic stem and progenitor cells. *Blood* **117**, 4253-4261 (2011).
16. Side, L.E. & Shannon, K.M. Myeloid disorders in infants with Noonan syndrome and a resident's "rule" recalled. *J Pediatr* **130**, 857-859 (1997).
17. Tartaglia, M., *et al.* Mutations in PTPN11, encoding the protein tyrosine phosphatase SHP-2, cause Noonan syndrome. *Nat Genet* **29**, 465-468 (2001).
18. Oishi, K., *et al.* Transgenic Drosophila models of Noonan syndrome causing PTPN11 gain-of-function mutations. *Hum Mol Genet* **15**, 543-553 (2006).
19. Tartaglia, M., *et al.* Diversity and functional consequences of germline and somatic PTPN11 mutations in human disease. *Am J Hum Genet* **78**, 279-290 (2006).
20. Kratz, C.P., *et al.* The mutational spectrum of PTPN11 in juvenile myelomonocytic leukemia and Noonan syndrome/myeloproliferative disease. *Blood* **106**, 2183-2185 (2005).
21. Martinelli, S., *et al.* Activating PTPN11 mutations play a minor role in pediatric and adult solid tumors. *Cancer Genet Cytogenet* **166**, 124-129 (2006).

22. Molteni, C.G., *et al.* PTPN11 mutations in childhood acute lymphoblastic leukemia occur as a secondary event associated with high hyperdiploidy. *Leukemia* **24**, 232-235 (2010).
23. Gripp, K.W., *et al.* HRAS mutation analysis in Costello syndrome: genotype and phenotype correlation. *Am J Med Genet A* **140**, 1-7 (2006).
24. Pai, E.F., *et al.* Structure of the guanine-nucleotide-binding domain of the Ha-ras oncogene product p21 in the triphosphate conformation. *Nature* **341**, 209-214 (1989).
25. Brunger, A.T., *et al.* Crystal structure of an active form of RAS protein, a complex of a GTP analog and the HRAS p21 catalytic domain. *Proc Natl Acad Sci U S A* **87**, 4849-4853 (1990).
26. Krengel, U., *et al.* Three-dimensional structures of H-ras p21 mutants: molecular basis for their inability to function as signal switch molecules. *Cell* **62**, 539-548 (1990).
27. Vojtek, A.B., Hollenberg, S.M. & Cooper, J.A. Mammalian Ras interacts directly with the serine/threonine kinase Raf. *Cell* **74**, 205-214 (1993).
28. Prontera, P., *et al.* Germline PTPN11 mutation affecting exon 8 in a case of syndromic juvenile myelomonocytic leukemia. *Leuk Res* **35**, e13-14 (2011).
29. Graham, J.M., Jr., *et al.* Genomic duplication of PTPN11 is an uncommon cause of Noonan syndrome. *Am J Med Genet A* **149A**, 2122-2128 (2009).
30. Goemans, B.F., *et al.* Differences in the prevalence of PTPN11 mutations in FAB M5 paediatric acute myeloid leukaemia. *Br J Haematol* **130**, 801-803 (2005).
31. Gripp, K.W., *et al.* A novel HRAS substitution (c.266C>G; p.S89C) resulting in decreased downstream signaling suggests a new dimension of RAS pathway dysregulation in human development. *Am J Med Genet A* **158A**, 2106-2118 (2012).
32. Weaver, K.N., *et al.* Early-lethal Costello syndrome due to rare HRAS Tandem Base substitution (c.35_36GC>AA; p.G12E)-associated pulmonary vascular disease. *Pediatr Dev Pathol* **17**, 421-430 (2014).
33. Sol-Church, K., *et al.* Male-to-male transmission of Costello syndrome: G12S HRAS germline mutation inherited from a father with somatic mosaicism. *Am J Med Genet A* **149A**, 315-321 (2009).
34. Gripp, K.W. & Lin, A.E. Costello syndrome: a Ras/mitogen activated protein kinase pathway syndrome (rasopathy) resulting from HRAS germline mutations. *Genet Med* **14**, 285-292 (2012).
35. Kelley, G.G., Reks, S.E., Ondrako, J.M. & Smrcka, A.V. Phospholipase C(epsilon): a novel Ras effector. *EMBO J* **20**, 743-754 (2001).
36. Chien, Y. & White, M.A. RAL GTPases are linchpin modulators of human tumour-cell proliferation and survival. *EMBO Rep* **4**, 800-806 (2003).
37. Song, C., *et al.* Regulation of a novel human phospholipase C, PLCepsilon, through membrane targeting by Ras. *J Biol Chem* **276**, 2752-2757 (2001).
38. Lopez, I., Mak, E.C., Ding, J., Hamm, H.E. & Lomasney, J.W. A novel bifunctional phospholipase c that is regulated by Galpha 12 and stimulates the Ras/mitogen-activated protein kinase pathway. *J Biol Chem* **276**, 2758-2765 (2001).
39. Lambert, J.M., *et al.* Tiam1 mediates Ras activation of Rac by a PI(3)K-independent mechanism. *Nat Cell Biol* **4**, 621-625 (2002).
40. Malliri, A., *et al.* Mice deficient in the Rac activator Tiam1 are resistant to Ras-induced skin tumours. *Nature* **417**, 867-871 (2002).
41. Kuriyama, M., *et al.* Identification of AF-6 and canoe as putative targets for Ras. *J Biol Chem* **271**, 607-610 (1996).

42. Han, L. & Colicelli, J. A human protein selected for interference with Ras function interacts directly with Ras and competes with Raf1. *Mol Cell Biol* **15**, 1318-1323 (1995).
43. Tall, G.G., Barbieri, M.A., Stahl, P.D. & Horazdovsky, B.F. Ras-activated endocytosis is mediated by the Rab5 guanine nucleotide exchange activity of RIN1. *Dev Cell* **1**, 73-82 (2001).
44. Vavvas, D., Li, X., Avruch, J. & Zhang, X.F. Identification of Nore1 as a potential Ras effector. *J Biol Chem* **273**, 5439-5442 (1998).
45. Khokhlatchev, A., *et al.* Identification of a novel Ras-regulated proapoptotic pathway. *Curr Biol* **12**, 253-265 (2002).
46. Vos, M.D., *et al.* RASSF2 is a novel K-Ras-specific effector and potential tumor suppressor. *J Biol Chem* **278**, 28045-28051 (2003).
47. Tommasi, S., *et al.* Tumor susceptibility of Rassf1a knockout mice. *Cancer Res* **65**, 92-98 (2005).
48. Matheny, S.A., *et al.* Ras regulates assembly of mitogenic signalling complexes through the effector protein IMP. *Nature* **427**, 256-260 (2004).
49. Chu, P.Y., Li, T.K., Ding, S.T., Lai, I.R. & Shen, T.L. EGF-induced Grb7 recruits and promotes Ras activity essential for the tumorigenicity of Sk-Br3 breast cancer cells. *J Biol Chem* **285**, 29279-29285 (2010).
50. Lee, J.H., *et al.* Drosophila PDZ-GEF, a guanine nucleotide exchange factor for Rap1 GTPase, reveals a novel upstream regulatory mechanism in the mitogen-activated protein kinase signaling pathway. *Mol Cell Biol* **22**, 7658-7666 (2002).
51. Barcelo, C., *et al.* Ribonucleoprotein HNRNPA2B1 interacts with and regulates oncogenic KRAS in pancreatic ductal adenocarcinoma cells. *Gastroenterology* **147**, 882-892 e888 (2014).
52. Johnson, L., *et al.* K-ras is an essential gene in the mouse with partial functional overlap with N-ras. *Genes Dev* **11**, 2468-2481 (1997).
53. Esteban, L.M., *et al.* Targeted genomic disruption of H-ras and N-ras, individually or in combination, reveals the dispensability of both loci for mouse growth and development. *Mol Cell Biol* **21**, 1444-1452 (2001).
54. Potenza, N., *et al.* Replacement of K-Ras with H-Ras supports normal embryonic development despite inducing cardiovascular pathology in adult mice. *EMBO Rep* **6**, 432-437 (2005).
55. Winter, J., Jung, S., Keller, S., Gregory, R.I. & Diederichs, S. Many roads to maturity: microRNA biogenesis pathways and their regulation. *Nat Cell Biol* **11**, 228-234 (2009).
56. Johnson, S.M., *et al.* RAS is regulated by the let-7 microRNA family. *Cell* **120**, 635-647 (2005).
57. Takamizawa, J., *et al.* Reduced expression of the let-7 microRNAs in human lung cancers in association with shortened postoperative survival. *Cancer Res* **64**, 3753-3756 (2004).
58. Chin, L.J., *et al.* A SNP in a let-7 microRNA complementary site in the KRAS 3' untranslated region increases non-small cell lung cancer risk. *Cancer Res* **68**, 8535-8540 (2008).
59. Nelson, H.H., *et al.* KRAS mutation, KRAS-LCS6 polymorphism, and non-small cell lung cancer. *Lung Cancer* **69**, 51-53 (2010).
60. Paranjape, T., *et al.* A 3'-untranslated region KRAS variant and triple-negative breast cancer: a case-control and genetic analysis. *Lancet Oncol* **12**, 377-386 (2011).

61. Smits, K.M., *et al.* A let-7 microRNA SNP in the KRAS 3'UTR is prognostic in early-stage colorectal cancer. *Clin Cancer Res* **17**, 7723-7731 (2011).
62. Lampson, B.L., *et al.* Rare codons regulate KRas oncogenesis. *Curr Biol* **23**, 70-75 (2013).
63. Pershing, N.L., *et al.* Rare codons capacitate Kras-driven de novo tumorigenesis. *J Clin Invest* **125**, 222-233 (2015).
64. Prior, I.A. & Hancock, J.F. Ras trafficking, localization and compartmentalized signalling. *Semin Cell Dev Biol* **23**, 145-153 (2012).
65. Ahearn, I.M., Haigis, K., Bar-Sagi, D. & Philips, M.R. Regulating the regulator: post-translational modification of RAS. *Nat Rev Mol Cell Biol* **13**, 39-51 (2012).
66. Apolloni, A., Prior, I.A., Lindsay, M., Parton, R.G. & Hancock, J.F. H-ras but not K-ras traffics to the plasma membrane through the exocytic pathway. *Mol Cell Biol* **20**, 2475-2487 (2000).
67. Choy, E., *et al.* Endomembrane trafficking of ras: the CAAX motif targets proteins to the ER and Golgi. *Cell* **98**, 69-80 (1999).
68. Chandra, A., *et al.* The GDI-like solubilizing factor PDEdelta sustains the spatial organization and signalling of Ras family proteins. *Nat Cell Biol* **14**, 148-158 (2012).
69. Lu, A., *et al.* A clathrin-dependent pathway leads to KRas signaling on late endosomes en route to lysosomes. *J Cell Biol* **184**, 863-879 (2009).
70. Bivona, T.G., *et al.* PKC regulates a farnesyl-electrostatic switch on K-Ras that promotes its association with Bcl-XL on mitochondria and induces apoptosis. *Mol Cell* **21**, 481-493 (2006).
71. Jura, N., Scotto-Lavino, E., Sobczyk, A. & Bar-Sagi, D. Differential modification of Ras proteins by ubiquitination. *Mol Cell* **21**, 679-687 (2006).
72. Sasaki, A.T., *et al.* Ubiquitination of K-Ras enhances activation and facilitates binding to select downstream effectors. *Sci Signal* **4**, ra13 (2011).
73. Shukla, S., *et al.* KRAS protein stability is regulated through SMURF2: UBCH5 complex-mediated beta-TrCP1 degradation. *Neoplasia* **16**, 115-128 (2014).
74. Serrano, M., Lin, A.W., McCurrach, M.E., Beach, D. & Lowe, S.W. Oncogenic ras provokes premature cell senescence associated with accumulation of p53 and p16INK4a. *Cell* **88**, 593-602 (1997).
75. Dimauro, T. & David, G. Ras-induced senescence and its physiological relevance in cancer. *Curr Cancer Drug Targets* **10**, 869-876 (2010).
76. Steckel, M., *et al.* Determination of synthetic lethal interactions in KRAS oncogene-dependent cancer cells reveals novel therapeutic targeting strategies. *Cell Res* **22**, 1227-1245 (2012).
77. Deshpande, R., *et al.* A comparative genomic approach for identifying synthetic lethal interactions in human cancer. *Cancer Res* **73**, 6128-6136 (2013).
78. Luo, J., *et al.* A genome-wide RNAi screen identifies multiple synthetic lethal interactions with the Ras oncogene. *Cell* **137**, 835-848 (2009).
79. Dephoure, N., *et al.* A quantitative atlas of mitotic phosphorylation. *Proc Natl Acad Sci U S A* **105**, 10762-10767 (2008).

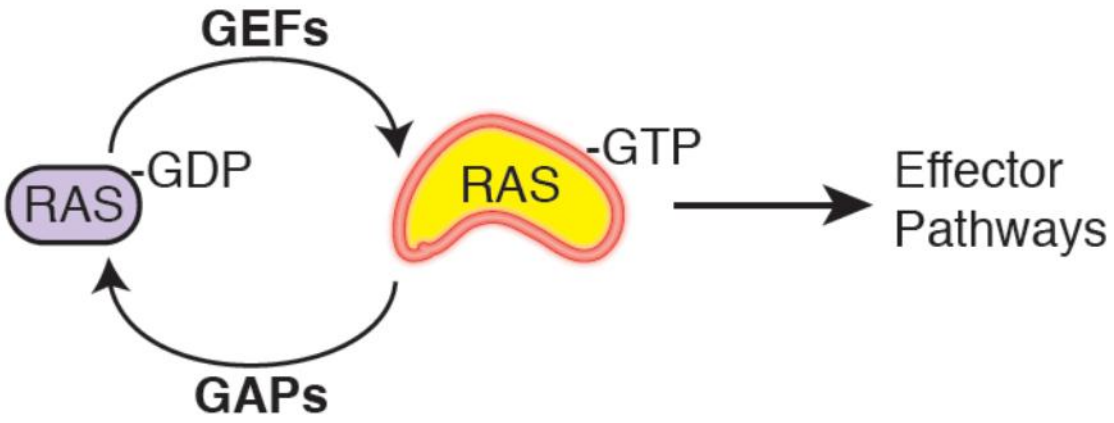

Figure 1.1 The RAS-GTPase cycle. RAS proteins cycle between an inactive GDP or active GTP bound form. In its activated state, RAS-GTP triggers various effector pathways that trigger cell proliferation.

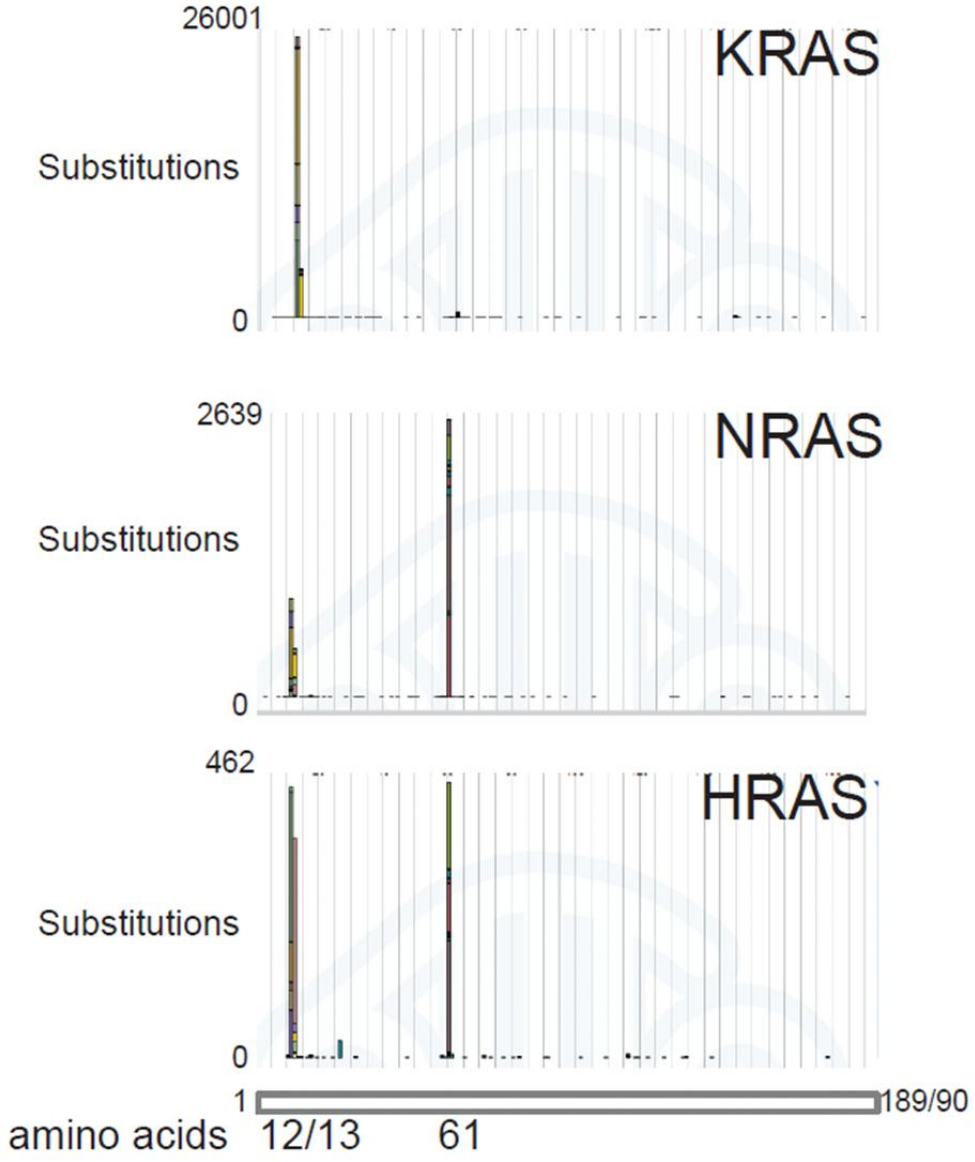

Figure 1.2 Frequency of mutations at amino acid 12, 13 and 61in different RAS proteins in human cancers (COSMIC analysis, 2015)

Syndrome	Gene	Protein	Protein Function	Mutation Frequency (%)
Noonan	PTPN11	SHP2	Phosphatase	50%
	SOS1	SOS1	RasGEF	17%
	KRAS	KRAS	GTPase	2%
	RAF1	CRAF	Kinase	17%
	MAP2K1	MEK1	Kinase	<1%
	RIT1	RIT1	GTPase	9%
Cardiofaciocutaneous	KRAS	KRAS	GTPase	2%
	BRAF	BRAF	Kinase	75%
	MAP2K1	MEK1	Kinase	25%
	MAP2K2	MEK2	Kinase	
Costello	HRAS	HRAS	GTPase	90%
	KRAS	KRAS	GTPase	6%
Type-1 Neurofibromatosis	NF1	Neurofibromin	RasGAP	50%
Legius	SPRED1	SPRED1	MAPK signaling	5%
LEOPARD	PTPN11	SHP2	Phosphatase	90%
	RAF1	CRAF	Kinase	3-5%
	BRAF	BRAF	Kinase	5%
Capillary malformation-arteriovenous	RASA1	P120GAP	RasGEF	50%

Table 1. Germline mutations of RAS/MAPK pathway in developmental disorders

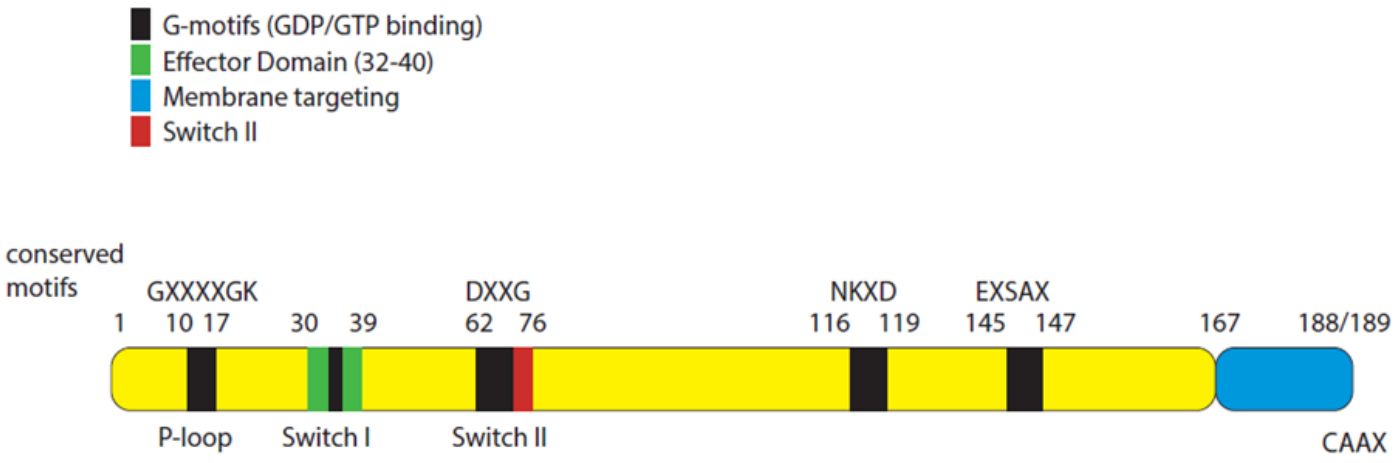

Figure 1.3 Structural motifs of the RAS-GTPase

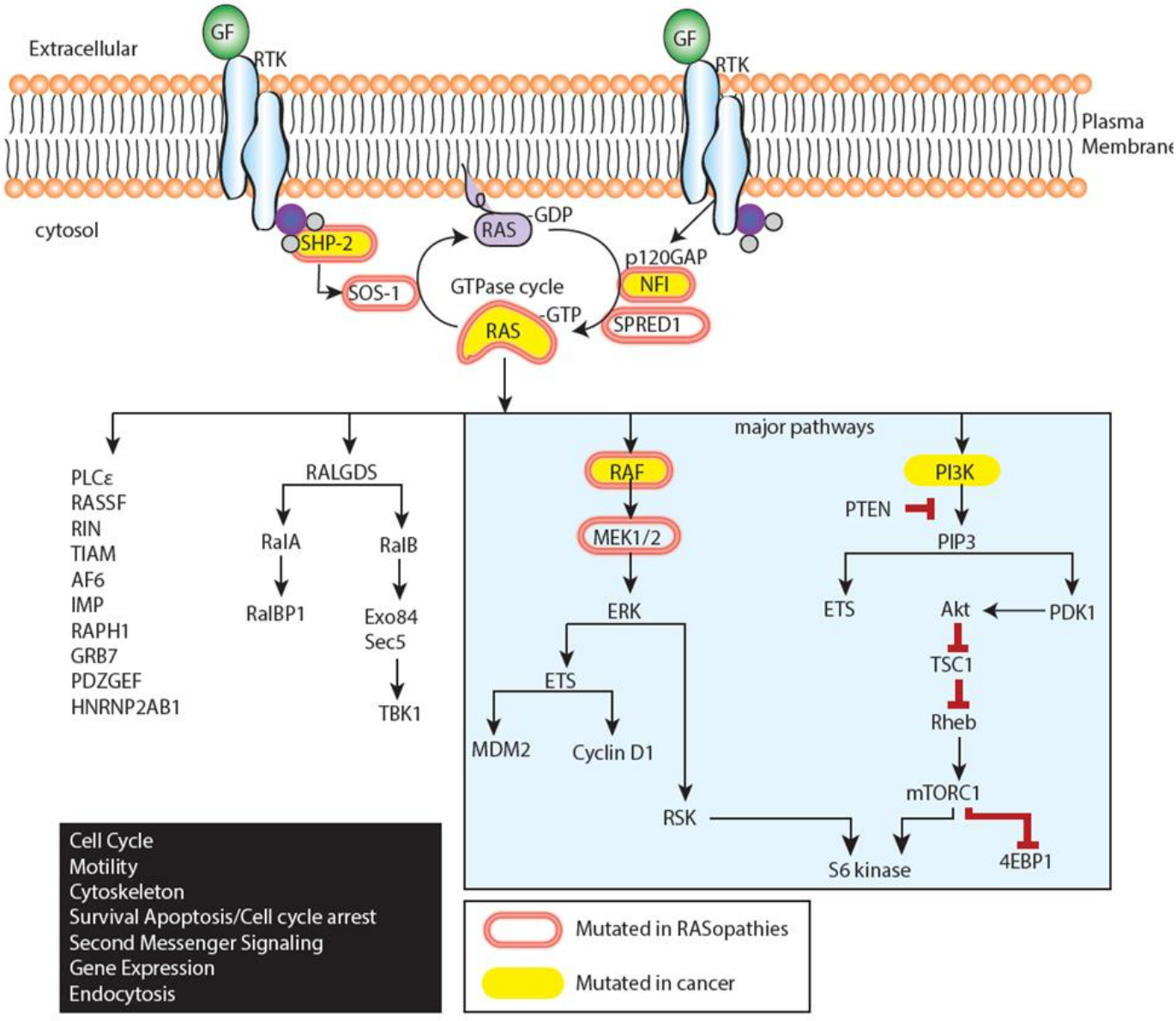

Figure 1.4 RAS signaling. Mitogenic signals translocate RAS to the plasma membrane and activate various signaling pathways. Adapted from *Dragging Ras Back in the Ring*. Cancer Cell 25, March 17, 2014

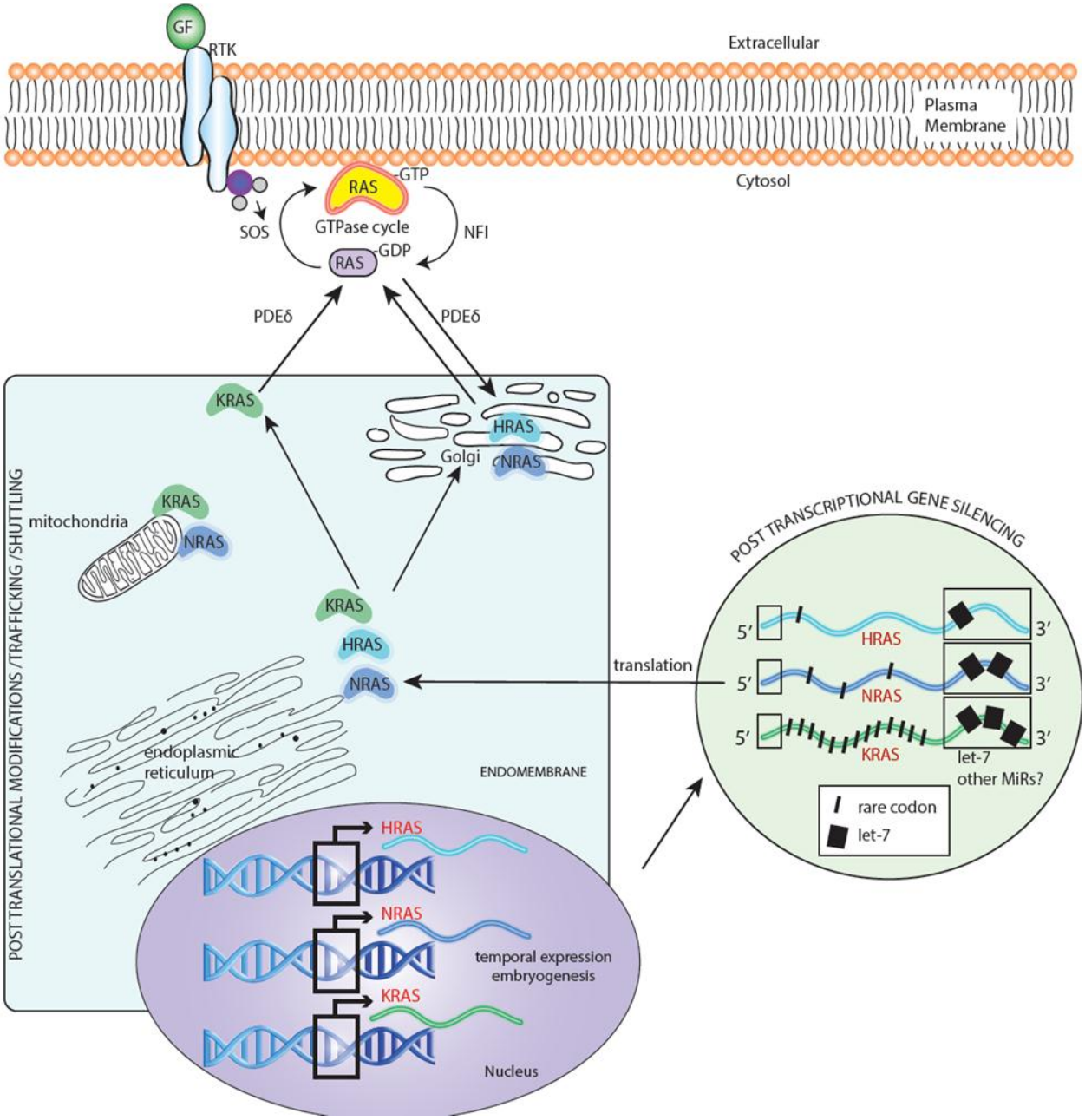

Figure 1.5 Regulation of RAS. RAS undergoes transcriptional, post transcriptional and post translational regulation. Post translational modification further traffic RAS to various cellular compartments for differential signaling outputs.

CHAPTER 2

CHARACTERIZATION OF *KRAS* REARRANGEMENTS IN METASTATIC PROSTATE CANCER

SUMMARY

Using an integrative genomics approach called Amplification Breakpoint Ranking and Assembly (ABRA) analysis, we nominated *KRAS* as a gene fusion with the ubiquitin-conjugating enzyme *UBE2L3* in the DU145 cell line- which was originally derived from a metastatic prostate cancer to the brain. Interestingly, analysis of tissues revealed that 2 out of 62 metastatic prostate cancers harbored aberrations at the *KRAS* locus. In DU145 cells, *UBE2L3-KRAS* produces a fusion protein and specific knock-down of the fusion attenuates cell invasion and xenograft growth. Ectopic expression of the UBE2L3-KRAS fusion protein exhibits transforming activity in NIH 3T3 fibroblasts and RWPE prostate epithelial cells *in vitro* and *in vivo*. In NIH 3T3 cells, UBE2L3-KRAS attenuates the MEK/ERK pathway, which is commonly engaged by oncogenic mutant KRAS, and instead diverts signaling to the AKT and p38 MAPK pathways. This is the first report of a gene fusion involving Ras family genes and suggests that this aberration may drive metastatic progression in a subset of prostate cancers.

INTRODUCTION

To date, oncogenic alterations in the RAS oncogenes have been restricted to activating point mutations including the most commonly observed substitutions in codon 12, 13 and 61 of the different *RAS* isoforms [1-3]. Gene fusions involving *RAS* genes have thus far not been described as a class of cancer-related aberrations.

Consolidating the characteristic features of driving gene fusions in cancer, previously we carried out a large-scale integrative analysis of cancer genomic datasets matched with gene rearrangement data [4]. As part of this analysis, we observed that in many instances, a small subset of tumors or cancer cell lines harboring an oncogenic gene fusion, often display characteristic amplification at the site of genomic rearrangements [5-9] . High level copy number changes that result in the marked over-expression of oncogenes usually encompass the target genes at the center of overlapping amplifications across a panel of tumor samples. In contrast, amplification loci usually include only a portion of fusion genes, and are considered secondary genetic lesions associated with disease progression, drug resistance, and/or poor prognosis[5,7-11]. Thus, a "partially" amplified cancer gene may be indicative that this gene participates in a genomic fusion event important in cancer progression. This is the result of several independent genetic accidents including the formation of the gene fusion and subsequent amplification, suggesting possible selective pressure in cancer cells for this aberration. To systematically analyze this aspect, we developed an integrative genomic approach called amplification breakpoint ranking and assembly (ABRA) to discover causal gene fusions from cancer genomic datasets.

To uncover driving gene fusions contributing to prostate cancer progression, we applied ABRA analysis to genomic data from ten prostate cancer cell lines. Most interestingly, this led to the identification of a *KRAS* gene fusion in a rare subset of metastatic prostate cancer. This is the

first description of a mutant chimeric version of KRAS and may represent a new class of RAS aberrations.

RESULTS

According to the fusion breakpoint principle previously described [4], amplifications associated with gene fusions usually involve the 5' region of 5' partners, and 3' region of 3' partners. Further, the amplification levels of 5' and 3' fusion genes will be similar due to their co-amplification as a single fusion gene. This rationale was used to assemble putative gene fusions associated with amplification breakpoints by matching the amplification levels of candidate 5' and 3' partners. We initially focused this analysis on cancer cell lines, as breakpoint analyses are more reliable in uniform cellular populations as opposed to tumors, which are often admixed with non malignant cells, diluting genomic aberration profiles.

The ABRA approach was tested using a high resolution single nucleotide polymorphism microarray (aSNP) dataset [5] generated from 36 leukemia cell lines including the K-562 chronic myeloid leukemia cell line known to harbor the amplified *BCR-ABL1* fusion [14]. We inferred the relative DNA copy number data and identified all 5' and 3' amplified genes from the 36 cell lines ($\geq$2 copies). In this dataset, *ABL1* was the top ranking gene with a 3' copy number increase. The amplification levels of all 5' amplified genes in K-562 were then matched with *ABL1* to nominate potential 5' partners. In total, six 5' amplified genes were found in K-562 and five matched the level of *ABL1* 3' amplification. After curation of the amplification breakpoints, *BCR* and *NUP214* were nominated as *ABL1* fusion partner candidates. This demonstrated the feasibility of this method in nominating driver gene fusions from genomic datasets.

To nominate novel gene fusions in advanced prostate cancer cells, we applied this method to an array comparative genomic hybridization (aCGH) dataset of 10 prostate cancer cell lines. Interestingly, the top candidate nominated in the ETS gene fusion-negative prostate cancer cell line, DU145, was the *KRAS* locus exhibiting a clear breakpoint accompanied by a 3' amplification of *KRAS* (**Figure 2.1a, left panel,**). This result was particularly intriguing considering that activating point mutations of *KRAS* are rarely seen in prostate cancer [13]. Interestingly, the activation of downstream signaling intermediaries of the RAS-MAPK pathway have been observed in prostate cancer by a number of studies [15-17]. To assemble amplification breakpoints in the *KRAS* gene with more confidence, we carried out replicate array CGH hybridizations for DU145. Matching the amplification level of *KRAS* with the 5' amplified genes from DU145 cells we identified 10 potential 5' partner candidates that were suggested by either of the two array CGH hybridizations. After curation, *C14orf166, SOX5* and *UBE2L3* were shortlisted as the top 5' partner candidates for *KRAS* (**Figure 2.1a, right panel)**

To experimentally assess the predicted fusions of *C14orf166-KRAS, SOX5-KRAS* and *UBE2L3-KRAS*, we designed primer pairs from the first exons of candidate 5' partners and last exon of *KRAS*, as well as the exons across the breakpoints. Reverse transcription polymerase chain reaction (RT-PCR) analysis of DU145 cells identified a specific fusion band for *UBE2L3-KRAS* but not for the other candidates. Sequencing of the RT-PCR product confirmed the fusion of the *UBE2L3* exon 3 to the *KRAS* exon 2, schematically depicted in **Figure 2.1b**. To assess the expression level of the *UBE2L3-KRAS* fusion transcripts, we analyzed a panel of prostate cell lines by SYBR green quantitative PCR (QPCR) (**Figure 2.1c**) and RNase protection assay. UBE2L3-KRAS was highly expressed in DU145 cells but not in the other prostate cancer cell lines; this was further confirmed by paired-end transcriptome sequencing of DU145 cells.

Importantly, RNAseq also confirmed that the fusion allele of *KRAS* from DU145 cells did not harbor canonical activating mutations, suggesting that the fusion may represent the oncogenic aberration in this sample.

To characterize the chromosomal rearrangements involving *UBE2L3* and *KRAS* loci in DU145, we carried out fluorescence in situ hybridization (FISH) analysis. Using *KRAS* split probe and *UBE2L3-KRAS* fusion probe, DU145 cells clearly showed a rearrangement at the *KRAS* genomic locus and fusion with *UBE2L3* (Figure **2.1d**). In addition, we also observed low level amplification (3 copies) of the *UBE2L3-KRAS* fusion consistent with its nomination by the ABRA approach. To extend our studies to prostate cancer tissues we carried out a combination of KRAS split probe FISH (n= 103 total cases) and array CGH breakpoint analysis (n=218 total cases) of 259 clinically localized prostate cancers, and 62 metastatic prostate cancers from the University of Michigan and Memorial Sloan Kettering Cancer Center (MSKCC). Interestingly, while clinically localized cases did not show aberrations at the KRAS locus, we identified 2 out of 62 metastatic prostate cancers that harbored a rearrangement at the KRAS locus (**Figure 2.1d**). One of the index cases, PCA0216, which was a soft tissue metastasis, was validated by both array CGH and FISH; while the other index PCA0211 was a bone metastasis and was validated by arrayCGH (but optimal hybridization for FISH analysis was not achieved following decalcification protocol) (**Figure 2.1d)**. Interestingly, the available gene and exon expression data for case PCA0211 suggested that this case was ETS fusion negative, and exhibited high expression of KRAS Exons 2-6 (not Exon 1) similar to the DU145 cell line.

We next examined expression of the UBE2L3-KRAS protein. The predicted 296 amino acid fusion protein trims 17 amino acids from the C-terminus of UBE2L3 (**Figure 2.2a**). The full length KRAS protein is preserved, with a 4 amino acid insertion between UBE2L3 and KRAS.

Using both a monoclonal antibody raised against the Ras family and a polyclonal antibody specific to KRAS, we detected a 33 kDa fusion protein in addition to the 21 kDa band corresponding to wild-type KRAS in DU145 cells (**Figure 2.2b**). Specificity of the band corresponding to the predicted UBE2L3-KRAS protein was confirmed by siRNA based knock down of *KRAS*, *UBE2L3* and the chimeric junction of *UBE2L3-KRAS*. The UBE2L3-KRAS protein was found specifically in DU145 cells and not in a panel of other prostate cell lines (**Figure 2.2c**). Specific expression of the protein was also independently confirmed by mass spectrometric assessment of DU145 cells using a multiple reaction monitoring (MRM) assay (which does not require antibody based detection) (**Figure 2.2d**). Over-expression of UBE2L3-KRAS in HEK293 cells, however, did not result in detectable fusion protein. Interestingly, in the presence of the proteosomal inhibitor, bortezomib, expression of the fusion protein was clearly apparent suggesting decreased stability of the fusion protein in the over-expression system (**Figure 2.2c**).

UBE2L3 is a ubiquitin-conjugating enzyme (E2) [18] and may account for the apparent instability of the fusion protein. We therefore attempted to detect possible ubiquitination of UBE2L3-KRAS protein. We identified a Rat anti-Ras monoclonal antibody which precipitated the 33kDa UBE2L3-KRAS protein as well as additional bands in the 40-55kDa region which were specific to HEK 293T cells expressing the fusion. These shifted bands are recognized by both anti-Ras and anti-HA tagged ubiquitin antibodies, and their molecular weights match the prediction for ubiquitinated fusion proteins. We further detected these ubiquitinated UBE2L3-KRAS proteins in DU145 cells. These data suggest that the UBE2L3-KRAS protein is ubiquitinated, which may contribute to its decreased stability.

To determine the function of the UBE2L3-KRAS fusion, we over-expressed it in NIH 3T3 cells, a system classically used to study RAS biology [1,19]. Of note, enforced expression of UBE2L3-KRAS induced loss of fibroblast morphology, increased cell proliferation and foci formation **(Figure 2.3a-b**). Cell cycle analysis revealed an increase in the S phase fraction of cells. To determine the effects of UBE2L3-KRAS expression on tumor growth *in vivo* we implanted nude mice with the stable NIH 3T3 vector control cells or NIH 3T3 *UBE2L3-KRAS* fusion expressing cells. We observed robust tumor formation by the UBE2L3-KRAS expressing cells but not the vector transfected cells (**Figure 2.3c**). To interrogate the potential RAS-related signaling pathways engaged by UBE2L3-KRAS in NIH 3T3 cells we carried out a series of immunoblot analyses on key signaling intermediaries. As reported in the literature for NIH 3T3 cells, KRAS is a stronger inducer of the MEK/ERK cascade; whereas HRAS is a stronger activator of the PI3K/AKT pathway [6]. Interestingly, UBE2L3-KRAS over-expression resulted in attenuated endogenous MEK and ERK phosphorylation (**Figure 2.3d**) in NIH 3T3 cells, instead, the signaling was directed to AKT and p38 MAP Kinase cascades, both of which have been implicated in prostate cancer [15,17].

As activation of the MEK-ERK pathway is dependent on membrane attachment of Ras proteins, we investigated their sub-cellular localization using immunofluorescence assays. Interestingly, Ras proteins, which are normally distributed in the cytoplasm, were found to be highly enriched in the late endosome after ectopic expression of UBE2L3-KRAS fusion in NIH3T3 cells. We speculate that this relocation of Ras proteins may decrease their association with the cellular membrane, and possibly enhance the growth-factor receptor signaling in the endosome.

To investigate the role of the *UBE2L3-KRAS* fusion in a prostate background, we over-expressed the fusion in RWPE prostate epithelial cells. The expression of the fusion protein was enhanced by incubation with bortezomib (**Figure 2.4a, insert**). Over-expression of the *UBE2L3-KRAS* fusion in RWPE cells led to increased cell invasion, proliferation, and a transient increase of tumor growth in nude mice (**Figure 2.4a**). It is notable that in the RWPE model, signaling pathway analysis did not reveal inhibition of the MEK/ERK pathway or activation of AKT/p38 MAPK, (data not shown). Although the MEK inhibitor U0126 inhibits the invasion of RWPE cells over-expressing either wild type or mutant KRAS, treatment of RWPE cells over-expressing the fusion continued to exhibit invasive properties in the presence of U0126, suggesting that downstream effectors other than MEK/ERK may be engaged by the fusion in the prostate context.

To further confirm the function of endogenous UBE2L3-KRAS in DU145 cells, we performed stable knock-down of UBE2L3-KRAS fusion and generated chicken embryo chorioallantoic membrane and mouse xenograft models. This resulted in decreased cell invasion and proliferation *in vitro*, as well as the inhibition of tumor formation in the *in vivo* models (**Figure 2.4b-c**).

DISCUSSION

The addiction of cancer cells to causal gene fusions often results in *in vivo* amplification, which may be exploited to reveal unbalanced recurrent gene rearrangements. Based on this rationale, we developed an integrative genomic-based approach called ABRA to explore driving gene fusions contributing to the progression of prostate cancer. This led to the nomination of the *UBE2L3-KRAS* fusion in DU145 prostate cancer cells. This fusion encodes a protein

encompassing most of the UBE2L3 protein and full length KRAS, which is ubiquitinated in DU145 cells. Importantly, recurrent genomic rearrangements at the *KRAS* locus were found in 2 out of 62 metastatic prostate tumors in addition to the DU145 metastatic prostate cancer cell line. While a number of oncogenic activating point mutations of *KRAS* have been identified, this is the first description of a mutant chimeric version of *KRAS* that is oncogenic and thus may represent a new class of cancer-related alteration. Consistent with this finding, we recently described gene fusions of *BRAF* and *RAF1* in 1-2 % of prostate tumors, further implicating the RAS-RAF-MAPK signaling pathway in subsets of prostate cancer[20].

While both KRAS G12V and UBE2L3-KRAS exhibit an oncogenic phenotype *in vitro* and *in vivo*, UBE2L3-KRAS over-expression leads to attenuation, rather than activation, of the MEK-ERK pathway in NIH 3T3 cells. Instead, it appears that the KRAS fusion enriches Ras proteins in the endosome, and switches signaling to the AKT and p38 MAPK cascades. This observation may have important implications in understanding the biology of this most studied proto-oncogene. Future studies will be needed to elucidate the details of how chimeric KRAS engages endogenous RAS- related signaling pathways in the context of prostate cancer.

MATERIALS AND METHODS

Amplification Breakpoint Ranking and Assembly. The microarray CGH data from prostate cancer cell lines were segmented by the circular binary segmentation (CBS) algorithm [21], and the genomic position of each amplification breakpoint was mapped with the genomic regions of all human genes. The 3' amplified genes were rated by their *r*ConSig Score, which identify *KRAS* as the top candidate. Matching the amplification level of 3' *KRAS* with 5' amplified genes from DU145 nominated *UBE2L3*, *SOX5* and *C14orf166* as 5' partner candidates.

Reverse Transcription PCR, Nuclease protection assay and Fluorescence In Situ Hybridization. RT-PCR with the fusion primers confirmed the *UBE2L3-KRAS* fusion in DU145 cells. Fusion qPCR was performed on a panel of prostate cancer cell lines (StepOne Real Time PCR system, Applied Biosystems). Ribonuclease protection assays were performed utilizing a 230 bp fragment spanning the UBE2L3-KRAS fusion junction. Interphase FISH was done on cell lines, paraffin-embedded tissue sections, and tissue microarrays using bacterial artificial chromosome probes.

Western Blotting and Multiple Reactions Monitoring Mass Spectrometry. Lysates from DU145, PrEC, RWPE, 22RV1, VCaP and PC3 cells, either untreated or treated with 500nM bortezomib for 12 hours, were probed with anti-RAS monoclonal (Millipore) and anti-KRAS rabbit polyclonal antibodies (Proteintech Group Inc). Cell lysates from DU145 and LnCaP cells treated with bortizomib were analyzed by Multiple Reactions Monitoring Mass Spectrometry to identify the fusion peptides.

In Vitro Overexpression and Stable Knockdown of UBE2L3-KRAS Fusion. Expression plasmids for UBE2L3-KRAS were generated with the pDEST40 (with or without 5' FLAG) and pLenti-6 vectors (without 5'FLAG). The expression plasmids were introduced into HEK (5' FLAG-UBE2L3-KRAS pDEST40 vector), NIH/3T3 (UBE2L3-KRAS pDEST40 vector) and RWPE cells (UBE2L3-KRAS pLenti-6 vector) using standard protocols. The prostate cancer cell line DU145 was infected with lentiviruses with scrambled shRNA or UBE2L3-KRAS shRNA, and stable cell lines were generated by selection with puromycin (Invitrogen).

Cell Proliferation, Invasion and Pathway Analysis, Xenograft Mice Model. Cell counting analysis and basement membrane matrix invasion assays were performed as described previously [22,23]. Protein lysates from NIH/3T3 stable cell lines expressing UBE2L3-KRAS, V600E mutant

BRAF, G12V mutant KRAS, and vector controls were probed with phospho and total MEK1/2, p38 MAPK, Akt, and ERK antibodies (Cell Signaling Technologies). The stable NIH/3T3 and RWPE cells expressing UBE2L3-KRAS, and pooled or single clone population of DU145 cells with the stable knockdown of UBE2L3-KRAS were implanted subcutaneously into nude mice.

REFERENCES

1 Seeburg, P. H., Colby, W. W., Capon, D. J., Goeddel, D. V. & Levinson, A. D. Biological properties of human c-Ha-ras1 genes mutated at codon 12. *Nature* **312**, 71-75 (1984).

2 Karnoub, A. E. & Weinberg, R. A. Ras oncogenes: split personalities. *Nat Rev Mol Cell Biol* **9**, 517-531, doi:10.1038/nrm2438
nrm2438 [pii] (2008).

3 Schubbert, S., Shannon, K. & Bollag, G. Hyperactive Ras in developmental disorders and cancer. *Nat Rev Cancer* **7**, 295-308 (2007).

4 Wang, X. S. *et al.* An integrative approach to reveal driver gene fusions from paired-end sequencing data in cancer. *Nat Biotechnol* **27**, 1005-1011 (2009).

5 Mullighan, C. G. *et al.* BCR-ABL1 lymphoblastic leukaemia is characterized by the deletion of Ikaros. *Nature* **453**, 110-114 (2008).

6 Graux, C. *et al.* Fusion of NUP214 to ABL1 on amplified episomes in T-cell acute lymphoblastic leukemia. *Nat Genet* **36**, 1084-1089 (2004).

7 Barr, F. G. *et al.* In vivo amplification of the PAX3-FKHR and PAX7-FKHR fusion genes in alveolar rhabdomyosarcoma. *Hum Mol Genet* **5**, 15-21 (1996).

8 Ferreira, B. I. *et al.* Array CGH and gene-expression profiling reveals distinct genomic instability patterns associated with DNA repair and cell-cycle checkpoint pathways in Ewing's sarcoma. *Oncogene* **27**, 2084-2090 (2008).

9 Koivunen, J. P. *et al.* EML4-ALK fusion gene and efficacy of an ALK kinase inhibitor in lung cancer. *Clin Cancer Res* **14**, 4275-4283 (2008).

10 Stergianou, K., Fox, C. & Russell, N. H. Fusion of NUP214 to ABL1 on amplified episomes in T-ALL--implications for treatment. *Leukemia* **19**, 1680-1681 (2005).

11 Attard, G. *et al.* Duplication of the fusion of TMPRSS2 to ERG sequences identifies fatal human prostate cancer. *Oncogene* **27**, 253-263 (2008).

12 Rodriguez-Viciana, P. *et al.* Cancer targets in the Ras pathway. *Cold Spring Harb Symp Quant Biol* **70**, 461-467, doi:10.1101/sqb.2005.70.044 (2005).

13 Moul, J. W., Friedrichs, P. A., Lance, R. S., Theune, S. M. & Chang, E. H. Infrequent RAS oncogene mutations in human prostate cancer. *Prostate* **20**, 327-338 (1992).

14 Wu, S. Q. *et al.* Extensive amplification of bcr/abl fusion genes clustered on three marker chromosomes in human leukemic cell line K-562. *Leukemia* **9**, 858-862 (1995).

15 Graff, J. R. *et al.* Increased AKT activity contributes to prostate cancer progression by dramatically accelerating prostate tumor growth and diminishing p27Kip1 expression. *J Biol Chem* **275**, 24500-24505 (2000).

16 Daniel Gioeli, S. K., Michael J. Weber, and Michael J. Weber. in *Current Clinical Oncology: Prostate Cancer: Signaling Networks, Genetics, and New Treatment Strategies* Vol. 11 (ed R. G. Pestell and M. T. Nevalainen) 223-256 (Humana Press, 2008).

17 Xu, L., Chen, S. & Bergan, R. C. MAPKAPK2 and HSP27 are downstream effectors of p38 MAP kinase-mediated matrix metalloproteinase type 2 activation and cell invasion in human prostate cancer. *Oncogene* **25**, 2987-2998 (2006).

18 Moynihan, T. P. *et al.* Fine-mapping, genomic organization, and transcript analysis of the human ubiquitin-conjugating enzyme gene UBE2L3. *Genomics* **51**, 124-127 (1998).
19 Der, C. J., Krontiris, T. G. & Cooper, G. M. Transforming genes of human bladder and lung carcinoma cell lines are homologous to the ras genes of Harvey and Kirsten sarcoma viruses. *Proc Natl Acad Sci U S A* **79**, 3637-3640 (1982).
20 Palanisamy, N. *et al.* Rearrangements of the RAF kinase pathway in prostate cancer, gastric cancer and melanoma. *Nat Med* **16**, 793-798, doi:nm.2166 [pii] 10.1038/nm.2166 (2010).
21 Olshen, A. B., Venkatraman, E. S., Lucito, R. & Wigler, M. Circular binary segmentation for the analysis of array-based DNA copy number data. *Biostatistics* **5**, 557-572 (2004).
22 Kleer, C. G. *et al.* EZH2 is a marker of aggressive breast cancer and promotes neoplastic transformation of breast epithelial cells. *Proc Natl Acad Sci U S A* **100**, 11606-11611 (2003).
23 Varambally, S. *et al.* Genomic loss of microRNA-101 leads to overexpression of histone methyltransferase EZH2 in cancer. *Science* **322**, 1695-1699 (2008).

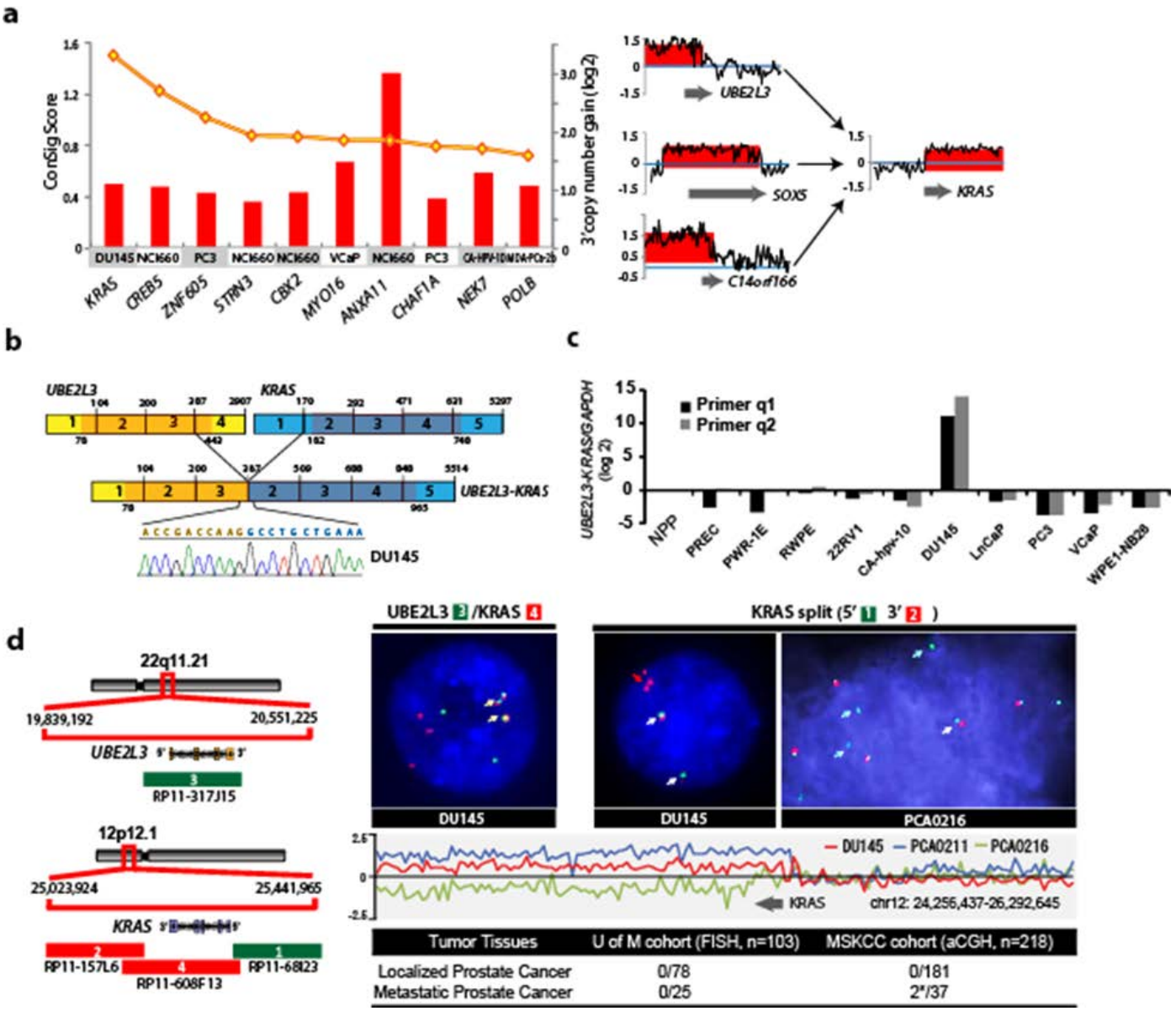

Figure 2.1. Identification and characterization of a novel KRAS rearrangement in metastatic prostate cancer. (a) Left panel, amplification breakpoint analysis and ConSig scoring of 3' amplified genes from a panel of advanced prostate cancer cell lines nominated *KRAS* as a top fusion gene candidate with 3'amplification in the DU145 prostate cancer cells. The ConSig scores are depicted by the yellow line and the level of 3' amplification for each 3' fusion gene candidate is depicted by red columns. Right panel, matching the amplification level of 5' amplified genes in DU145 cells nominates *SOX5*, *C14orf166*, and *UBE2L3* as 5' fusion partner candidates for *KRAS*. The relative quantification of DNA copy number data from the genomic regions 1Mb apart from the candidate fusion genes is shown. The x axis indicates the physical position of the genomic aberrations. The fusion partners are indicated by grey arrows. **(b)** Schematic of sequencing result from Reverse Transcription PCR revealing fusion of *UBE2L3* with *KRAS* in DU145. Structures for the *UBE2L3* and *KRAS* genes have their basis in the Genbank reference sequences. The numbers above the exons (indicated by boxes) indicate the last base of each exon. Open reading frames are shown in darker shades. The exons of *UBE2L3-KRAS* fusion are numbered from the original reference sequences. Line graphs show the position and DNA sequencing of the fusion junction. **(c)** A panel of prostate cancer cell lines was analyzed for *UBE2L3-KRAS* mRNA expression by SYBR assay with the fusion primers. * NPP, normal prostate pool. **(d)** Left panel, the genomic organizations of *UBE2L3* and *KRAS* loci were shown in the schematic, with red and green bars indicating the location of BAC clones. Genes are shown with the direction of transcription indicated by the arrows and exons indicated by bars. Right panel, FISH assay (upper) and copy number data analysis (lower) confirms the fusion of *UBE2L3* to *KRAS* in DU145 cells and recurrent rearrangements at the *KRAS* locus. Left FISH figure shows three copies of fusion signals as indicated by yellow arrows, using co-localizing probes for the fusion. Right FISH figure shows triplicate *KRAS* 3' signals in DU145, and 3' deletion of *KRAS* in a metastatic prostate tumor, PCA0216, using probes that tightly encompass the *KRAS* locus. Relative quantification of copy number array CGH data at the *KRAS* locus in DU145, metastatic prostate tumors PCA0211 and PCA0216 are shown in the lower panel.

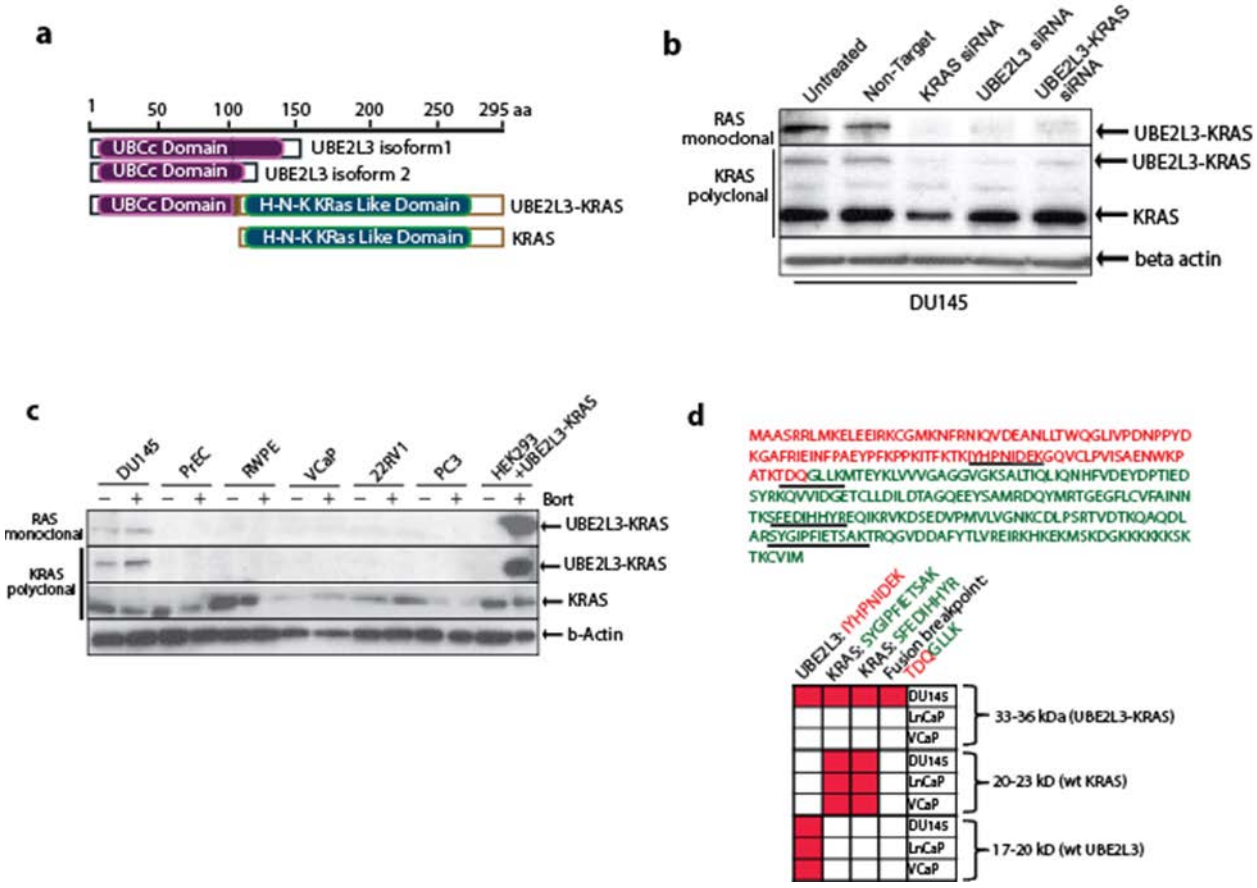

Figure 2.2. Characterization of the UBE2L3-KRAS fusion protein. **(a)** Schematic representations of UBE2L3, KRAS and the predicted UBE2L3-KRAS fusion protein. **(b)** Expression of the UBE2L3-KRAS fusion protein in DU145 cells. Immunoblot analysis of DU145 cells using an anti-RAS mouse monoclonal antibody and an anti-KRAS rabbit polyclonal antibody detects a 33kDa fusion protein specific to DU145 cells. siRNA duplexes employed are indicated. β-actin was used to demonstrate equal loading. **(c)** Survey of the UBE2L3-KRAS fusion protein in a panel of prostate cancer cell lines and stabilization of protein expression with a proteosomal inhibitor, bortezomib. Cell lines are indicated and treated in the presence or absence of 500nM bortezomib for 24 hours. HEK293 cells were transfected with an expression construct encoding UBE2L3-KRAS. Immunoblot analysis was carried out using KRAS polyclonal and RAS monoclonal antibodies. **(d)** Mass spectrometric assay for the detection of the UBE2L3-KRAS protein in DU145 cells. An MRM-MS assay was developed to detect the UBE2L3-KRAS fusion protein. Upper panel, sequence of the UBE2L3-KRAS fusion protein with amino acids colored in red from UBE2L3 and colored in green from KRAS. Tryptic peptides used for MRM-MS analysis are underlined. Matrix represents positive measurement (highlighted in red) of peptides from corresponding gel fraction of DU145, LNCaP and VCaP whole cell lysates.

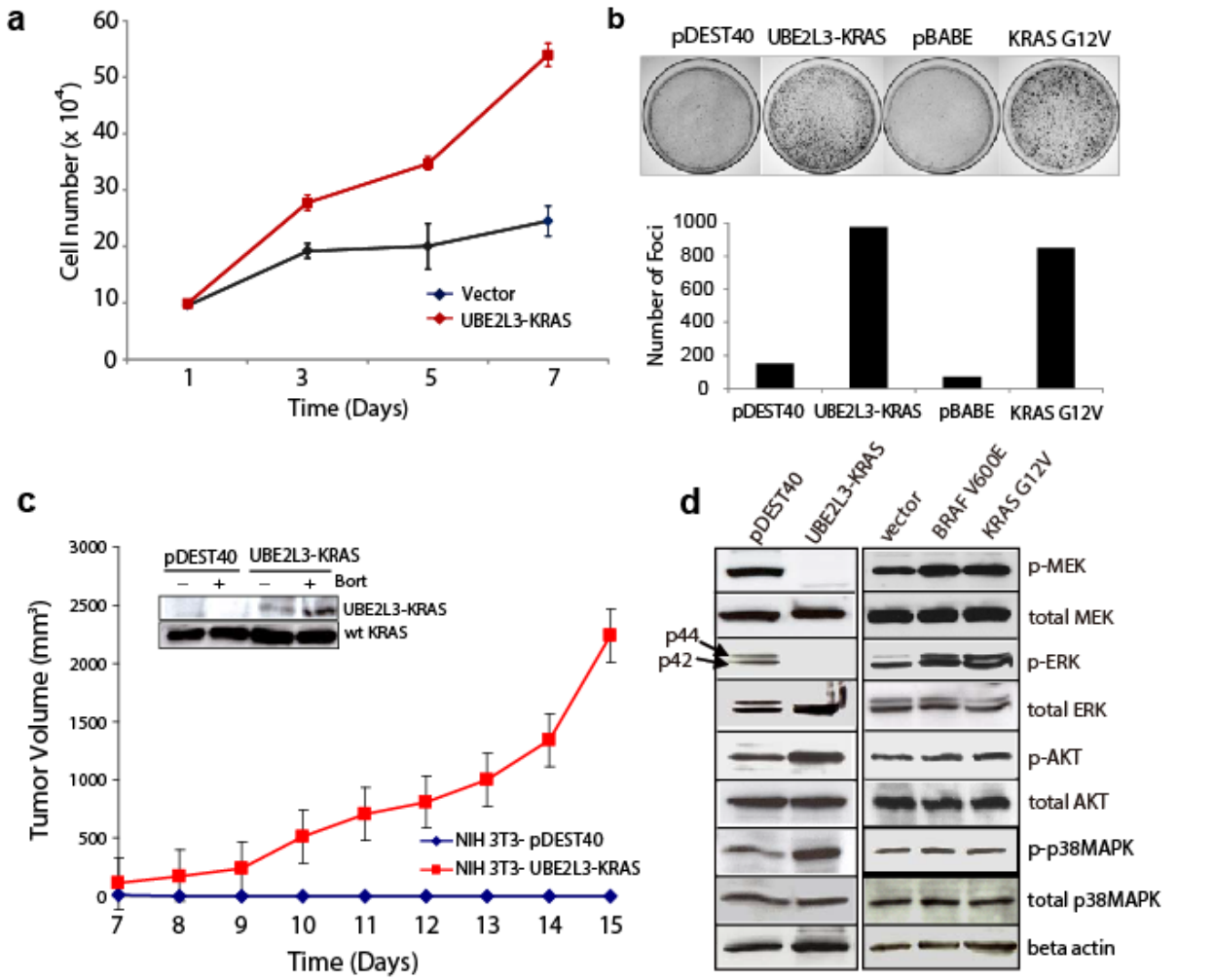

Figure 2.3. Transforming activities of the UBE2L3-KRAS fusion in NIH 3T3 cells. (a) Overexpression of UBE2L3-KRAS in NIH 3T3 cells increases cellular proliferation. pDEST40 represents an empty vector. **(b)** Overexpression of UBE2L3-KRAS induces foci formation in NIH 3T3 cells. Oncogenic KRAS G12V was used as a positive control with respective empty vectors as negative controls (pDEST40 and pBABE). Photographs of representative plates are shown in the upper panel and quantification of foci formation is shown in the bar graph of the lower panel. **(c)** The UBE2L3-KRAS transfected NIH 3T3 cells form tumors in nude mice. Stable polyclonal populations of NIH 3T3 cells expressing either the vector or UBE2L3-KRAS fusion gene were injected subcutaneously into nude mice. Tumor growth was monitored from day 7 to day 15 as indicated. The insert shows the presence of the fusion protein in the stably transfected NIH 3T3 cells which is further stabilized upon bortezomib treatment. **(d)** Investigation of the downstream signaling pathways engaged by the UBE2L3-KRAS fusion in NIH 3T3 cells. Lysates prepared from stably transfected NIH 3T3 polyclonal populations and vector controls were subject to immunoblot analysis for phospho- and total MEK, ERK, AKT and p38 MAPK. Oncogenic BRAFV600E and KRASG12V were included as controls. β-actin was used as a loading control.

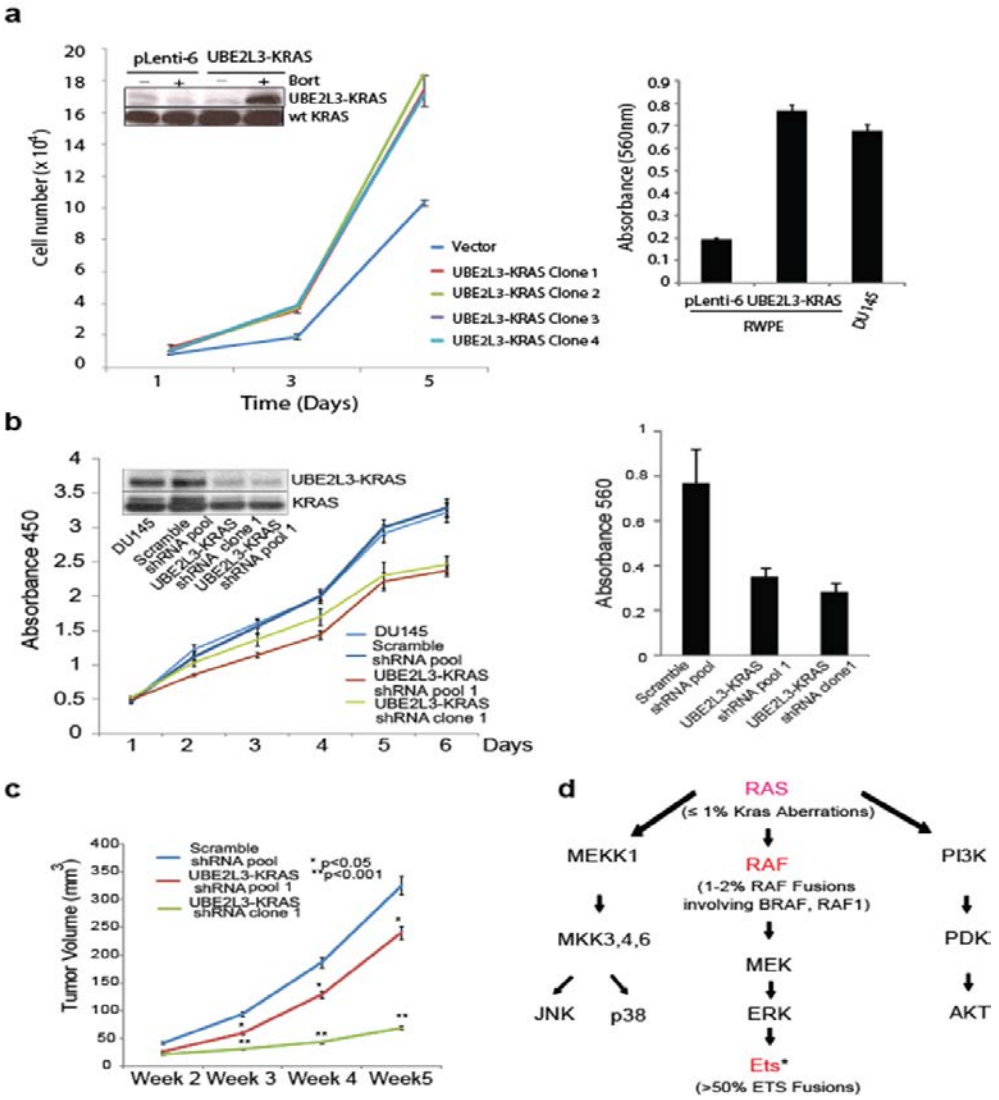

Figure 2.4. The oncogenicity of UBE2L3-KRAS fusion in the prostate context. (a) Expression of the UBE2L3-KRAS fusion in RWPE benign prostate epithelial cells leads to increased cellular proliferation and invasion. Left, the results of cell proliferation assays using stable RWPE cell clones infected with either the pLenti-6 vector or UBE2L3-KRAS. The inset shows the 33kd fusion protein detected only in the fusion transfected cells treated with bortezomib to enhance protein stability (data from a representative clone is shown (Clone 2)). Right, modified Boyden chamber-matrigel assays using the pLenti-6 vector and the fusion expressing cells (Clone 2). Invading cells were stained with crystal violet and quantitated. DU145 prostate cancer cells were used as a positive control. (**b**) Knockdown of the UBE2L3-KRAS fusion reduces cell proliferation and invasion in DU145 cells. Left, cell growth relative to the control shRNA was monitored using WST-1 assay for 6 days. Insert shows the immunoblot analysis for the 33kd fusion protein detected using Ras monoclonal antibody. Right, results of matrigel invasion assay for DU145 pool and clone with UBE2L3-KRAS knock-down. Scrambled shRNA duplexes are used as control. (**c**) Knock-down of the UBE2L3-KRAS fusion attenuates prostate tumor growth in mouse xenograft models. The figure shows a plot of mean tumor volume trajectories over time for mice inoculated with DU145 pool (red) or single clone (green) after UBE2L3-KRAS stable knock-down. Error bars represent the standard error of the mean at each time point. (**d**) A summary of RAS-RAF signaling pathways in relation to recurrent gene fusions characterized in prostate cancer. Genes that participate in fusion events are indicated in red. In parenthesis are the percentage of prostate cancers harboring aberrations in the ETS family, RAF family, and KRAS gene locus. * ETS family members involved in gene fusions include ERG, ETV1, 4, and 5. Figure adapted and modified from: Gioeli, Kraus, Weber et al, Current Clinical Oncology: Prostate Cancer.

CHAPTER 3

OUTLIER KINASES IN INDIVIDUAL CANCER SAMPLES REPRESENT PERSONALIZED THERAPEUTIC TARGETS

SUMMARY

Cancer-specific oncogene ‘dependence’ provides the basis for targeted therapeutic approaches. Protein kinases provide some of the most effective targets in personalized cancer treatment; therefore determination of tumor-specific kinase aberrations is a major objective of cancer genomic analyses. In this study, we analyzed high-throughput transcriptome sequencing data from a compendium of 485 cancer and benign samples from 25 different tissue types to delineate sample-specific ‘kinome’ expression profiles. Comparing gene expression data across different sample sets, we identified distinct ‘outlier kinases’ in individual cancer samples, defined as genes showing the highest levels of absolute *and* differential expression. In pancreatic cancer, frequent outlier kinases included therapeutic targets like MET, MST1R, AKT2, EPHA2, AXL, and PLK2, distinct from breast cancer where predominant outlier kinases included ERBB2, RET, and FGFR4 etc.. These outlier kinases were found to impart sample-specific dependencies in various cell lines tested by siRNA knockdown or therapeutic inhibition, both *in vitro* and *in vivo*. Interestingly, we observed that a subset of KRAS-dependent pancreatic cancer cell lines display outlier expression of polo-like kinases (PLKs) and show increased sensitivity to the PLK inhibitor BI6727 in combination with KRAS knockdown. Together, our results suggest that outlier kinases represent effective personalized therapeutic targets that are readily identifiable through clinical RNA-sequencing of tumors.

INTRODUCTION

The dependence of cancers on a primary driver gene known as 'oncogene addiction'[1] forms the guiding principle of targeted therapy that has had some outstanding successes, such as imatinib for BCR-ABL-positive chronic myeloid leukemia, Herceptin and lapatinib for ERBB2-positive breast cancers, gefitinib for lung cancers with kinase domain mutations in EGFR, and more recently crizotinib for lung cancers with ALK gene fusions. Evidently, protein kinases are the mainstay of a majority of the current targeted therapeutic strategies for cancers, and inhibitors of several common driver kinases such as AKT, BRAF, CDKs, KIT, RET, SRC, MAPKs, MET, PIK3CA, PLKs, AURKs, S6Ks, and VEGFR are under various stages of clinical use, trials or development [2,3]. While activating somatic mutations or amplifications are associated with some of these genes, overexpression of kinases (presumably resulting from underlying cancer genomic aberrations) is often a strong indicator of increased activity that may impart dependence on cancer cells.

Pancreatic cancer is the 4th leading cause of cancer related deaths in the U.S., with the worst prognosis (5 year survival < 3%) of all major malignancies [4], attributed to diagnosis of the disease at an advanced, unresectable stage and poor responsiveness to chemo-/ radiation-therapy [5,6]. The overarching oncogenic driver of pancreatic cancer is mutant-KRAS that has eluded therapeutic interventions [7,8], spurring the search for alternative targets [8]. The identification of distinct kinases in independent screens for synthetic lethal interactors of KRAS [9-11] led us to systematically explore potential 'personalized kinase targets' in a panel of pancreatic cancer cell lines, based on kinome expression profiling.

Next-generation sequencing of cancer transcriptomes affords a direct readout of gene expression that offers significant advantages over microarrays in terms of throughput,

eliminating probe bias, and simultaneous monitoring of diverse components of transcriptome biology [12], including gene expression [12-15], alternative splicing [16,17], chimeric/-readthrough transcripts [18,19] and non-coding transcripts [20]. Here, we set out to use transcriptome data from a compendium of 485 cancer and benign samples from 25 different tissue types to carry out gene expression profiling of the complete complement of kinases in the human genome, the kinome, to identify 'individual sample-specific outlier kinases' inspired by the concept of cancer outlier profile analysis (COPA)[21,22]. Importantly, while COPA analysis was used to identify subsets of samples displaying outlier expression of candidate genes, here we interrogated individual samples to identify outlier genes, focusing on kinases that display the highest levels of absolute expression among all the kinases in a sample *and* the highest levels of differential expression compared to the median level of expression of the respective gene(s) across the compendium. We hypothesized that such sample-specific outlier kinases may impart 'dependence' on the cells due to extremely high expression and thus potentially provide personalized therapeutic targets.

Here, we analyzed the expression profiles of breast and pancreatic cancer kinomes to identify sample-specific outlier kinases. Focusing on cell lines displaying outlier expression of kinases with available therapeutics, we tested their dependence on specific outlier kinases compared with random targets using siRNA/ small molecule inhibitors to test their effects on cell proliferation. Using this approach we identified several cell line-specific dependencies as well as kinase targets showing enhanced effects with ERBB2-inhibition in breast and KRAS-knockdown in pancreatic cancer cells.

RESULTS

Delineation of cancer specific kinome outlier profiles using transcriptome sequencing data

Taking advantage of the direct and unbiased readout of gene expression in terms of defined RNA-Seq reads, we carried out a systematic analysis of the human kinome expression in cancer. RNA-Seq-based normalized read-counts of all 468 kinases available in our transcriptome compendium, comprised of 485 samples from 25 different tissue types, revealed distinct kinases expressed at very high levels- both in absolute terms and in the context of their typical range of expression levels- in virtually all samples examined. Querying individual breast cancer samples (123 samples) for kinases that display the highest levels of absolute expression among all the kinases in an individual sample (>20 RPKM) *and* the highest levels of differential expression compared to the median level of expression of the respective gene(s) across the compendium of non-breast samples (>5 fold), we identified common outlier kinases across the cohort of breast cancer samples (**Figure 3.1A**). Thus, for example, all breast cancer cell lines known to be ERBB2-positive scored an outlier expression of ERBB2. Interestingly, many ERBB2-positive cell lines also displayed outlier expression of additional therapeutic target kinases like RPS6KB1, FGFR4, and RET, among others (**Figure 3.1A, inset; Figure 3.2**). Multiple outlier kinases in individual cancer samples could represent multiple therapeutic avenues and were thus explored further. Similarly, kinome expression data from 22 pancreatic cancer cell lines and 18 tissues revealed a set of kinases specifically overexpressed in pancreatic cancers as compared to other tissues and cell lines (**Figure 3.1B**). Assessment of outlier kinases in pancreatic and breast cancer cohorts revealed distinct outlier kinase profiles between the two diseases. For example, common outlier kinases in breast cancer included ERBB2, FGFR4, and RET, while kinases displaying outlier expression across multiple pancreatic cancer samples included EPHA2, MST1R, MET, PLK2, and AKT2. Interestingly, AXL and EGFR demonstrated outlier expression in both pancreatic and breast cancer samples.

FGFR4 as a targetable outlier kinase in ERBB2-positive breast cancer cell lines

Among the ERBB2-positive breast cancer cell lines analyzed, ZR-75-30 exhibited singular outlier kinase expression of ERBB2, whose knockdown resulted in a strong growth inhibition, while knockdown of RPS6KB1, another oncogenic kinase with potent activity in the mTOR signaling pathway, did not have any effect on the proliferation rate of ZR-75-30 cells (**Figure 3.2**). Among the additional kinases showing outlier expression in ERBB2-positive samples, FGFR4 was observed frequently**,** such as in MDA-MB-361 and MDA-MB-453 (**Figure 3.2),** as well as in MDA-MB-330, HCC202, and HCC1419. To assess the significance of FGFR4 outlier expression in the backdrop of ERBB2 overexpression, MDA-MB-361 and MDA-MB-453 cells were treated with Herceptin and or short hairpin RNA-encoding lentiviral constructs against FGFR4. In MDA-MB-361 cells, targeting ERBB2 using Herceptin had no effect on cell proliferation, while shRNA-mediated knockdown of FGFR4 impaired the growth rate of these cells significantly (**Figure 3.2**). In MDA-MB-453 cells, both Herceptin treatment and FGFR4 knockdown diminished cell proliferation rates significantly, but an even greater effect was obtained with combined treatment, demonstrating dependence on both FGFR4 and ERBB2 in this cell line.

To further examine the dependency of a subset of ERBB2-positive cells on FGFR4, we generated Herceptin-resistant sub-lines for MDA-MB-453 cells and BT474, an ERBB2-positive breast cancer cell line that does not exhibit FGFR4 outlier expression (**Figure 3.3A**). Consistent with the experiment using Herceptin combined with shRNA-mediated FGFR4 inhibition (**Figure 3.2**), MDA-MB-453 cells were found to be independently responsive to both Herceptin and PD170374, a small molecule inhibitor of FGFR, with the strongest effect on cell proliferation seen upon combined treatment with the two reagents (**Figure 3.3B, left**). Interestingly, the

MDA-MB-453 cells grown to be resistant to Herceptin, continued to display responsiveness to the FGFR inhibitor PD170374 (**Figure 3.3B, right**), suggesting that FGFR4 represents an independent therapeutic target in a subset of ERBB2-positive breast cancer cells. Similar effect was obtained using another FGFR inhibitor Dovinitib, which significantly decreased cell proliferation in both the MDA-MB-453 parental and Herceptin-resistant sub-lines (**Figure 3.3C, left**) but did not affect BT-474 parental or Herceptin-resistant sub-lines (**Figure 3.3C, right**). Taken together, these results suggest that a subset of ERBB2-positive breast cancers that display outlier expression of FGFR4 may respond to combined treatment more effectively compared to only ERBB2-directed therapy.

Pancreatic cancer cell lines are sensitive to knockdown of cell-specific outlier kinases

Extending the kinome outlier analysis to pancreatic cancer, a tumor type critically lacking in rational therapeutic targets, particularly in the realm of actionable kinases, kinome expression profiles of individual pancreatic cancer cell lines were used to identify sample-specific outlier kinases (**Figure 3.4, left**). Next, the pancreatic cancer cell lines were tested for effect on cell proliferation following siRNA-based knockdown of sample-specific outlier and non-outlier kinases. Knockdown of the sample-specific outlier kinases for example EGFR in L3.3, PLK2 in MIA-PaCa-2, MET in BxPC-3 and AKT2 in PANC-1 cells, inhibited the proliferation of respective cells, (**Figure 3.4, middle**)., A similar growth inhibition was observed following knockdown of MET in HPAC and AXL in Panc08.13 and PL45 cells. Conversely, knockdown of the non-outlier kinases AXL in L3.3 and BxPC-3 cells, MET in MIA-Paca-2, and PLK2 in PANC-1 cells did not significantly affect cell growth (**Figure 3.4, right**), as well as PLK2 in BxPC-3 and L3.3 cells -despite comparable levels of siRNA-mediated knockdown of target

genes. These observations strongly support the notion that outlier kinases represent potential therapeutic targets in individual cancer samples.

Notably, knockdown of the outlier kinase PLK2 in MIA-PaCa-2 cells did not have as profound an effect on cell proliferation as outlier kinase-targeting in many other samples. We hypothesized that this could be due to a pervasive influence of oncogenic KRAS in these cells, and therefore tested the effect of KRAS knockdown in pancreatic cancer cell lines with PLK outlier expression.

Effect of KRAS knockdown combined with PLK inhibition

The impact of KRAS knockdown in the context of PLK outlier expression in pancreatic cancer cell lines (**Figure 3.5, left**) was assessed using pooled clones of pancreatic cancer cell lines stably transduced with two different inducible shRNAs against KRAS. Following induction by doxycycline, the cells expressing KRAS-shRNAs were distinguished by red fluorescence (resulting from red fluorescent protein co-expressed with the shRNA) (**Figure 3.5**, **middle**). KRAS knockdown efficiency of 50% or more was obtained in all the cells tested. Of the cell lines tested, knockdown of KRAS significantly inhibited the proliferation of L3.3, MIA-PaCa-2, and Panc-03.27, which all harbor oncogenic mutations in KRAS and were designated as KRAS-dependent (in the context of sensitivity to KRAS knockdown) (**Figure 3.5A, right**). The BxPC-3 cells with wild type KRAS as well as HPAC and PANC-1 cells, with mutant KRAS, were not affected by KRAS knockdown and were categorized as KRAS-independent (**Figure 3.5B, right**).

Incidentally, all three PLK outlier cell lines tested here, L3.3, MIA-PaCa-2 and Panc-03.27, were found to be KRAS-dependent, based on their reduced proliferation upon KRAS

knockdown (**Figure 3.5A**). Treatment with the PLK inhibitor BI6727 alone significantly inhibited cell proliferation only those cell lines with PLK outlier expression (**Figure 3.5A, right**) but had no effect in cell lines without PLK outlier expression (**Figure 3.5B, right**). The decrease in cell proliferation following BI6727 treatment was associated with increased apoptosis, as measured by flow cytomteric analysis of Annexin V/Propidium Iodide-stained cells (Supplemental figure S2A) Further, treatment with BI6727 in combination with knockdown of KRAS enhanced the inhibition of cell proliferation in the KRAS-dependent, PLK outlier cells (**Figure 3.5A, right**) but had no effect in the KRAS-independent cells without PLK outlier expression (**Figure 3.5B, right**). Investigating the likely reason for intriguing lack of sensitivity to KRAS knockdown in a subset of pancreatic cancer cells harboring oncogenic KRAS, we observed that following KRAS knockdown, the levels of phospho-ERK, one of the major effector proteins in the RAS signaling pathway, were reduced in the KRAS-dependent cell lines L3.3 and MIA-PaCa-2 but not in the KRAS-independent cell line PANC-1, in which kinase activity was likely sustained by other outlier kinases. Interestingly, the KRAS-independent cell lines BxPC-3 and PANC-1 did respond to inhibition of their respective outlier kinases, both *in vitro* (**Figure 3.4, middle**) as well as *in vivo*, described below.

XL184 treatment in BxPC-3 and PANC-1 pancreatic cancer xenografts

To test the effect of inhibiting sample-specific outlier kinases *in vivo*, we examined tumor xenografts of the KRAS-independent pancreatic cancer cell lines BxPC-3 and PANC-1 established in NOD/SCID mice, treated with the MET inhibitor XL184. As predicted, growth of BxPC-3 cells, which display outlier expression of MET, was significantly inhibited, as measured by tumor volume and weight (**Figure 3.6A-C**). However, growth of PANC-1 cells, which do not harbor MET outlier expression, was also significantly inhibited.

As PANC-1 displays significant outlier expression of and dependence on AKT2 (**Figure 3.4**), we queried whether the profound inhibitory effect of XL184 on PANC-1 *in vivo* was mediated by non-specific targeting of AKT2. Western blot analysis of PANC-1 xenograft tumor lysates revealed markedly decreased phospho-AKT expression after XL184 treatment (**Figure 3.6D**). This suggests that XL184 suppresses PANC-1 proliferation through inhibition of AKT signaling. Importantly, there was no difference in body weight between treated and untreated BxPC-3 and PANC-1 xenografts, demonstrating that XL184 had no significant *in vivo* toxicity.

DISCUSSION

The advent of high-throughput sequencing enables a comprehensive characterization of the genomic and transcriptomic landscape of individual cancer samples, inexorably leading to the challenge of defining and prioritizing clinically relevant findings to translate into improved diagnostic and therapeutic options [23,24]. Clinical sequencing of cancers aims to identify actionable genomic aberrations and match patients with available therapies. Protein kinases, being central to biological and disease processes, including cancer, and being therapeutically targetable, comprise a large proportion of available and potential targets; thus any novel disease-specific kinase aberrations are of great clinical interest. This study proposes and tests the hypothesis that specific kinases showing outlier expression in individual cancer samples impart 'dependence' on the cells, which may be targeted in combination with existing treatment modalities. Importantly, a case is made for considering the entire profile of kinome aberrations to prioritize potentially effective targets.

The ‘sample-centric’ analysis of kinome expression revealed unique profiles of outlier kinases that were tested for dependency. Importantly, this approach uncovers multiple potent targets in an unbiased manner. For example, the well-known ‘ERBB2-positive’ breast cancer cell lines MDA-MB-361 and MDA-MB-453 were found to display outlier expression of the additional therapeutic target FGFR4. Notably, a subset of ERBB2-positive primary breast cancer tissues was found to display outlier expression of FGFR4 in Oncomine (data not shown). Targeting outlier FGFR4 in ERBB2-positive breast cancer samples was found to confer independent as well as additive effects upon their combined knockdown (**Figure 3.2**), highlighting the potential of combining two or more therapeutic targets in treating cancer, even in cases with a predominant driver such as ERBB2. Interestingly, we also showed that even after the ERBB2-positive cell line MDA-MB-453 becomes resistant to Herceptin treatment, cell proliferation still remained dependent on FGFR4 and responded to FGFR inhibitors (**Figure 3.3**). Our results suggest that the ERBB2-positive breast cancers may be partly dependent on additional drivers, such as FGFR4, RET, EGFR, and MET, which may sustain these cancers despite elimination of ERBB2 activity. Another important corollary to our observations is that combinatorial targeting of ERBB2 and additional outlier kinases at the outset may be much more effective than approaching one target at a time. Further, each cancer sample needs to be investigated individually to rationally determine patient-specific target combinations.

Next, we extended the approach of nominating sample-specific outlier kinases to pancreatic cancer, which is characterized by a bleak prognosis due to presentation at an advanced stage and resistance to tradiational chemoradiation therapy in the setting of its pancreatic cancer sanctuary, encompassing tumor stroma, extracellular matrix, tumor infiltrating immune cells, and cancer stem cells. Given the paucity of effective targets in pancreatic cancer, the strong response

of pancreatic cancer cell lines to knockdown/inhibition of *a priori* designated outlier kinases is a promising lead. Our results also underscore the importance of matching sample-specific actionable targets with the appropriate therapeutics. For example targeting MET was found to be more effective in pancreatic cancer cell lines with MET outlier expression compared to non-outlier samples. Notably, many of our experimental results are consistent with several anecdotal studies using kinase inhibitors against EGFR, MET and AKT2 [25-29]. Considering the outlier kinases in pancreatic cancer in the context of the predominant oncogenic KRAS mutation, our results suggest that subsets of KRAS-dependent cells are significantly affected upon combined inhibition of KRAS and the PLK outlier kinases. Previously Luo et al, demonstrated a synthetic lethal interaction between mutant KRAS and PLK in lung and colorectal cancer cell lines [9]. Further, successful demonstration of the dependence of pancreatic cancer cells on outlier kinases in an *in vivo* setting provides a platform to carry out pre-clinical investigations of primary human tumors in mouse 'avatars' with unique outlier kinase profiles. Overall, our study provides a metric to define and prioritize personalized target spectra specific to individual tumors.

MATERIALS AND METHODS

Kinome analysis

Transcriptome sequencing data from 485 cancer and benign samples from 25 different tissue types previously generated on Illumina GA and GAII platforms, was mapped using Bowtie [30] against UCSC genes in hg18 human genome assembly (http://genome.ucsc.edu). Unique best match hit sequences normalized for the number of reads per kb transcript per million total reads in the given sequencing run (RPKM) [13] were used to generate gene expression data matrix for the

entire compendium [31]. The expression data for the complete list of kinase genes [32] was used to identify 'outlier kinases' in individual samples based on their absolute expression (>20 RPKM) within the sample *and* differential expression (>5 fold) across the compendium, as well as separately for breast and pancreatic cancer samples.

Cell culture

All human breast and pancreatic cancer and benign epithelial cell lines were procured from the American Type Culture Collection (ATCC), except the benign immortalized pancreatic epithelial cell line HPDE provided by Dr. Diane Simeone and the pancreatic adenocarcinoma cell line L3.3 obtained from the University of Texas MD Anderson Characterized Cell Line Core (Houston, TX). All cell lines were grown in recommended culture media and maintained at 37°C in 5% CO_2. To ensure cellular identities, a panel of cell lines was genotyped at the University of Michigan Sequencing Core using Profiler Plus (Applied Biosystem) and compared with the short-tandem repeat (STR) profiles of respective cell lines available in the STR Profile Database (ATCC).

Transcript knockdowns and cell proliferation assays

ON-TARGETplus siRNA against AKT2, AXL, EGFR, MET, PLK2, and non-targeted control (siNTC) from Dharmacon were used at 100nM. Cells were transfected in 6-well plates at a density of 50,000 cells per well using Oligofectamine (Invitrogen), as per the manufacturer's protocol. Transfection was repeated 24 hours later, the cells grown for an additional 48 hours, and the cells replated at a density of 5,000 cells per well in 24-well plates. Cells were counted over a period of 1 to 6 days using Beckman Coulter cell counter (Beckman Coulter).

Transient transductions with shRNA against ERBB2, RPS6KB1, FGFR4, or non-targeted control (shNTC) were carried out in 6-well plates in the presence of 8ug/mL Polybrene (Sigma). For Herceptin (Trastuzumab; Roche) experiments, cells were grown for 3 days in 24-well plates with and without Herceptin (100ug/mL), in combination with FGFR inhibitors PD173074 (TOCRIS Bioscience) at 1uM or TKI-258 (Dovitinib; Selleck Chemicals) at 0.1 uM.

Herceptin-resistant cell lines were generated from MDA-MB-453 and BT-474 by maintaining the cells in the continuous presence of 100ug/mL Herceptin over 1 month. Cell proliferation assays were carried out over a period of 1 to 7 days using Beckman Coulter cell counter and growth curves were plotted using GraphPadPrism software. Standard deviation was calculated by one-way ANOVA.

Generation of stable cell lines with doxycycline-inducible KRAS-shRNA lentiviral constructs

Doxycycline-inducible shRNAmir-TRIPZ lentiviral constructs targeting KRAS or non-targeted control (Open Biosystems) were used to transduce a panel of pancreatic cell lines in the presence of 8µg/mL Polybrene. Constructs were marked by red fluorescence protein (RFP) expression. Forty-eight hours post-transduction, cells were selected in medium containing 1µg/mL puromycin (Invitrogen) for 4 days. shRNA expression was induced by growing cells in medium containing 1µg/mL doxycycline (Sigma) for 72 hours. The enrichment of stable cells and efficiency of shRNA induction were assessed by measuring the percentage of cells displaying red fluorescence by flow cytometry (FACSAria Cell Sorter BD Biosciences). Experiments with stable cell lines were performed in the presence of 1µg/mL doxycycline, refreshed daily. Experiments with the PLK inhibitor BI6727 (Volasertib; Selleck Chemicals) were carried out

with cells plated in 96-well culture plates at a density of 3000- 4000 cells/well and treated with 10nM BI6727 or DMSO. This concentration was selected based on IC_{50} values calculated from prior proliferation assays using 1-500nM BI6727 (data not shown). At 0, 1, 3, and 5 days following drug treatment, viable cells were quantified using WST-1 reagent (Roche) and absorbance measured at 440nm, as per the manufacturer's protocol. Growth curves were plotted using GraphPadPrism software. Standard deviation was calculated by one-way ANOVA.

Quantitative real-time PCR assay

RNA was isolated from cell lysates by the RNeasy Micro Kit (Qiagen), and cDNA was synthesized from 1μg RNA, using SuperScript III (Invitrogen) and Random Primers (Invitrogen), as per the manufacturer's protocol. SYBR Green (Invitrogen)-based quantitative real-time PCR (qPCR) was carried out on StepOne Real Time PCR system (Applied Biosystems) using gene specific primers designed with Primer-BLAST and synthesized by IDT Technologies. QPCR data were analyzed using relative quantification method and plotted as average fold-change compared to control siRNA/shRNA treatments. GAPDH was used as an internal reference.

Apoptosis assay

Apoptosis assay was carried out using ApoScreen Annexin V Apoptosis Kit (Southern Biotech), as per the manufacturer's protocol. Briefly, cells treated for 48 hours with DMSO or increasing concentrations of BI6727 were washed with cold PBS, suspended in cold 1X binding buffer, stained with Annexin V and Propidium Iodide (PI), and subjected to flow cytometry by FACSAria Cell Sorter (BD Biosciences). Results were analyzed and plotted using Summit 6.0 Software (Beckman Coulter).

Western blot

10μg cell or tissue lysates were separated on 4-12% SDS polyacrylamide gels (Novex) and blotted on PVDF membranes (Amersham) by semi-dry transfer. Antibodies to phospho-AKT, total AKT, phosho-ERK, and total ERK (Cell Signaling) were used at 1:1000 dilutions for standard immunoblotting and detection by enhanced chemiluminescence (ECL Prime), as per the manufacturer's protocol.

***In Vivo* Tumorigenicity Studies**

Six-week-old male NOD/SCID mice (Taconic) were housed under pathogen-free conditions approved by the American Association for Accreditation of Laboratory Animal Care in accordance with current regulations and standards of the US Department of Agriculture and Department of Health and Human Services. Animal experiments were approved by the University of Michigan Animal Care and Use Committee and performed in accordance with established guidelines. Mice anesthetized with an intra-peritoneal injection of xylazine (9 mg/kg) and ketamine (100 mg/kg) were implanted with $1x10^6$ BxPC-3 or PANC-1 cells suspended in 50 μL 1:1 mixture of Media 199 and Matrigel (BD Biosciences) injected subcutaneously into their flanks using a 30-gauge needle.

When tumors reached 0.4 mm, mice were randomized into control and treatment groups (n=8 per group). The MET inhibitor XL184 (Selleck Chemicals) was orally administered at 30mg/kg twice per week for three weeks. Tumor growth was monitored weekly. Tumor caliper

measurements were converted into tumor volumes using the formula: ½[length x $(width)^2$] mm^3 and plotted using GraphPadPrism software. Standard deviation was calculated by one-way ANOVA. At three weeks of treatment, mice were weighed and euthanized and the tumors harvested. Statistical comparisons were conducted using one-way ANOVA.

REFERENCES

1. Weinstein, I.B. & Joe, A. Oncogene addiction. *Cancer Res* **68**, 3077-3080; discussion 3080 (2008).
2. Manning, B.D. Challenges and opportunities in defining the essential cancer kinome. *Sci Signal* **2**, pe15 (2009).
3. Zhang, J., Yang, P.L. & Gray, N.S. Targeting cancer with small molecule kinase inhibitors. *Nat Rev Cancer* **9**, 28-39 (2009).
4. Maitra, A. & Hruban, R.H. Pancreatic cancer. *Annu Rev Pathol* **3**, 157-188 (2008).
5. Zanini, N., Masetti, M. & Jovine, E. The definition of locally advanced pancreatic cancer. *British journal of cancer* **102**, 1306-1307; author reply 1308 (2010).
6. Cardenes, H.R., Chiorean, E.G., Dewitt, J., Schmidt, M. & Loehrer, P. Locally advanced pancreatic cancer: current therapeutic approach. *Oncologist* **11**, 612-623 (2006).
7. Fleming, J.B., Shen, G.L., Holloway, S.E., Davis, M. & Brekken, R.A. Molecular consequences of silencing mutant K-ras in pancreatic cancer cells: justification for K-ras-directed therapy. *Mol Cancer Res* **3**, 413-423 (2005).
8. Strimpakos, A., Saif, M.W. & Syrigos, K.N. Pancreatic cancer: from molecular pathogenesis to targeted therapy. *Cancer Metastasis Rev* **27**, 495-522 (2008).
9. Luo, J., *et al.* A genome-wide RNAi screen identifies multiple synthetic lethal interactions with the Ras oncogene. *Cell* **137**, 835-848 (2009).
10. Barbie, D.A., *et al.* Systematic RNA interference reveals that oncogenic KRAS-driven cancers require TBK1. *Nature* **462**, 108-112 (2009).
11. Scholl, C., *et al.* Synthetic lethal interaction between oncogenic KRAS dependency and STK33 suppression in human cancer cells. *Cell* **137**, 821-834 (2009).
12. Wang, Z., Gerstein, M. & Snyder, M. RNA-Seq: a revolutionary tool for transcriptomics. *Nature reviews* **10**, 57-63 (2009).
13. Mortazavi, A., Williams, B.A., McCue, K., Schaeffer, L. & Wold, B. Mapping and quantifying mammalian transcriptomes by RNA-Seq. *Nat Methods* **5**, 621-628 (2008).
14. Sultan, M., *et al.* A global view of gene activity and alternative splicing by deep sequencing of the human transcriptome. *Science* **321**, 956-960 (2008).
15. Li, H., *et al.* Determination of tag density required for digital transcriptome analysis: application to an androgen-sensitive prostate cancer model. *Proc Natl Acad Sci U S A* **105**, 20179-20184 (2008).
16. Pan, Q., Shai, O., Lee, L.J., Frey, B.J. & Blencowe, B.J. Deep surveying of alternative splicing complexity in the human transcriptome by high-throughput sequencing. *Nat Genet* **40**, 1413-1415 (2008).
17. Trapnell, C., Pachter, L. & Salzberg, S.L. TopHat: discovering splice junctions with RNA-Seq. *Bioinformatics* **25**, 1105-1111 (2009).
18. Maher, C.A., *et al.* Chimeric transcript discovery by paired-end transcriptome sequencing. *Proc Natl Acad Sci U S A* **106**, 12353-12358 (2009).
19. Maher, C.A., *et al.* Transcriptome sequencing to detect gene fusions in cancer. *Nature* **458**, 97-101 (2009).
20. Morin, R., *et al.* Profiling the HeLa S3 transcriptome using randomly primed cDNA and massively parallel short-read sequencing. *Biotechniques* **45**, 81-94 (2008).

21. MacDonald, J.W. & Ghosh, D. COPA--cancer outlier profile analysis. *Bioinformatics* **22**, 2950-2951 (2006).
22. Tomlins, S.A., *et al.* Recurrent fusion of TMPRSS2 and ETS transcription factor genes in prostate cancer. *Science* **310**, 644-648 (2005).
23. Hutchinson, L. Personalized cancer medicine: era of promise and progress. *Nat Rev Clin Oncol* **8**, 121 (2011).
24. Hood, L. & Friend, S.H. Predictive, personalized, preventive, participatory (P4) cancer medicine. *Nat Rev Clin Oncol* **8**, 184-187 (2011).
25. Buck, E., *et al.* Inactivation of Akt by the epidermal growth factor receptor inhibitor erlotinib is mediated by HER-3 in pancreatic and colorectal tumor cell lines and contributes to erlotinib sensitivity. *Molecular cancer therapeutics* **5**, 2051-2059 (2006).
26. Ali, S., El-Rayes, B.F., Sarkar, F.H. & Philip, P.A. Simultaneous targeting of the epidermal growth factor receptor and cyclooxygenase-2 pathways for pancreatic cancer therapy. *Molecular cancer therapeutics* **4**, 1943-1951 (2005).
27. Morgan, M.A., *et al.* The combination of epidermal growth factor receptor inhibitors with gemcitabine and radiation in pancreatic cancer. *Clin Cancer Res* **14**, 5142-5149 (2008).
28. Cheng, J.Q., *et al.* Amplification of AKT2 in human pancreatic cells and inhibition of AKT2 expression and tumorigenicity by antisense RNA. *Proceedings of the National Academy of Sciences of the United States of America* **93**, 3636-3641 (1996).
29. Miwa, W., *et al.* Isolation of DNA sequences amplified at chromosome 19q13.1-q13.2 including the AKT2 locus in human pancreatic cancer. *Biochemical and biophysical research communications* **225**, 968-974 (1996).
30. Langmead, B. Aligning short sequencing reads with Bowtie. *Curr Protoc Bioinformatics* **Chapter 11**, Unit 11 17 (2010).
31. Kalyana-Sundaram, S., *et al.* Expressed Pseudogenes in the Transcriptional Landscape of Human Cancers. *Cell* **149**, 13 (2012).
32. Manning, G., Whyte, D.B., Martinez, R., Hunter, T. & Sudarsanam, S. The protein kinase complement of the human genome. *Science* **298**, 1912-1934 (2002).

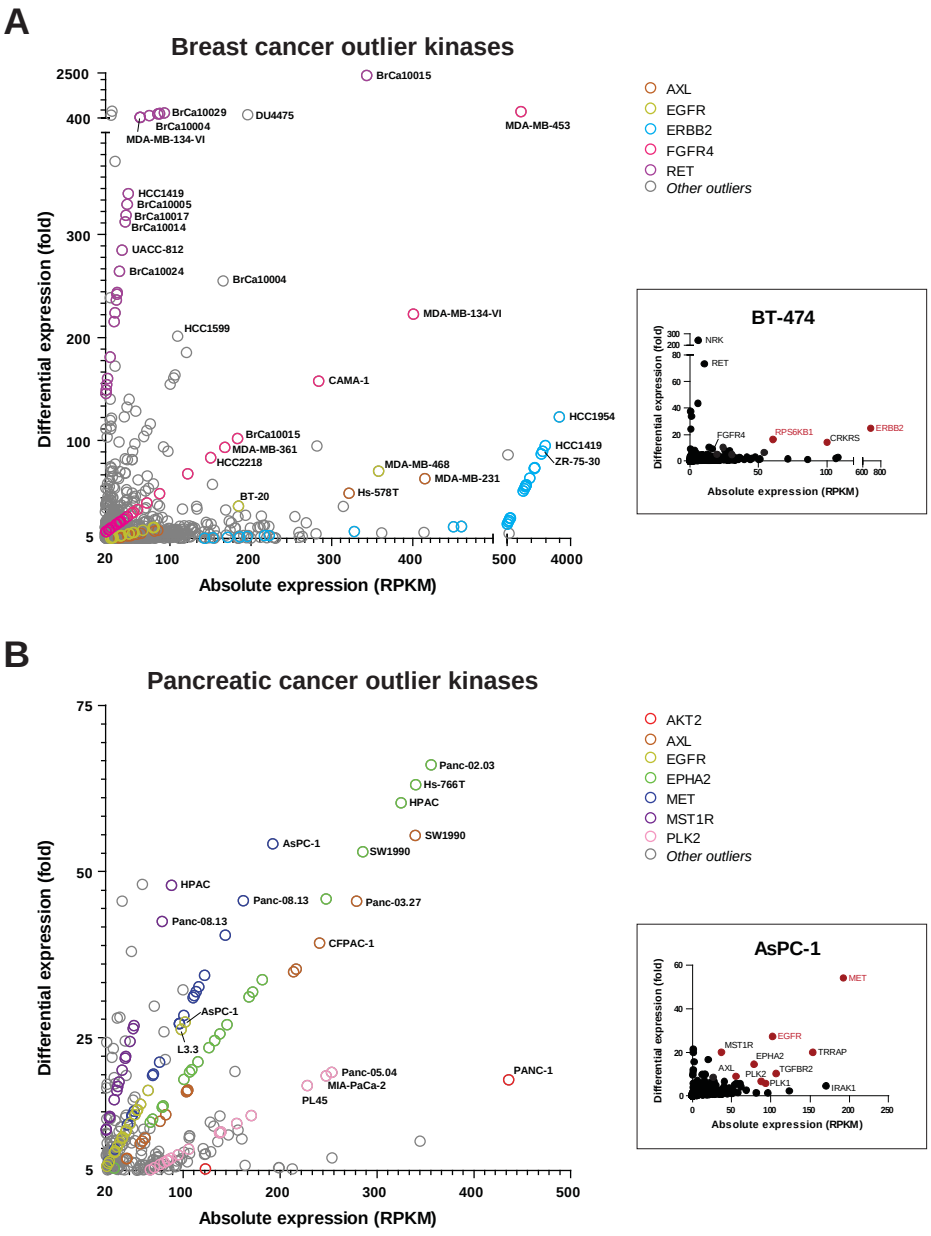

Figure 3.1: Scatter plot representation of outlier kinases in (A) breast and (B) pancreatic cancer samples. Kinases displaying an absolute expression >20 RPKM (reads per kilobase transcript per million total reads) and differential expression >5 fold (versus non-breast or non-pancreas samples, respectively) were designated as outliers. The colored circles represent salient kinases displaying outlier expression in multiple samples. Examples of sample-specific kinome profiles are shown in the insets (BT-474 breast cancer and AsPC-1 pancreatic cancer cell lines), with kinases displaying high outlier expression highlighted in red.

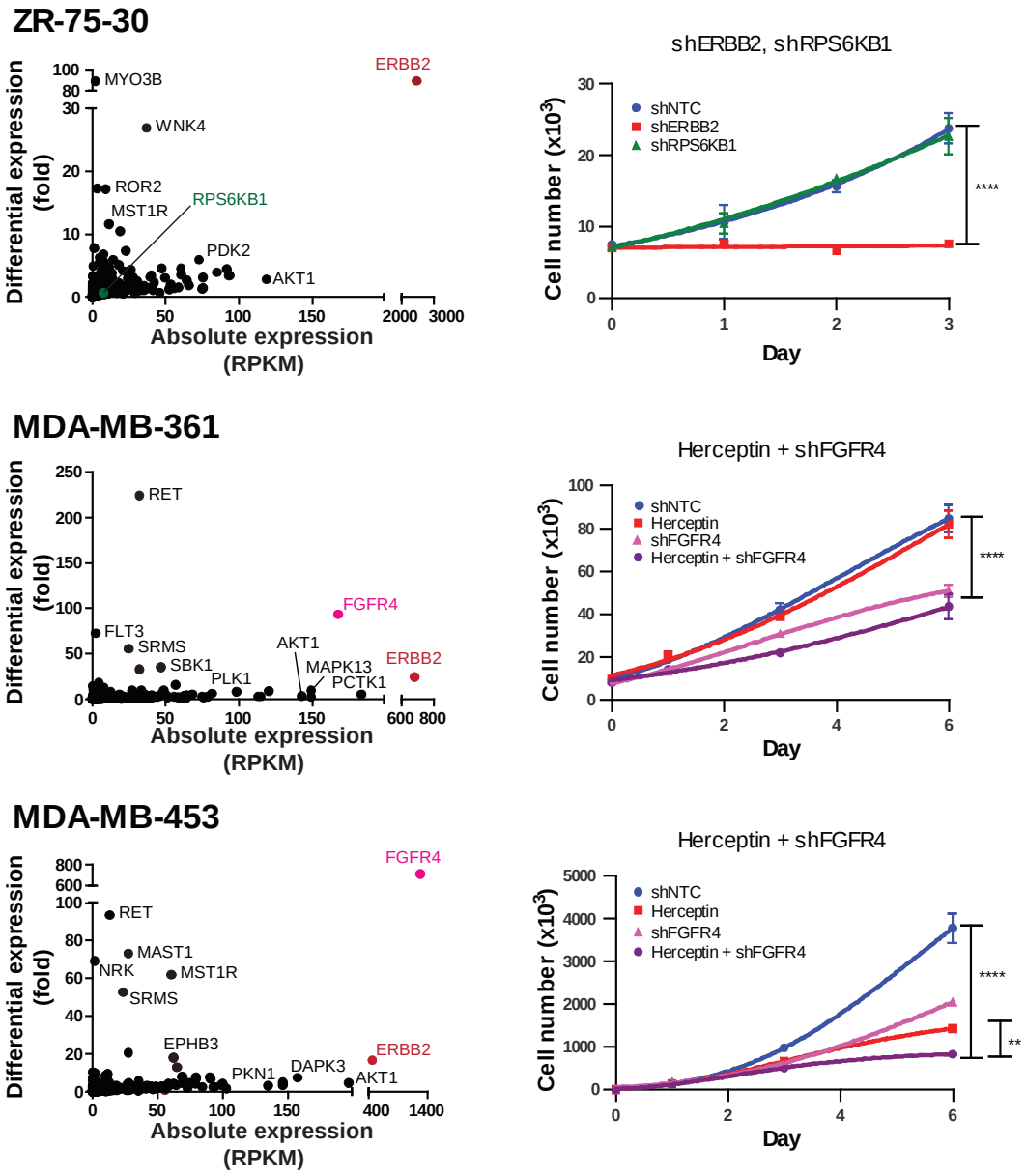

Figure 3.2: Sample-wise outlier kinases in ERBB2-positive breast cancer cell lines. (Left) The scatter plots display kinome expression profiles of individual breast cancer cell lines. Kinases targeted for knockdown are shown in color. (Right) Growth curves show the effect of targeting outlier (ERBB2) versus non-outlier (RPS6KB1) kinases in ZR-75-30 cells and the effects of Herceptin and/or knockdown of the outlier FGFR4 in MDA-MB-361 and MDA-MB-453 cells. Values represent mean ± SD. **, P<0.01; ****, P<0.0001.

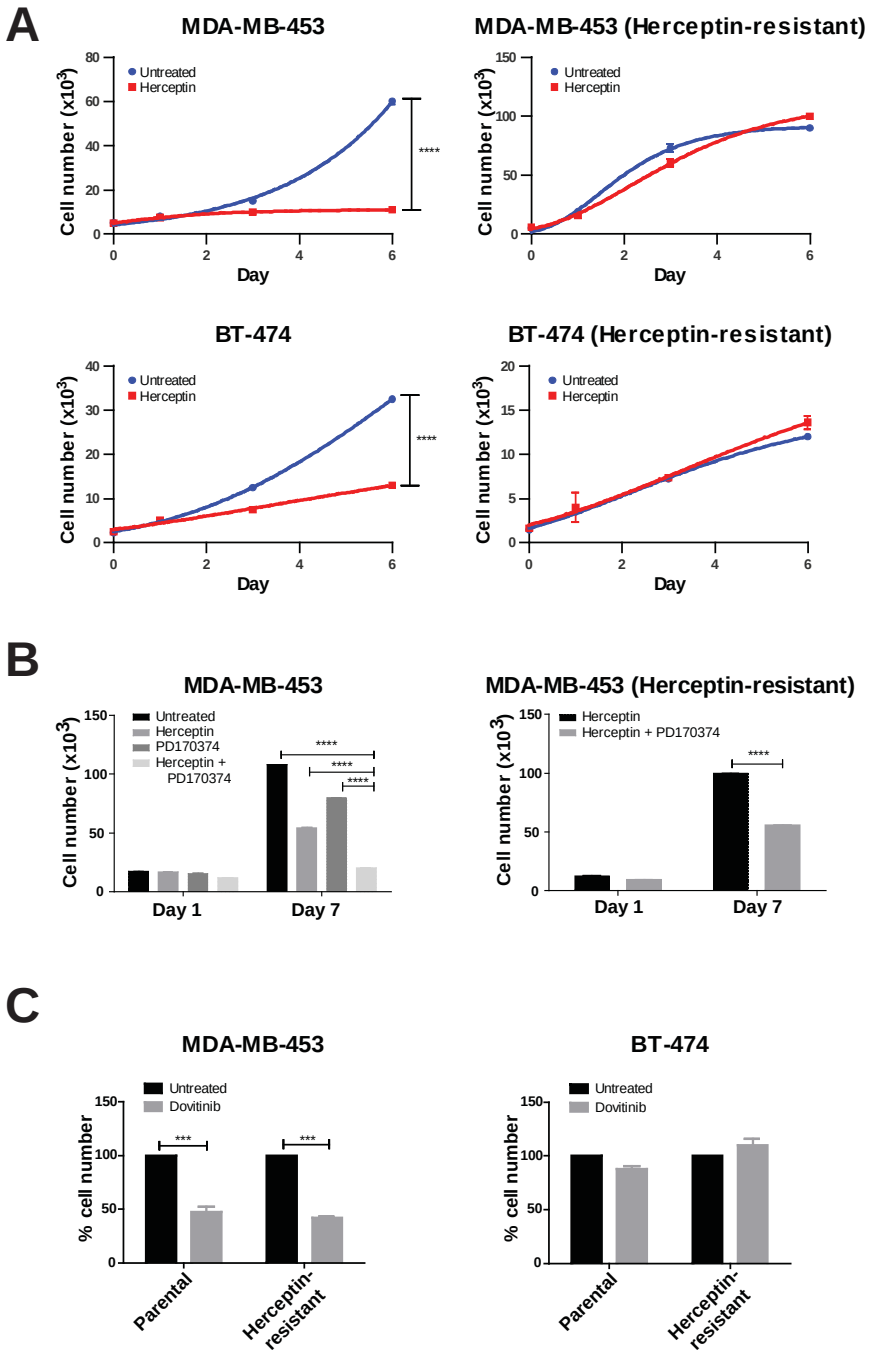

Figure 3.3. Herceptin-resistant cell lines respond to targeting of the outlier kinase FGFR4. (A) The growth curves show the effect of Herceptin treatment on MDA-MB-453 and BT-474 (left) and their Herceptin-resistant sublines (right). (B) The bar graphs demonstrate the individual and combined effects of Herceptin and the FGFR inhibitor PD170374 on cell proliferation in MDA-MB-453 (left) and its Herceptin-resistant subline (right). (C) The bar graphs display the effect of the FGFR inhibitor Dovitinib on parental and Herceptin-resistant sublines of MDA-MB-453 (with FGFR4 outlier expression) and BT-474 (without FGFR4 outlier expression). Values represent mean ± SD. ***, $P<0.001$; ****, $P<0.0001$.

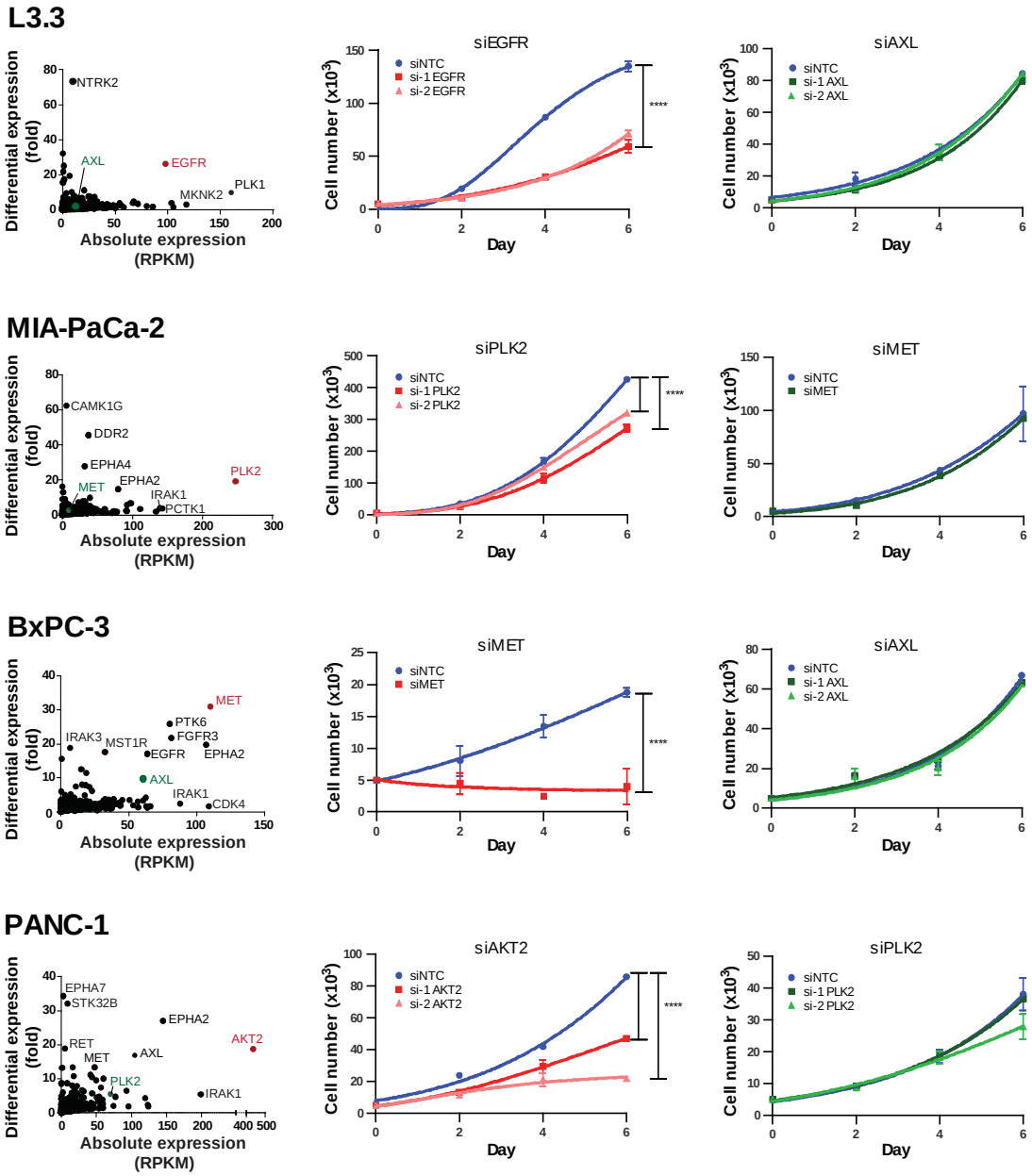

Figure 3.4. Pancreatic cancer cell lines are sensitive to knockdown of outlier kinases. Scatter plots display kinome profiles of select pancreatic cancer cell lines; kinases targeted for knockdown are shown in color (left). The growth curves display the effects of siRNA-mediated knockdown of sample-specific outliers (middle) and non-outliers (right) for each cell line. Values represent mean ± SD. ****, P<0.0001.

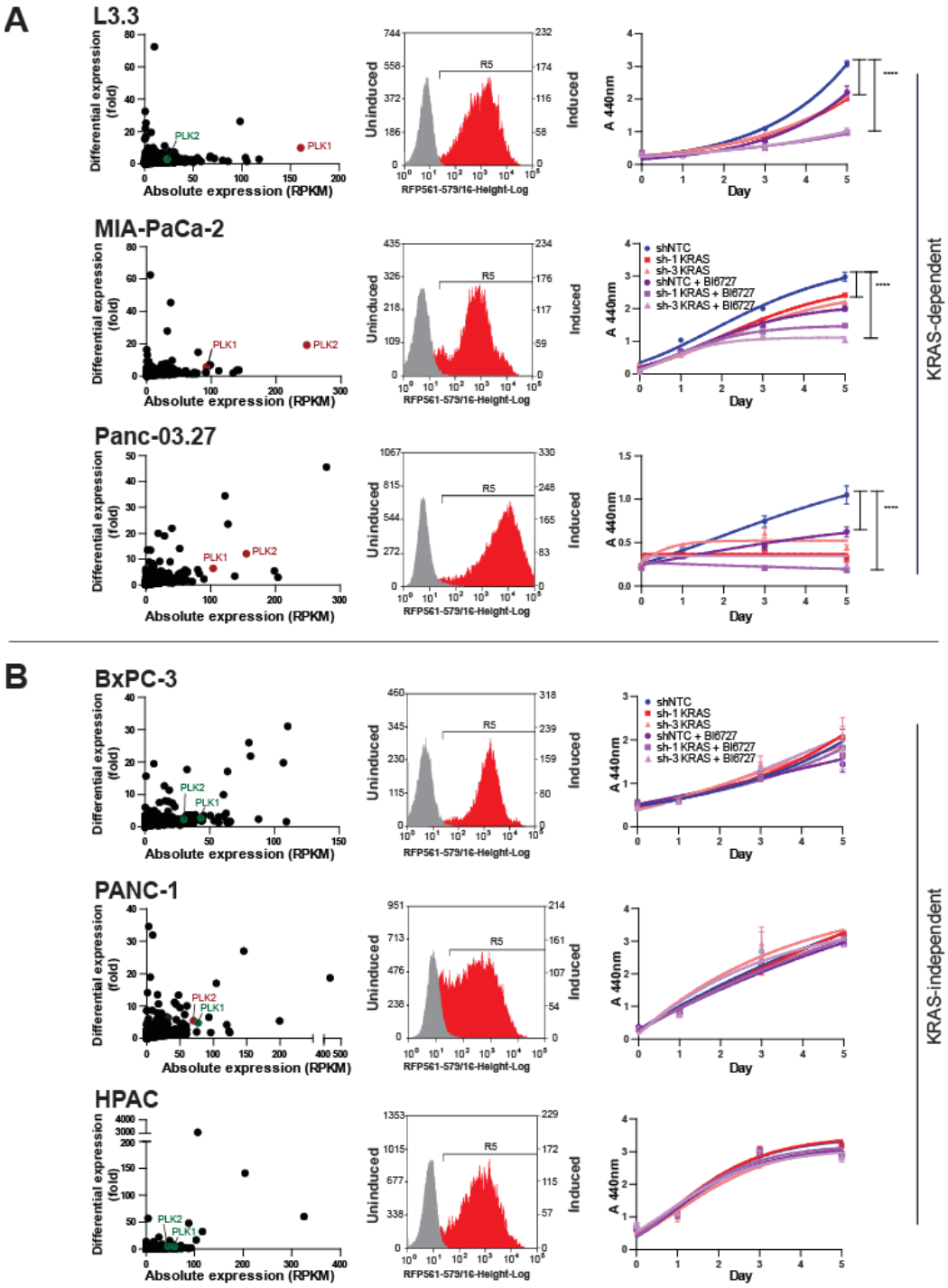

Figure 3.5. Knockdown of KRAS combined with PLK inhibition reduces cell proliferation in indicated KRAS-dependent cell lines (A) but not in KRAS-independent cell lines (B). The scatter plots demonstrate the absolute and differential expressions of PLK1/2 for each cell line (left). The flow cytometric profiles of doxycycline-induced cells expressing KRAS shRNA with RFP expression (red) versus un-induced cells (gray) are displayed (middle).The growth curves show the individual and combined effects of KRAS shRNA and the PLK inhibitor BI6727, using WST-1 assay (right). Values represent mean ± SD. ****, $P<0.0001$.

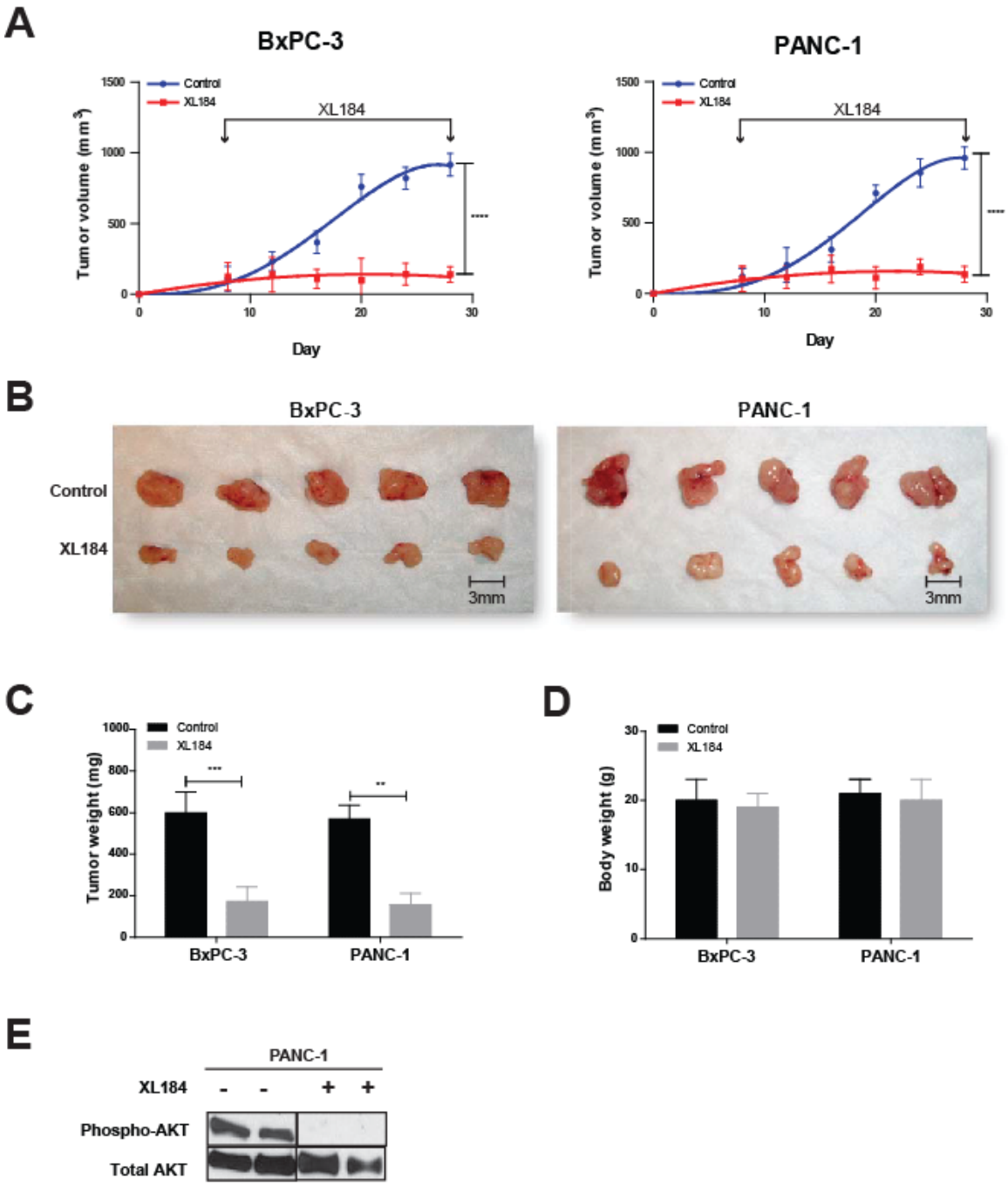

Figure 3.6. XL184 treatment suppresses tumor growth in BxPC-3 and PANC-1 pancreatic cancer xenografts. (A) The growth curves demonstrate the effect of the MET inhibitor XL184 on tumor growth in BxPC-3 and PANC-1 xenografts. (B) BxPC-3 and PANC-1 xenograft tumors after 3 weeks of XL184 treatment are shown as compared to the controls. The bar graphs display tumor weight (C) and total body weight (D) after 3 weeks of XL184 treatment. Values represent mean ± SE. **, $P<0.01$; ***, $P<0.001$; ****, $P<0.0001$. (E) The western blot shows the effect of XL184 treatment on phospho-AKT levels in PANC-1 xenografts.

CHAPTER 4

MASS SPECTROMETRIC ANALYSIS IDENTIFIES ARGONAUTE-2 AS A RAS INTERACTING PARTNER

SUMMARY

Since the discovery of *RAS* family of small GTPases over thirty years ago, targeting RAS still remains an intractable therapeutic target. To potentially expand therapeutic avenues for blocking RAS function, we explored endogenous interactors of RAS in a panel of cancer cell lines using co-immunoprecipitation mass spectrometry (co-IP MS) and discovered a specific interaction between RAS and Argonaute 2 (AGO2), a key component of RNA silencing pathways. In fractionated cell lysates, RAS protein co-sediments with AGO2 in membrane fractions, whereas *in situ* the two proteins co-localize in intracellular membrane organelles. Using antibodies that bind the Switch regions in RAS, we determined that the Switch II domain was critical for AGO2 interaction. We also demonstrate a direct, nucleotide independent binding of KRAS and AGO2 *in vitro,* using purified components, with the conserved Y64 residue as a critical amino acid. Further interaction analysis revealed that the N-terminal "wedge" domain of AGO2 (amino acids, aa 112-114) was essential for RAS binding only to the RAS Switch II domain, suggesting that unlike RAF, AGO2 is likely not a RAS effector.

INTRODUCTION

Despite extensive characterization of the RAS/GAP molecular switch (es) and downstream signaling axes, therapeutic targeting of RAS driven cancers remains elusive, suggesting potential gaps in our understanding of the spectrum of RAS mediated signaling[1-3].

RAS effectors bind RAS through the conserved Switch I and Switch II domains, and drive cellular transformation by activating downstream kinases and GTPase signaling modules. These interactors have been identified using conventional approaches of yeast two hybrid analysis[4] and ectopically expressed epitope-tagged *RAS* constructs [5,6]. Recently, we performed co-immunoprecipitation followed by mass spectrometry (co-IP MS) to analyze the endogenous interactome of oncogenic ERG in the prostate cancer cell line VCaP that harbors the TMPRSS2-ERG gene fusion, and discovered interactions with PARP and DNAPK[7]. Here, we employed a RAS antibody for a similar co-IP MS based strategy to investigate endogenous interactors of RAS in a panel of lung and pancreatic cancer cell lines representing the spectrum of *KRAS* mutation status and dependency. Surprisingly, the most prominent interacting protein, across all cell lines analyzed, was EIF2C2, commonly known as Argonaute 2 (AGO2), a key effector of the RNA silencing pathway. Recent studies have demonstrated a role for AGO2 in RAS induced senescence[8,9]. Multiple reports also showed that phosphorylation of AGO2 by MAPK/PI3K pathway activators alters its microRNA related function through different mechanisms [10-13], portending that signaling molecules may have direct effects on RNA silencing mechanisms [14]. Considering the potential functional implications of RAS-AGO2 interaction, here we corroborated and characterized this interaction in detail.

RESULTS

Endogenous interaction of RAS and AGO2

To analyze RAS-interacting proteins in an endogenous setting, we first used the pan-RAS antibody RAS10 [15], which efficiently immunoprecipitates RAS proteins by binding to the Switch I domain (amino acids, aa, 32-40) (**Figure 4.1A-C**). Co-immunoprecipitation of RAS followed by tandem mass spectrometry (RAS co-IP-MS) was performed using NIH3T3 cells ectopically overexpressing human wild-type or mutant *KRAS* and a panel of ten lung and pancreatic cancer cell lines of known *KRAS* mutation status, according to the schema in **Figure 4.1D**. As expected, the spectral counts of peptide fragments obtained through MS analyses showed robust detection of the bait protein (RAS) in all of the 12 cell lines analyzed. Intriguingly the RAS co-IP MS identified peptides spanning *EIF2C2*, commonly known as Argonaute 2 (*AGO2*), the catalytic component of the RNA-induced silencing complex (RISC) in NIH3T3 cells expressing $KRAS^{WT}$ or $KRAS^{G12V}$, as well as all of the ten cancer cell lines tested (**Figure 4.2A)**. Remarkably, only the RAS and AGO2 peptides were consistently detected in every cell line tested, with cumulative spectral counts of 576 and 253, for RAS and AGO2 peptides respectively. Analyzing the RAS co-IP MS data further, we noted that peptides mapping uniquely to KRAS, NRAS and HRAS were readily detected in most cell lines (**Figure 4.2B**). By contrast, among all AGO family proteins only AGO2 peptides were observed in all of the 12 cell lines (only one peptide uniquely mapped to AGO1 in a single sample) (**Figure 4.2B**).

The putative endogenous interaction between RAS and AGO2 was corroborated by reciprocal IPs of RAS and AGO2 using two different antibodies for each, in two different lung cancer cell lines, H358 and H460 harboring distinct *KRAS* mutations (**Figure 4.2C**). Further, consistent with the co-IP MS analyses (**Figure 4.2A**), the RAS-AGO2 interaction was readily detected by co-IP followed by immunoblot analysis in two cell lines with wild-type *KRAS* and representative lung and pancreatic cancer cells harboring various activating mutations of *KRAS*

(**Figure 4.2D**). The RAS-AGO2 interaction was robustly maintained even under a highly stringent condition of 1 M NaCl (**Figure 4.3A**). Furthermore, this interaction was unaffected in the presence of RNase (considering that AGO2 is RNA bound), suggesting that the RAS-AGO2 is not RNA-dependent (**Figure 4.3B-C**). RAS was also detected in FLAG immunoprecipitates when FLAG-tagged *AGO2* construct was expressed in HEK293 cells (**Figure 4.3D**), further corroborating the endogenous co-IP MS observations.

Colocalization of RAS and AGO2 in Membrane Organelle Fractions

RAS proteins are restricted to the plasma membrane and membranes of various intracellular organelles like the endoplasmic reticulum, Golgi, mutivesicular bodies and the mitochondria and it is generally accepted that distinct RAS localization affects signaling outputs [16,17]. On the other hand, AGO2 is known to assemble into cytoplasmic messenger ribonucleoprotein particles (mRNPs) [18]., and AGO2 is also known to function inside the nucleus [19,20]. Studies have also detected functional AGO2 complexes in organelle structures like the endoplasmic reticulum [21] , multi vesicular bodies [22] and mitochondria [23]. To investigate the cellular compartment where RAS and AGO2 could interact we performed cell fractionation analysis using H358 cells. As expected, AGO2 was detected in the cytoplasm, slightly enriched in the membrane/organelle fraction and within the nucleus (**Figure 4.4A**). The RAS10 antibody detected RAS only in the membrane/organelle enriched fraction, indicating that RAS and AGO2 may reside in intracellular organellar structures. Further, AGO2 is also known to form low to high molecular weight complexes depending on its association with RNA [18]. Similar sucrose density sedimentation analysis of H358 cells showed the presence of total RAS as well as KRAS predominantly in smaller molecular weight fractions (Complex I) with AGO2 and AGO1

(**Figure 4.4B**). To demonstrate endogenous RAS and AGO2 co-localization using immunofluorescence, we used RAS10 antibody for immunostaining in H358 (*KRAS*^{G12C}) cells **(Figure 4.5A**) and determined the specificity of the RAS10 Ab staining using RAS peptides recognized by the antibody prior to immunostaining. As seen in **Figure 4.5B**, the immunostaining by RAS10 was abrogated upon pre-incubation with a RAS peptide that spans the RAS10 Ab epitope in the Switch I effector domain (aa 30-39) (**right**) but not by a RAS peptide spanning aa 34-43 (**left**). To validate the specificity of AGO2 antibodies for immunofluorescence analyses, we performed AGO2 immunofluorescence in mouse embryonic fibroblast (MEFs) with homozygous knockout of AGO2 (*AGO2*-/- MEF) and in *AGO2*-/- MEF cells expressing *AGO2* (*AGO2*-/- MEF +*AGO2*). As expected, AGO2 was detected only in MEF *AGO2*-/- +*AGO2* cells **(Figure 4.5C),** mostly in the intracellular fraction and weaker nuclear staining. Using these experimentally validated, highly specific antibodies, we performed co-localization analyses for RAS and AGO2 in two independent lung cancer cell lines, H358 (*KRAS*^{G12C}) and H1793 (*KRAS*^{WT}) (**Figure 4.5C-D**) and observed a significant overlap in the immunofluorescence signals localized within intracellular organelles. The acquired images were analyzed using ImageJ software (version 1.41) and as a measure of co-localization, Manders coefficient was used to evaluate the overlap in fluorescence [24]. The Manders co-efficient for RAS and AGO2 was assessed as 0.4 and 0.6 in H358 and H1793 cells respectively (a value of 0.99 is considered as complete overlap while 0 or below signifies no overlap). Together these data suggests that a considerable fraction of RAS and AGO2 co-localize in intracellular organelles.

AGO2 binds RAS through the wedge domain within its N-terminus

Next, to identify specific region(s) in AGO2 involved in the interaction with RAS, a panel of FLAG-epitope tagged AGO2 expression constructs (summarized in the schematic in **Figure 4.6A**) was employed. RAS co-IP analysis of the FLAG tagged AGO2 deletion constructs showed that the N-terminal domain of AGO2 was necessary (**Figure 4.6B**) and sufficient (**Figure 4.6C**) for RAS binding. Further analysis of a panel of deletion constructs spanning the N-terminal domain suggested that the region spanning 50-139 amino acids was critical for RAS binding (**Figure 4.7A**). Interestingly, this stretch of amino acids was recently shown to be part of the so called "wedging" domain, important for microRNA duplex unwinding prior to RISC assembly [25]. To further define AGO2 residues critical for interaction with RAS, we focused on amino acid residues within the aa 50-139 stretch that are unique to AGO2 (as compared to AGO1, 3 and 4), considering that amongst the Argonaute family proteins, AGO2 was almost singularly represented in the RAS co-IP MS data. ClustalW alignment of all human Argonaute proteins (AGO1-4) was used to identify the amino acid residues that are unique to AGO2 in the wedging domain (**Figure 4.7B**). Alanine substitution of each of the 10 residues unique to AGO2 within the aa 50-139 stretch was followed by RAS co-IP analysis, and amino acids K112 and E114 of AGO2 were found to be critical for a direct association with RAS (**Figure 4.7C**).

Y64 residue within the Switch II domain of RAS is critical for direct AGO2 binding

In parallel analyses aiming to define the residues in RAS that are critical for AGO2 association, we first employed the two antibodies that exclusively bind to the Switch I (RAS10 mAb) or the Switch II (Y13-259) domains in RAS (summarized in **Figure 4.8A**). Using H358 cell lysates for RAS IP we observed that in contrast to the Switch I specific RAS10 Ab, the Switch II specific

Y13-259 Ab failed to co-immunoprecipitate AGO2 (**Figure 4.8B**), strongly suggesting that the Switch II domain in RAS may be critical for AGO2 interaction.

Next, we sought to determine the specific residues in the RAS Switch II region involved in its interaction with AGO2, using *in vitro* co-IP analyses with a panel of mutations flanking the Y64 residue in the switch domain, known to be important for interactions with multiple effector/regulator proteins. First to validate the *in vitro* co-IP assay, purified recombinant KRASG12V or KRASWT proteins incubated with varying concentrations of AGO2 protein, followed by RAS immunoprecipitation showed a concentration dependent, direct interaction between recombinant AGO2 and RAS proteins (**Figure 4.8C**). Next, co-IP of recombinant AGO2 protein with the panel of Switch II mutant RAS proteins including and flanking the Y64 residue, showed that altering the Y64 residue (but not the adjoining amino acids) significantly reduced KRAS binding to AGO2 **(Figure 4.8D**).

To assess if GDP/GTP loading of KRAS may influence AGO2 interaction *in vitro*, we also carried out *in vitro* co-IP analyses using KRASWT and KRASG12V proteins loaded with GDP/GTPγS, and as seen in **Figure 4.9A**, AGO2 binding was seen to be independent of nucleotide loading on KRAS. To further substantiate this observation, and to obviate potential technical concerns inherent in antibody based co-IP, we carried out an antibody-independent pull down assay using His-tagged AGO2 protein bound to Co-NTA beads. Similar to the antibody based assay, both the KRASWT and KRASG12V proteins were observed to bind to His-tagged AGO2, independent of the nucleotide loading on KRAS (**Figure 4.9B**). To validate the efficiency and specificity of nucleotide loading onto KRAS in our experiments, we performed RAF-RBD pull down assays and observed the expected differential between GDP and GTP bound KRAS with respect to RAF-RBD binding (**Figure 4.9C)**. Also, consistent with the *in vitro*

co-IP analyses, the His-tagged AGO2 pull down assay also showed specific dependency of AGO2-RAS binding on the Y64 residue **(Figure 4.9D)**. Thus, these data define the amino acids in RAS (Y64) and AGO2 (K112/E114) as critical for the RAS-AGO2 interaction.

Lastly, we reasoned that if the RAS-AGO2 interaction is limited to Switch II domain we may be able to detect AGO2 in the RAS-GTP complexed with RAF on RAS binding domain of RAF (RBD) agarose beads which only involves the Switch I domain. As expected, we were able to detect AGO2 on RAS-GTP bound to RBD-agarose in H358 ($KRAS^{G12C}$) cells (**Figure 4.9E**), further suggesting that AGO2 binds through the Switch II domain with no involvement of the effector domain.

DISCUSSION

RAS, one of the earliest proto-oncogenes identified [26], has emerged as one of the most prevalent cancer aberrations with extensively characterized oncogenic driver functions[22,46-49], that remains a pertinent but as yet an unsuccessful therapeutic target. In recent years, there is a renewed interest in targeting RAS to alter its status from undruggable to druggable [3,27-30]. In this context, discovery of novel endogenous interactors of RAS could potentially advance our understanding of RAS biology as well as provide novel therapeutic avenues.

In this study, we identify a novel interaction of RAS with AGO2, a key mediator of RNA-based gene silencing[31-33]. The RAS-AGO2 interaction is independent of the mutation status of RAS (and thus, to GDP/GTP loading status *in vitro*), the two proteins co-localize in intracellular membrane organelles, sites that are known for RAS trafficking and AGO2 activity. The RAS-AGO2 interaction involves the Switch II domain of RAS (particularly the Y64 residue), and the N-terminal Wedge domain of AGO2 (K112-E114 residues).

Our study focused on analyzing endogenous interactors of RAS, common across a panel of cancer cells spanning the spectrum of KRAS mutation profiles. To the best of our knowledge, this is the first study using endogenous RAS as bait for mass spectrometric analyses; previous co-IP MS analyses used N-terminal epitope-tagged-*HRAS*, -*MRAS*, or -*RRAS* ectopically expressed in NIH3T3 cells [5,6]. Studies using tagged AGO2 as bait for mass spectrometry have also been reported[34,35], and as a 25kDa cutoff was employed for analyses, may have missed the detection of the 21 kDa RAS protein. In our study, the pull-down of AGO2 using multiple independent antibodies, consistently co-precipitated RAS (**Figure 4.2D**) and we found that this interaction is direct, as assessed using purified components (**Figures 4.8-4.9**). Endogenously, the RAS-AGO2 interaction is readily detected in both cancer and benign cells, independent of *RAS* mutation status (**Figure 4.2E**), together suggesting a more general role for this interaction in the cell.

Since the RAS-AGO2 interaction is restricted to the intracellular membrane bound organelles, we believe that the endogenous RAS interacts with AGO2 within membranous organelles, before it reaches the plasma membrane. While effector binding of activated RAS is extensively studied and restricted to the plasma membrane, the function of RAS in other organelles remains unappreciated. Since both RAS[16] and AGO2[23] associate with different proteins depending on their location in the cell, compartmentalized association of the two molecules could therefore have an effect both on RAS signaling and AGO2 silencing mechanisms.

The N-terminal domain represents the most distinct region in the highly conserved AGO protein family, that regulates the endonucleolytic activity unique to AGO2 [36]. Interestingly, the RAS interaction observed with AGO2, involves residues in the N-terminal, unique to AGO2. A

recent report [25] suggests that the region we identified in AGO2 as critical for RAS binding (i.e., the 'wedge domain'), is important for small RNA duplex unwinding, a prerequisite for RISC assembly. It is possible that mutant KRAS interaction directly involving the residues in the wedge domain attenuates AGO2 function through its effect on RISC assembly. Furthermore, AGO2 as a preferred RISC component among AGO family members suggests that unique properties of AGO2 such as endonucleolytic activity [37] and its ability to bind open reading frames of mRNA transcripts [38] may play an important role during oncogenic stress.

MATERIALS AND METHODS

Cell lines, specimen collection and DNA constructs

Lung and pancreatic cancer cell lines were purchased from the American Type Culture Collection (ATCC). No further testing for Mycoplasma was performed in the lab. PDX1319 cells were obtained through the Xenograft Core, University of Michigan, directed by Dr. Diane Simeone, University of Michigan, Ann Arbor. Cells were grown in specified media supplemented with 10% fetal bovine serum and antibiotics (Invitrogen).

Coimmunoprecipitation and Tandem Mass Spectrometric analysis

Methods used for immunoprecipitation with RAS/control IgG followed by Tandem Mass Spectrometric analysis and database searching are schematically outlined in. Clustal W analysis was performed using the online program, http://www.ebi.ac.uk/Tools/services/web/toolform.ebi?tool=clustalo with peptide sequences obtained from RAS co-IP MS analysis of H358 lung cancer cells.

Immunoprecipitation (IP) and Western blot Analysis

Fresh protein extracts were prepared by lysis of cells in K buffer (10mM Tris HCl, 0.1%, 150mM NaCl, 1% Triton X100 and protease inhibitors). After brief sonication, debris were removed by centrifugation. For IP, 50-400 µg of lysates were pre-cleared with Protein A/G agarose beads (Pierce) for 1 hour and treated overnight at 4^0C with 1-10 µg of control or specific antibody as indicated. The immune complexes were then precipitated with Protein A/G agarose beads, washed with K buffer and resuspended in sample loading buffer. RAS10 monoclonal antibody immunoprecipitates were routinely washed at 500mM NaCl for increased stringency and a final wash was carried out with buffer containing 150mM NaCl prior to SDS-PAGE analysis. RNase/DNase treatments of lysates were performed prior to pre-clearing of lysates followed by IP. After SDS-PAGE separation, proteins were transferred onto nitrocellulose membranes for immunoblot analysis. For IP using FLAG tagged constructs, FLAG M2 agarose beads (Sigma) were used as per manufacturers' protocol.

Sucrose Density Co-sedimentation analysis

Sucrose gradient fractionation was performed as described earlier[18]. Briefly, cells were lysed in buffer containing 25 mM Tris–HCl (pH 7.4), 150 mM KCl, 0.5% NP-40, 2 mM EDTA, 1 mM NaF, 0.5 mM dithiothreitol and protease inhibitors (Roche) and centrifuged at 10,000*g* for 10 min at 4°C. For fractionations, gradients from 15% (w/v) to 55% (w/v) sucrose in 150 mM KCl, 25 mM Tris (pH 7.4) and 2 mM EDTA were used. Lysates were separated by centrifugation at 30,000 r.p.m. for 18 h in an SW41 rotor at 4°C. For each lysate 22 fractions of 0.5ml each were collected, 45ul of which was used for immunoblot analysis.

***KRAS* and *AGO2* plasmid constructs**

Full length FH-*AGO2* and mutant $KRAS^{G12V}$ constructs were obtained from Addgene (pIRESneo-FLAG/HA-*AGO2* corrected plasmid 10822, PI:Thomas Tuschl; FLAG-*AGO2* plasmid 21538:

PI: Edward Chan and plasmid 12544 PI: Channing Der). Deletion constructs of *AGO2* spanning different domains (indicated in the figures) were subcloned as FLAG-tagged expression plasmids in pDEST40 (Life Technologies) vector backbone. Site directed mutagenesis was performed on *AGO2* encoded plasmid 10822 to obtain the constructs described in **Figure 3C**. Wild-type *KRAS4A* was cloned for mammalian expression in pDEST40 vector.

Cell transfection

NIH3T3 or HEK293T cells were transfected with the indicated plasmid constructs using Fugene HD (Promega) according to standard protocols.

Recombinant KRAS and AGO2 proteins

Human derived KRASWT and KRASG12V full length coding regions were cloned as HIS-SUMO tagged proteins in a pET21d plasmid backbone described earlier[39]. Site directed mutagenesis was used to introduce the specific mutations described in the figures. Individual recombinant KRAS proteins were transformed into Rosetta cells for bacterial expression (further details awaited).

His tagged KRASG12D (1-166aa) and KRASG12DY64G (1-166aa) were provided by Gideon Bollag (Plexxikon Inc.). His-tagged AGO2 was cloned in baculoviral vector and purified using Ni-NTA columns.

***In vitro* co-immunoprecipitation**

100ng of baculoviral AGO2 or AGO1 proteins (Sino Biologicals) and 50ng of the indicated KRAS protein, were incubated in the above mentioned K-buffer with the addition of 0.2% BSA. After 2 hours of incubation at 4^0C, 1µg of IgG (RAS or control) was added and incubated further for 2 hours. 10ul of Protein A/G agarose beads (50% slurry) equilibrated in K buffer were then

added to pull down the immune complexes, washed five times at RT and resolved using SDS-PAGE.

His-AGO2 pull down assay

30 µg of his-AGO2 (made in house) protein was incubated with 600ul of Ni-NTA beads, 50% slurry (Qiagen) resuspended in Ni-NTA buffer (20 mM Tris-HCl (pH.8), 0.1% beta-mercaptoethanol, 150 mM NaCl,0.5% Triton X-100). Loading performed at 4^0C for 1hr.Spin and wash the beads using Ni-NTA buffer and incubate 25 µl of control/His-AGO2 loaded beads with KRAS proteins in Ni-NTA buffer containing 0.2% BSA. Incubate for 1.5 h at 4 °C and wash 5 times. All washes were at room temperature with rotation for 5 minutes and spin at 4000 rpm for 2 min. Binding was assessed by immunoblot analysis (using RAS10 and AGO2, polyclonal antibodies).

RAS-GTP pull down assay

The RAS-RAF interaction was studied using the RBD agarose beads as per manufacturer's instructions (Millipore). Pull down assays were performed using the cell lysates as indicated. The pull down of RAS by RBD agarose beads indicates the presence of active GTP-bound RAS interacting with RAF1.

Immunofluorescence

Indicated cells were grown on poly-lysine coated cover slips. Cells were washed twice with PBS, fixed with 3.7% paraformaldehyde for 10 min, and then permeabilized with 0.1% (w/v) saponin (Sigma) for 10 min. Cells were co-incubated with primary antibodies against AGO2 and RAS for 12 h at 4 °C, followed by incubation with appropriate Alexa-Fluor-conjugated secondary antibodies for 30 min at 37 °C. Cells were washed and mounted onto glass slides using Vectashield mounting medium (Vector Laboratories, Burlingame, CA) containing DAPI.

Samples were analyzed using a Nikon A1 laser-scanning confocal microscope equipped with a Plan-Apo ×63/1.4 numerical aperture oil lens objective. Acquired images were then analyzed using ImageJ software (version 1.41).

REFERENCES

1. Baines, A.T., Xu, D. & Der, C.J. Inhibition of Ras for cancer treatment: the search continues. *Future Med Chem* **3**, 1787-1808 (2011).
2. Downward, J. Targeting RAS signalling pathways in cancer therapy. *Nat Rev Cancer* **3**, 11-22 (2003).
3. Stephen, A.G., Esposito, D., Bagni, R.K. & McCormick, F. Dragging ras back in the ring. *Cancer Cell* **25**, 272-281 (2014).
4. Vojtek, A.B., Hollenberg, S.M. & Cooper, J.A. Mammalian Ras interacts directly with the serine/threonine kinase Raf. *Cell* **74**, 205-214 (1993).
5. Vasilescu, J., Guo, X. & Kast, J. Identification of protein-protein interactions using in vivo cross-linking and mass spectrometry. *Proteomics* **4**, 3845-3854 (2004).
6. Goldfinger, L.E., *et al.* An experimentally derived database of candidate Ras-interacting proteins. *J Proteome Res* **6**, 1806-1811 (2007).
7. Brenner, J.C., *et al.* Mechanistic rationale for inhibition of poly(ADP-ribose) polymerase in ETS gene fusion-positive prostate cancer. *Cancer Cell* **19**, 664-678 (2011).
8. Yang, M., *et al.* Dephosphorylation of tyrosine 393 in argonaute 2 by protein tyrosine phosphatase 1B regulates gene silencing in oncogenic RAS-induced senescence. *Mol Cell* **55**, 782-790 (2014).
9. Benhamed, M., Herbig, U., Ye, T., Dejean, A. & Bischof, O. Senescence is an endogenous trigger for microRNA-directed transcriptional gene silencing in human cells. *Nat Cell Biol* **14**, 266-275 (2012).
10. Horman, S.R., *et al.* Akt-mediated phosphorylation of argonaute 2 downregulates cleavage and upregulates translational repression of MicroRNA targets. *Mol Cell* **50**, 356-367 (2013).
11. Rudel, S., *et al.* Phosphorylation of human Argonaute proteins affects small RNA binding. *Nucleic Acids Res* **39**, 2330-2343 (2011).
12. Zeng, Y., Sankala, H., Zhang, X. & Graves, P.R. Phosphorylation of Argonaute 2 at serine-387 facilitates its localization to processing bodies. *Biochem J* **413**, 429-436 (2008).
13. Shen, J., *et al.* EGFR modulates microRNA maturation in response to hypoxia through phosphorylation of AGO2. *Nature* **497**, 383-387 (2013).
14. Paroo, Z., Ye, X., Chen, S. & Liu, Q. Phosphorylation of the human microRNA-generating complex mediates MAPK/Erk signaling. *Cell* **139**, 112-122 (2009).
15. Cheng, C.M., *et al.* Compartmentalized Ras proteins transform NIH 3T3 cells with different efficiencies. *Mol Cell Biol* **31**, 983-997 (2011).
16. Prior, I.A. & Hancock, J.F. Ras trafficking, localization and compartmentalized signalling. *Semin Cell Dev Biol* **23**, 145-153 (2012).
17. Bivona, T.G., *et al.* PKC regulates a farnesyl-electrostatic switch on K-Ras that promotes its association with Bcl-XL on mitochondria and induces apoptosis. *Mol Cell* **21**, 481-493 (2006).
18. Hock, J., *et al.* Proteomic and functional analysis of Argonaute-containing mRNA-protein complexes in human cells. *EMBO Rep* **8**, 1052-1060 (2007).

19. Gagnon, K.T., Li, L., Chu, Y., Janowski, B.A. & Corey, D.R. RNAi factors are present and active in human cell nuclei. *Cell Rep* **6**, 211-221 (2014).
20. Dudley, N.R. & Goldstein, B. RNA interference: silencing in the cytoplasm and nucleus. *Curr Opin Mol Ther* **5**, 113-117 (2003).
21. Stalder, L., *et al.* The rough endoplasmatic reticulum is a central nucleation site of siRNA-mediated RNA silencing. *EMBO J* **32**, 1115-1127 (2013).
22. Gibbings, D.J., Ciaudo, C., Erhardt, M. & Voinnet, O. Multivesicular bodies associate with components of miRNA effector complexes and modulate miRNA activity. *Nat Cell Biol* **11**, 1143-1149 (2009).
23. Zhang, X., *et al.* MicroRNA directly enhances mitochondrial translation during muscle differentiation. *Cell* **158**, 607-619 (2014).
24. Bolte, S. & Cordelieres, F.P. A guided tour into subcellular colocalization analysis in light microscopy. *J Microsc* **224**, 213-232 (2006).
25. Kwak, P.B. & Tomari, Y. The N domain of Argonaute drives duplex unwinding during RISC assembly. *Nat Struct Mol Biol* **19**, 145-151 (2012).
26. DeFeo, D., *et al.* Analysis of two divergent rat genomic clones homologous to the transforming gene of Harvey murine sarcoma virus. *Proc Natl Acad Sci U S A* **78**, 3328-3332 (1981).
27. Ostrem, J.M., Peters, U., Sos, M.L., Wells, J.A. & Shokat, K.M. K-Ras(G12C) inhibitors allosterically control GTP affinity and effector interactions. *Nature* **503**, 548-551 (2013).
28. Spiegel, J., Cromm, P.M., Zimmermann, G., Grossmann, T.N. & Waldmann, H. Small-molecule modulation of Ras signaling. *Nat Chem Biol* **10**, 613-622 (2014).
29. Burns, M.C., *et al.* Approach for targeting Ras with small molecules that activate SOS-mediated nucleotide exchange. *Proc Natl Acad Sci U S A* **111**, 3401-3406 (2014).
30. Sun, Q., *et al.* Discovery of small molecules that bind to K-Ras and inhibit Sos-mediated activation. *Angew Chem Int Ed Engl* **51**, 6140-6143 (2012).
31. Wilson, R.C. & Doudna, J.A. Molecular mechanisms of RNA interference. *Annu Rev Biophys* **42**, 217-239 (2013).
32. Czech, B. & Hannon, G.J. Small RNA sorting: matchmaking for Argonautes. *Nat Rev Genet* **12**, 19-31 (2011).
33. Peters, L. & Meister, G. Argonaute proteins: mediators of RNA silencing. *Mol Cell* **26**, 611-623 (2007).
34. MacRae, I.J., Ma, E., Zhou, M., Robinson, C.V. & Doudna, J.A. In vitro reconstitution of the human RISC-loading complex. *Proc Natl Acad Sci U S A* **105**, 512-517 (2008).
35. Meister, G., *et al.* Identification of novel argonaute-associated proteins. *Curr Biol* **15**, 2149-2155 (2005).
36. Ender, C. & Meister, G. Argonaute proteins at a glance. *J Cell Sci* **123**, 1819-1823 (2010).
37. Liu, J., *et al.* Argonaute2 is the catalytic engine of mammalian RNAi. *Science* **305**, 1437-1441 (2004).
38. Detzer, A., Engel, C., Wunsche, W. & Sczakiel, G. Cell stress is related to re-localization of Argonaute 2 and to decreased RNA interference in human cells. *Nucleic Acids Res* **39**, 2727-2741 (2011).
39. Weeks, S.D., Drinker, M. & Loll, P.J. Ligation independent cloning vectors for expression of SUMO fusions. *Protein Expr Purif* **53**, 40-50 (2007).

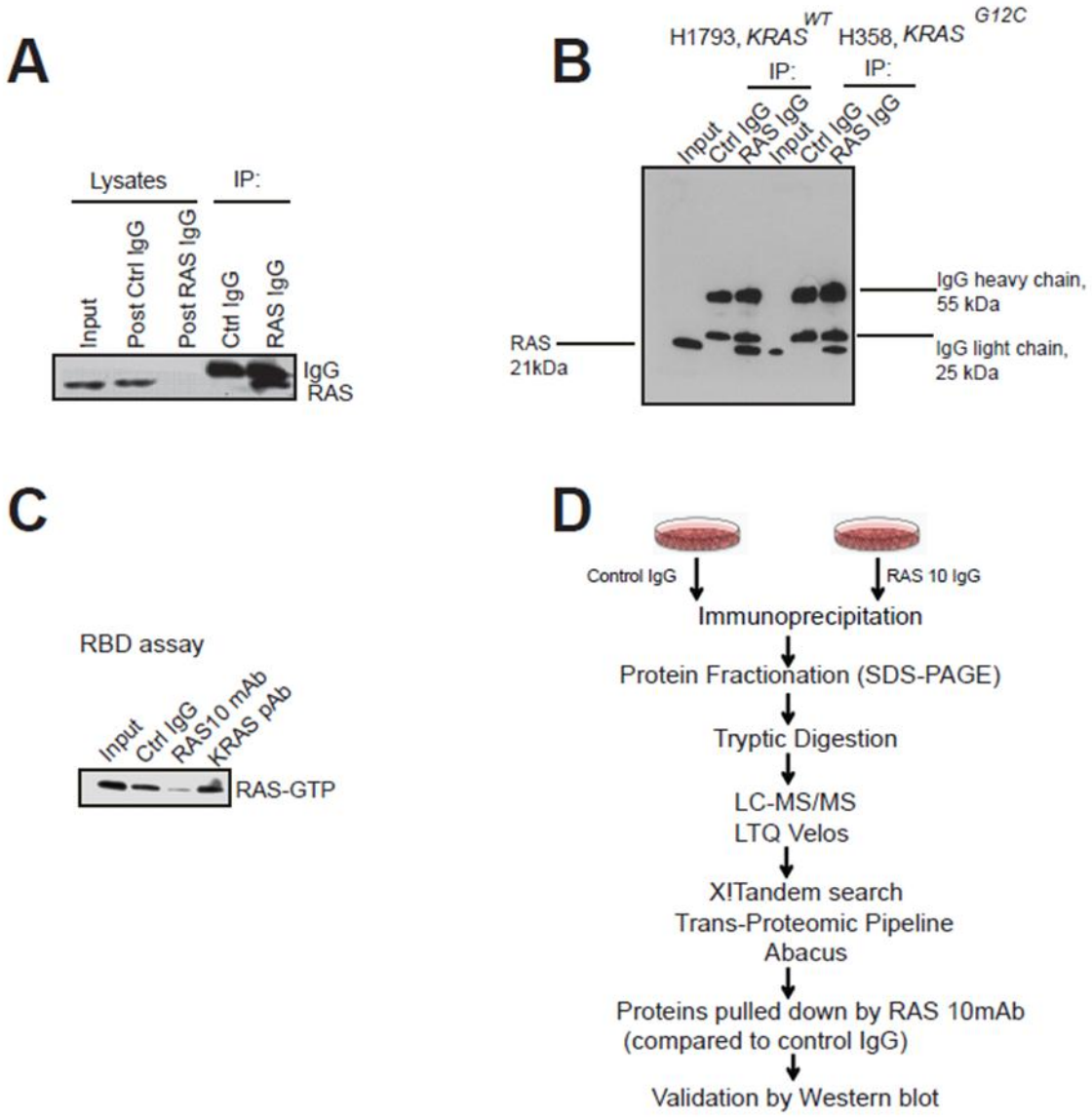

Figure 4.1. Characterization of RAS10 mAb (which binds the Switch1 domain of RAS) used for mass spectrometric identification of RAS binding proteins (A) Efficiency of the RAS10 mAb in pulling down RAS as seen by immunoblot analysis of RAS immunoprecipitates. The RAS10 mAb was used for both immunoprecipitation (IP) and immunoblot (IB) analysis. **(B)** Scan of the entire immunoblot using the RAS10 mAb demonstrating the specificity of detection using total cell lysates or immunoprecipitates. Both the IP and immunoblotting were performed using the RAS10 mAb. **(C)** Immunoblot analysis of RAS bound to RAS binding domain of RAF (RBD) in the presence of different RAS antibodies. RBD agarose beads were added to H358 cell lysates in the presence of RAS10 monoclonal or KRAS polyclonal (KRAS sc-521) antibody. Reduced interaction between RAS-GTP and RBD in the presence of RAS10 antibody indicates that the antibody binds the RAS Switch I domain and interferes with the RAS-RAF interaction. KRAS sc-521 polyclonal antibody, which binds the C-terminal region of KRAS was used as control. RAS10 mAb was used for IB analysis. **(D)** Schematic of the methodology used for RAS Co-IP MS. Proteins pulled down by the corresponding isotypic control IgG in each cell line were considered as non-specific hits and were excluded from the data obtained from RAS IP.

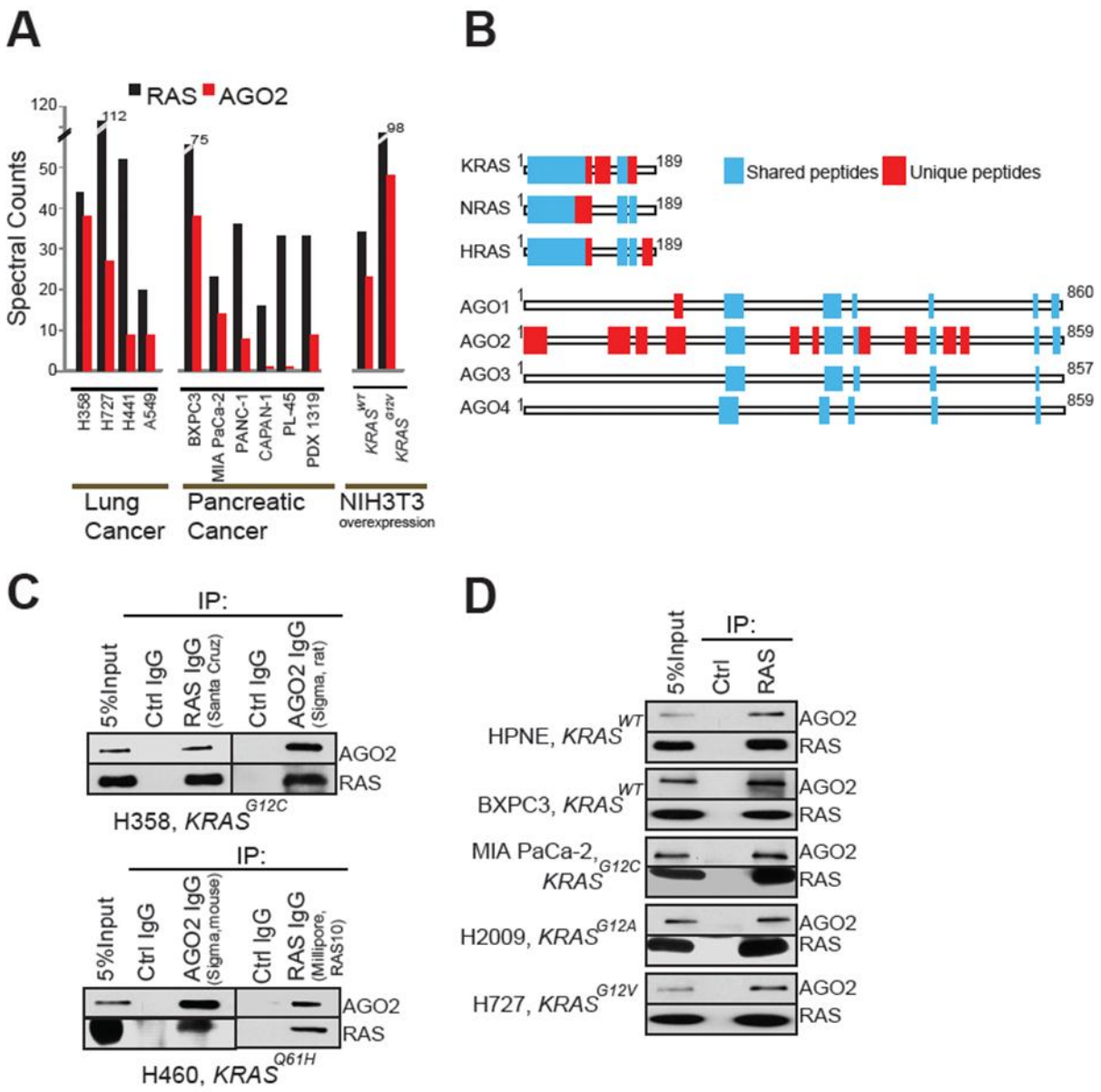

Figure 4.2. Identification of RAS-AGO2 interaction (A) Spectral counts of RAS and AGO2 peptides detected in RAS co-immunoprecipitation mass spectrometric (co-IP MS) analysis of NIH3T3 cells expressing *KRAS*^{WT} and *KRAS*^{G12V} and indicated cancer cell lines. (**B**) Distribution of peptides mapping to RAS and AGO gene families from RAS co-IP MS based on ClustalW alignments. Representative experiment from H358 cells is shown. Blue boxes indicate peptides mapping to multiple gene family members, and red boxes indicate peptides mapping uniquely to a protein. (**C**) Immunoprecipitation (IP) of RAS or AGO2 in H358 (left) and H460 (right) lung cancer cells followed by immunoblot analysis using multiple distinct antibodies, as indicated. (**D**) IP of RAS from a panel of benign and cancer cells with differing mutational status of *KRAS* (as indicated) followed by immunoblot analysis of AGO2 or RAS. RAS10 mAb was used for both IP and IB.

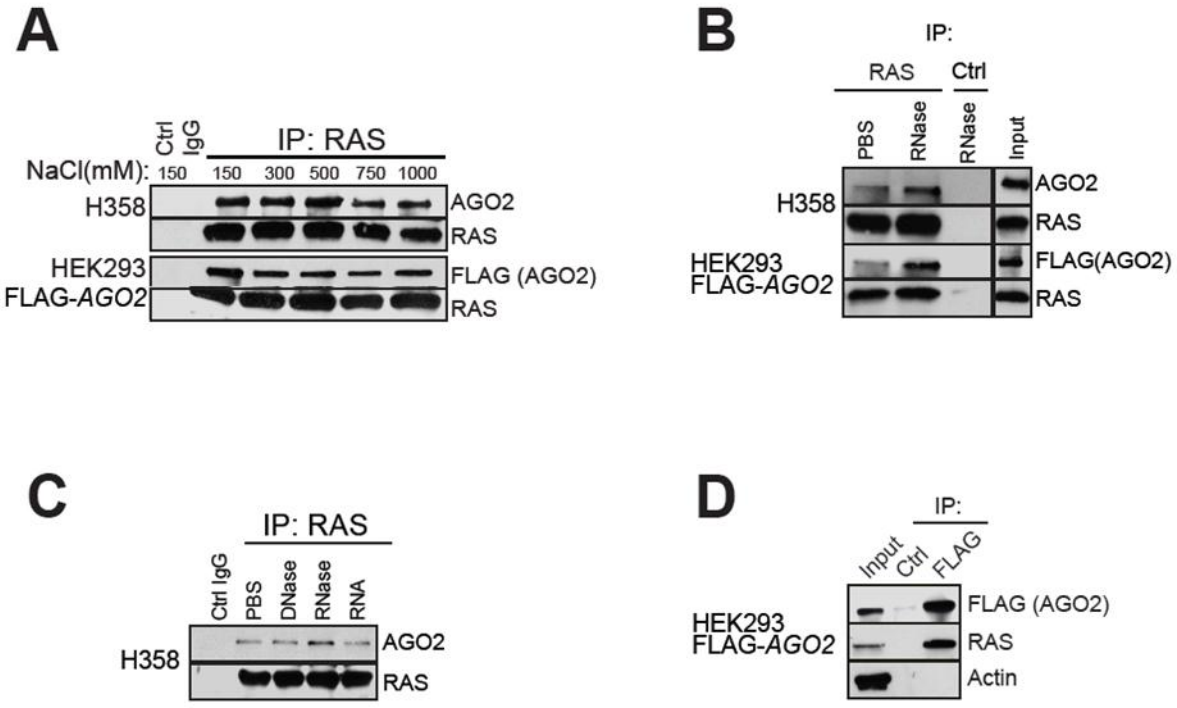

Figure 4.3. AGO2 associates with RAS proteins in the presence of RNase (A) IP of RAS in H358 and HEK293 FLAG-*AGO2* expressing cells under increasing concentrations of salt followed by immunoblot analysis. Immunoblot analysis of RAS10 Ab immunoprecipitates from H358 lung cancer (endogenous) and FLAG-*AGO2* overexpressing HEK293 cell lysates treated with RNase (**B**) and DNase (**C**). RAS10 mAb was used for both IP and IB. RAS10 mAb was used for both IP and IB. (**D**) FLAG tagged AGO2 expressed in HEK293 immunoprecipitates RAS. Actin was used as control.

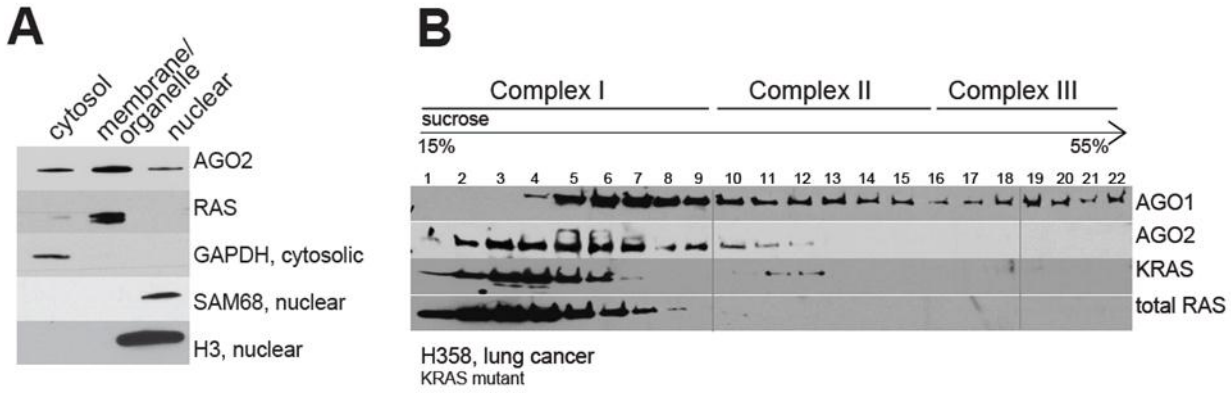

Figure 4.4. Co-sedimentation of RAS and AGO2 (**A**) Cell fractionation analysis of H358 cells to show enrichment of distinct proteins in the cytocolic/membrane or organelle/nuclear fractions. GAPDH was used as a cytosolic marker while SAM68 and H3 were used as nuclear markers. 2ug of various fractions were assessed for the different protein contents. (**B**) Sucrose density gradient fractionation of cell lysates from H358 and HEK293 cells followed by immunoblot detection of total RAS, KRAS, AGO1 and AGO2 proteins.

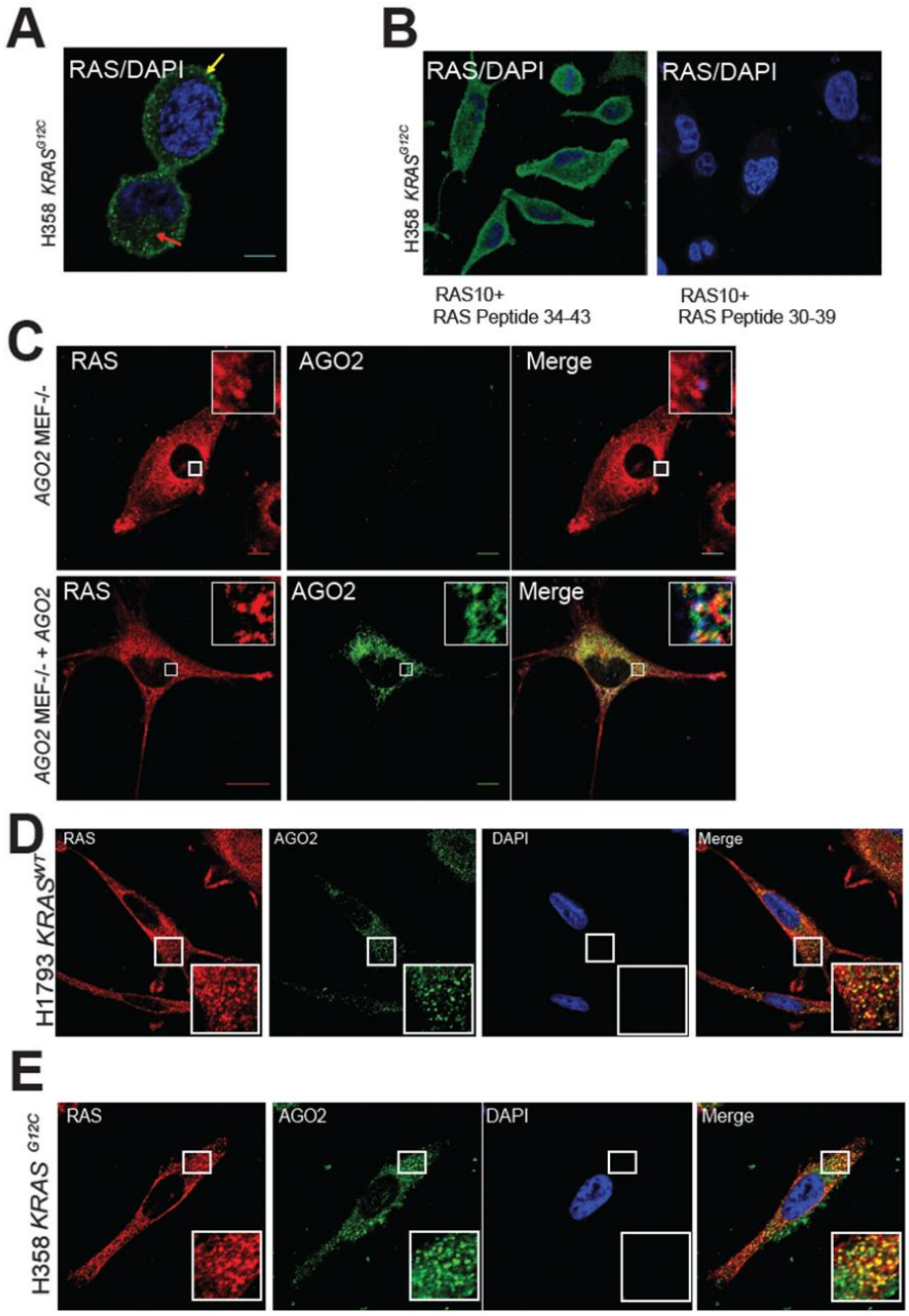

Figure 4.5. Co-localization of RAS and AGO2 proteins in the intracellular compartments (A) Membrane (yellow arrow) and intracellular organelle staining (red arrow) of RAS in H358 *KRAS*^{G12C} lung cancer cells, using RAS10 mAb that binds the switch I domain. (**B**) Specificity of the RAS10 mAb is demonstrated by pre-incubating the antibody with switch I domain specific (30-39aa) or non-specific (34-43aa) RAS peptides, prior to immunofluorescence analysis (**C**) Immunofluorescence analysis of RAS and AGO2 co-localization in AGO2 knock out mouse embryonic fibroblasts (*AGO2-/-* MEF upper panels) and AGO2 knock out MEF cells expressing AGO2 (*AGO2-/-* MEF *+AGO2*, lower panels). (**D**) Immunoflourescence analysis shows co-localization of RAS (red) and AGO2 (green) proteins in membrane bound organelles in H1793 *KRAS*^{WT} lung cancer cells. (**E**) Intracellular localization by immunofluorescence of RAS (red) and AGO2 (green) proteins in H358 *KRAS*^{G12C} lung cancer cells. Yellow color in the merged image indicates cytoplasmic co-localization of RAS and AGO2. The nucleus was visualized by DAPI staining (blue). Insets show magnified view of the areas marked.

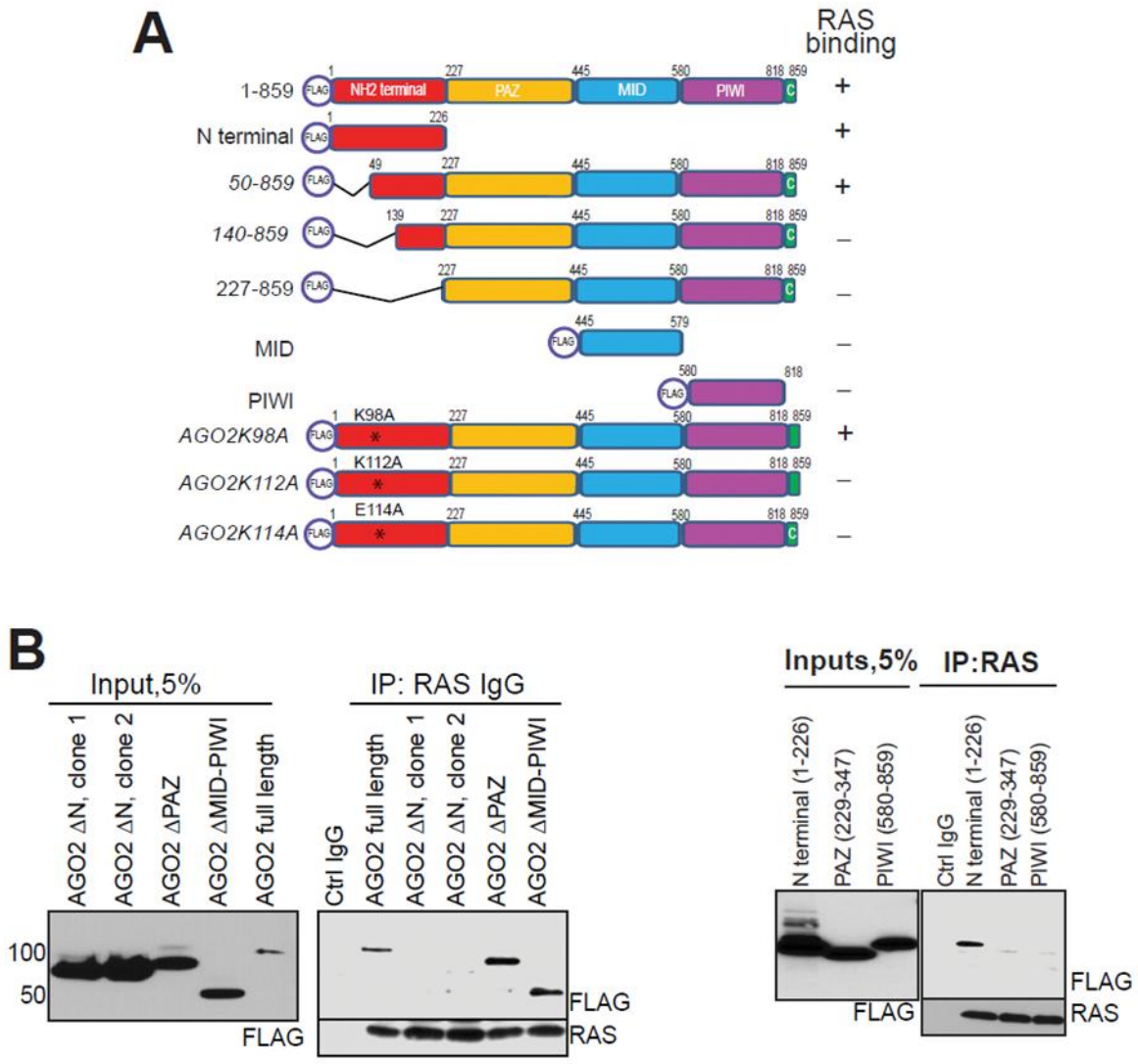

Figure 4.6. The N-terminal domain of AGO2 interacts with RAS (**A**) Schematic summary of FLAG tagged *AGO2* deletion and mutant constructs used for RAS co-IP analyses (**B**) Expression of FLAG tagged N-terminal, PAZ, or PIWI domains of *AGO2* in HEK293 cells (left panel), followed by RAS IP (right panel). Immunoblot analysis shows that deletion of (1-226aa) N terminal domain in AGO2 abrogates RAS interaction. (**C**) Expression (left panel) and RAS IP interaction analysis (right panel) of FLAG tagged N-terminal, PAZ, or PIWI domains of *AGO2* in HEK293 cells. Immunoblot analysis shows that (1-226aa) N terminal domain is sufficient for RAS interaction using RAS10mAb.

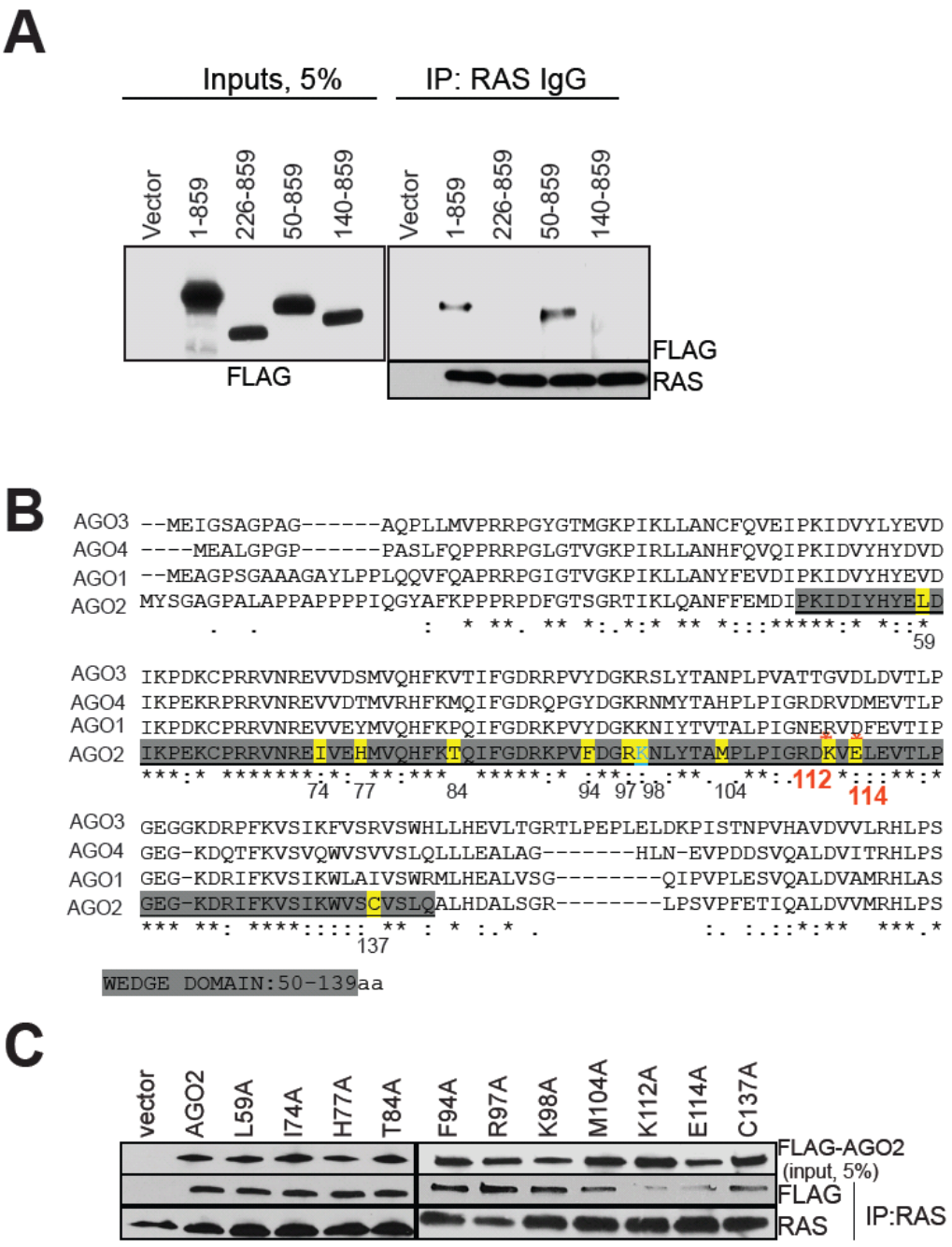

Figure 4.7. Residues 112-114 in AGO2 are critical for its association with RAS. (A) Expression (left panel) and RAS IP analysis (right panel) of various indicated *AGO2* N terminal deletion constructs in HEK293 cells. Immunoblot analysis indicates that 50-139 aa in the AGO2 N terminal domain is essential for RAS binding. Both RAS IP and IB were performed using RAS10 mAb. **(B)** ClustalW alignment of the Argonaute family proteins spanning the "wedge domain" (50-139 aa, marked in grey). Residues marked in yellow were identified as unique to AGO2 and were mutagenized to alanine for binding analysis. The numbers below indicate the amino acid position. *AGO2*^{K98} (marked in green) shared with AGO1 was also changed to alanine to be used as control. AGO2 residues K112 and E114, marked in red were critical for RAS interaction. (**C**) Expression of indicated *AGO2* N terminal point mutant constructs within the wedge domain (50-139aa) in HEK293 cells, followed by RAS co-IP analysis.

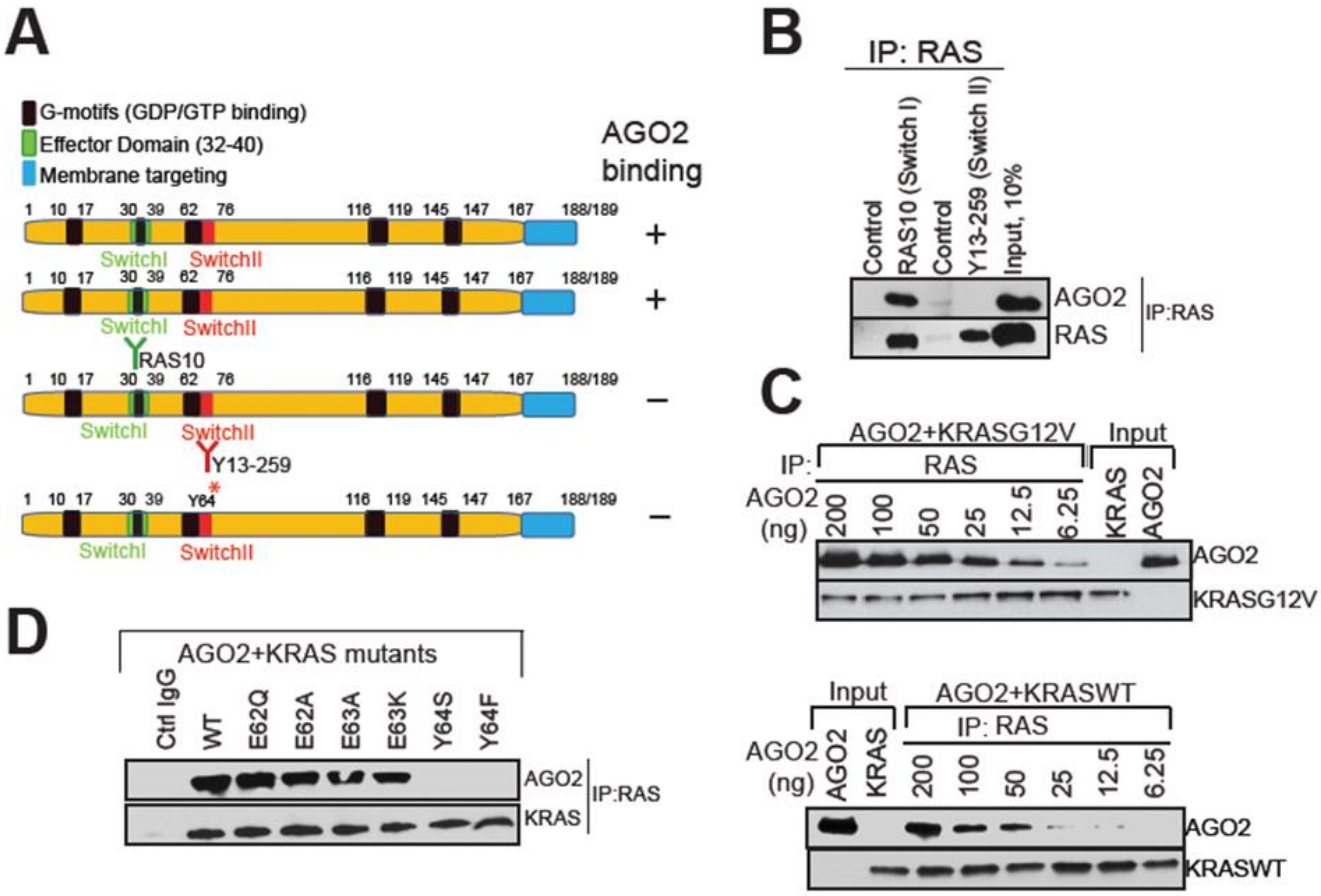

Figure 4.8. The Switch II domain of RAS interacts with AGO2 (**A**) Schematic summary of the antibodies and recombinant proteins used for RAS-AGO2 co-IP analysis to identify residues in RAS, critical for AGO2 interaction. (**B**) RAS co-IP using antibodies that bind switch I domain (RAS10 Ab) or switch II domain (Y13-259 Ab), followed by immunoblot analysis for RAS and AGO2. (**C-D**) Characterization of direct RAS-AGO2 interaction, *in vitro*. (C) Immunoblot analysis following *in vitro* co-IP of recombinant KRASG12V (top panel) and KRASWT (bottom panel) in the presence of varying concentrations of recombinant AGO2. (**D**) *In vitro* co-IP analysis of KRAS-AGO2 interaction using a panel of KRAS mutant proteins spanning amino acid residues 62-65 in the switch II domain.

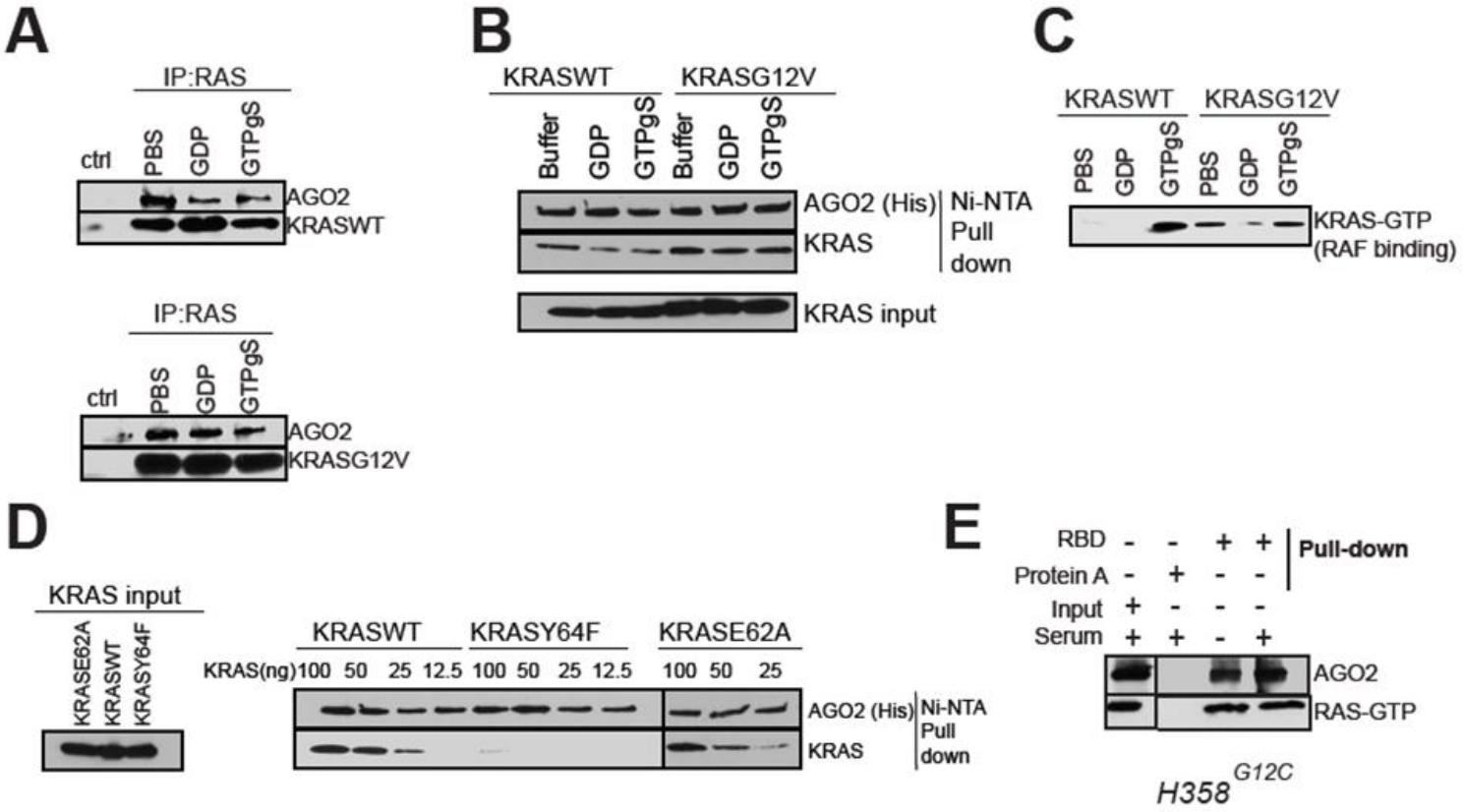

Figure 4.9. **Characterization of direct RAS-AGO2 interaction by *in vitro* co-IP** (**A**) GDP or GTPγS loading of recombinant KRASWT (top panel) and KRASG12V (bottom panel) proteins prior to RAS-AGO2 *in vitro* co-IP analysis using RAS10 Ab. (**B**) *In vitro* HIS-AGO2 pull down assay after GDP or GTPγS loading of recombinant KRASWT and KRASG12V proteins. (**C**) RBD pull down assay using recombinant KRASWT and KRASG12V proteins loaded with GDP or GTPγS to demonstrate efficiency and specificity of nucleotide loading. (**D**)Immunoblot analysis following His-AGO2 pull down assay using Ni-NTA beads upon incubation with different KRAS mutant proteins. (**E**) RBD pull down assay using lysates from H358 cells followed by immunoblot analysis for RAS (RAS10) and AGO2 (rat AGO2, Sigma). RBD associates only with the active form of RAS (RAS-GTP) which is more abundant in H358 cells (mutated KRAS dependent) compared to H460 cells (mutated KRAS independent).

Number	Cell Line	Source	Tissue	Type	*KRAS* or *AGO2* status	RAS co-IP Mass Spec	RAS co-IP Western
1	A549	Human	Lung	Cancer	*KRAS* G12S	X	ND
2	H358	Human	Lung	Cancer	*KRAS* G12C	X	X
3	H441	Human	Lung	Cancer	*KRAS* G12V	X	ND
4	H727	Human	Lung	Cancer	*KRAS* G12V	X	X
5	BXPC3	Human	Pancreas	Cancer	*KRAS* WT	X	X
6	CAPAN-1	Human	Pancreas	Cancer	*KRAS* G12V	X	ND
7	MIA PaCa-2	Human	Pancreas	Cancer	*KRAS* G12C	X	X
8	PANC-1	Human	Pancreas	Cancer	*KRAS* G12D	X	ND
9	PDX 1319	Human	Pancreas	Cancer	*KRAS* G12D	X	ND
10	PL-45	Human	Pancreas	Cancer	*KRAS* G12D	X	ND
11	NIH3T3, stable cell line	Mouse	Fibroblast	Benign	overexpressing, *KRAS* WT	X	ND
12	NIH3T3, stable cell line	Mouse	Fibroblast	Benign	overexpressing, *KRAS* G12V	X	ND
13	H2009	Human	Lung	Cancer	*KRAS* G12A	ND	X
14	H460	Human	Lung	Cancer	*KRAS* Q61H	ND	X
15	HPNE	Human	Pancreas	Benign	*KRAS* WT	ND	X
16	*AGO2* MEF-/-	Mouse	Embryonic fibroblast	Benign	*AGO2* knockout	ND	X
17	*AGO2* MEF-/- +*AGO2*	Mouse	Embryonic fibroblast	Benign	*AGO2* knockout overexpressing *AGO2*	ND	X
18	HEK293FT	Human	Embryonic kidney	Benign	for transient overexpression as indicated	ND	X
19	NIH3T3 *AGO2* -/-	Mouse	Fibroblast	Benign	CRISPR/Cas9 for AGO2 knockout	ND	ND

Table 4.1 Cell lines used in the study. Cell lines used in this study for RAS co- IP MS and/or RAS co-IP Western blot analysis, with their associated *KRAS* mutation status. NIH3T3 stable lines were generated using plasmids encoding $KRAS^{WT}$ or $KRAS^{G12V}$. HEK293 cells were used for transfection for assays in the transient mode. PDX 1319 is a pancreatic cancer derived xenograft cell line. ND: not determined

		Lung				Pancreas						Mouse fibroblast			
Protein_ID	Protein	A549	H358	H441	H727	BXPC3	Capan-1	MIA PaCa-2	PANC-1	PL45	PDX 1319	NIH3T3 $KRAS^{G12V}$	NIH3T3 $KRAS^{WT}$	Cumulative spectral counts	Number of cancer cell lines
NP_004976/ NP_002515/ NP_005334	KRAS/NRAS/HRAS	20	44	52	112	75	33	23	36	16	33	98	34	556	12
NP_036286	EIF2C2 (AGO2)	9	39	9	28	38	1	14	8	1	9	48	25	229	12
NP_004090	STOM	0	40	16	56	21	3	0	13	3	2	5	6	165	10
NP_001138303	PHB2	0	3	23	0	5	48	0	15	48	4	7	9	162	10
NP_258260	FCHSD1	26	20	0	0	0	13	0	11	13	0	8	11	76	7
NP_057018	NOP58	10	19	31	0	3	4	4	2	4	6	0	0	73	9
NP_001028886	NOP2	10	13	15	0	2	9	0	0	9	2	0	0	50	7
NP_542193	BRI3BP	0	3	3	20	0	3	3	2	3	3	0	0	40	8
NP_005605	RHEB	10	3	9	0	5	0	0	0	0	7	11	0	35	6
NP_055315	HTATSF1	9	29	0	0	0	2	0	2	2	0	0	0	35	5
NP_036473	GTPBP4	6	2	13	0	0	0	8	0	0	1	0	0	24	5
NP_055118	PES1	5	5	9	0	0	0	5	0	0	3	0	0	22	5
NP_078938	NAT10	6	9	1	0	0	2	4	1	2	1	0	0	20	8
NP_001092688	RAD51AP2	5	4	0	0	0	6	0	4	6	0	0	0	20	5

Table 4.2 Summary of shared peptide hits in RAS coIP mass spectrometry in cancer cell lines. Spectral counts of peptides detected in at least 5 of 10 cancer cell lines tested by tandem mass spectrometry of RAS co-immunoprecipitation.

Number	Antibody	Vendor	Catalog Number	Experiments	Validation method/s
1	Anti-Ras Clone 10	Millipore	05-516	IP, IB, IF	recombinant protein detection, peptide competition
2	K-Ras-2B Antibody (C-19)	Santa Cruz	sc-521	IP, IB	recombinant protein detection, KRAS siRNA
3	K-Ras monoclonal Ab	Santa Cruz	sc-30	IB	recombinant protein detection
4	Ago2 rabbit pAb	Millipore	07-590	IB, IF	recombinant protein detection, MEF AGO2-/-
5	AGO2 mouse mAb, clone 2E12-1C9	Sigma	WH0027161M1	IP, IB, IF	recombinant protein detection
6	AGO2, 11A9, rat mAb	Sigma	SAB4200085	IP, IB	recombinant protein detection
7	Anti-FLAG	Sigma	F1804	IB, IP	FLAG-AGO2 detection in HEK 293 cells
8	Y13-259 rat mAb	EMD-Millipore	OP01, Y13-259	IP	recombinant protein detection
9	Phospho-Akt (S473)	Cell Signaling	9271	IB	ND
10	Phospho-ERK (S473)	Cell Signaling	9101	IB	ND
11	Phospho-S6 Ribosomal (S236/236)	Cell Signaling	2211	IB	ND
12	AGO1	Sigma	SAB4200084	IB	recombinant protein detection
13	Normal Rat IgG	Abcam	ab18450	control IP	ND
14	Normal mouse IgG	Millipore	12-371	control IP	ND
15	Normal rabbit IgG	Millipore	12-370	control IP	ND

Table 4.3. Antibodies used in this study. IB: Immunoblotting, IP:Immunoprecipitation, IF: Immunoflourescence

CHAPTER 5

ARGONAUTE-2 PROMOTES *KRAS* MEDIATED CELLULAR TRANSFORMATION

SUMMARY

In the earlier chapter we describe a specific interaction between endogenous RAS and AGO2 in cells expressing both wild type and mutant RAS. To probe this interaction at a functional level, we characterized the role of AGO2 in established KRAS mutant cell line models of lung and pancreatic cancer and its effect on cellular transformation using NIH3T3 model. Using shRNA, we demonstrate that knock-down of AGO2 attenuates *KRAS*-mediated cell proliferation, while *KRAS*-mediated transformation is enhanced by overexpression of AGO2. Mechanistically, the intracellular KRAS-AGO2 interaction increases mutant KRAS levels and affects signaling outputs through modulation of Akt activation. We also provide evidence that expression of mutant KRAS inhibits the assembly of regulatory messenger ribonucleoprotein particles (mRNPs) in NIH3T3 cells. Employing NIH3T3 *AGO2-/-* cells, we observed that interaction with AGO2 is required for maximal KRAS-mediated transformation, such that cells lacking AGO2 fail to elevate mutant KRAS levels and limit phospho-Akt activation. The repurposing of RNA-based gene silencing by RAS through its interaction with AGO2 expands its range of oncogenic activities, identifies a critical regulator of mutant RAS levels, and suggests a novel avenue for therapeutic intervention.

INTRODUCTION

The discovery of a direct RAS-AGO2 interaction brings to the foreground a direct association of signaling networks and silencing mechanisms. Known functions of AGO2, its interacting partners and role in MAPK pathway are described below.

AGO2: Core component of the RNA silencing pathway

Protein encoding transcripts are transcribed from just 2% of the eukaryotic genome and are further regulated by 21-35 nucleotide containing small non-coding microRNAs which regulate gene expression. These double stranded microRNAs are themselves regulated at the transcriptional level and their biogenesis (from long dsRNA primary transcripts) is largely controlled by the Dicer and Drosha proteins through multiple pathways reviewed in literature [1,2]. Once the mature dsRNAs are transported to the cytoplasm, they are loaded onto Argonaute proteins, where the non-complementary or passenger strand is removed and the guide strand helps enhance the affinity of the AGO protein to its target transcript. Perfect complementarity between the small RNA and its target mRNA, as seen with the small interfering RNA or siRNA, results in AGO2 mediated endonucleolytic cleavage of the target transcript. In case of microRNAs (with partial complementarity to its target sequence), the target sequence is either held in a repressive complex preventing translation or deadenylated to prevent degradation [3]. While all human Argonaute AGO1, AGO2, AGO3 and AGO4 proteins have overlapping functions and can form such RNA induced silencing complexes or RISC [4], only AGO2 has been shown to have endonucleolytic activity to cleave the target mRNA sequence.

Argonaute proteins have two conserved RNA binding domains called the PAZ (PIWI-Argonaute-Zwille) domain and an RNAse like PIWI domain. The different AGO proteins are

most divergent at their N-terminal. Recently independent groups demonstrated that four catalytic residues in the PIWI domain and critical residues in its N-terminal domain are sufficient for AGO2 endonucleolytic activity [5,6]. Given that majority of the eukaryotic gene silencing is mediated through microRNAs, the role of the endonucleolytic activity, which requires perfect complementarity of the guide and target sequences, remains unclear.

Localization and post translational modifications controls AGO2 activity

Most of the AGO associated activities have been demonstrated in the cytoplasmic compartment of the cell, where it resides in non-membrane bound, ribosome free cytoplasmic structures called Processing bodies (P-bodies) [7] or in stress bodies [8]. Here, untranslated mRNA associates with AGO2 to form miRNA containing RibonucleoProtein (mRNP) complexes such that the transcripts can either be degraded or return for translation[9]. The movement of AGO2 is further regulated by post translational modification such that phosphorylation at tyrosine residue 387 [10], and tyrosine 529 prevents its accumulation in P-bodies[11], suggesting that phosphorylation of AGO2 is an emerging critical regulator of AGO2 function.. Proline residue hydroxylation of AGO2 was also recently identified as important for its stability and efficient RNA silencing activities [12]. Recently, AGO2 was found to be sumolyated by SUMO1 and SUMO2/3 enzymes which results in increased stability of the AGO2 protein [13]. These studies providing clues to the fine tuning of AGO2 function through various mechanisms in different cellular contexts.

Like RAS proteins, AGO2 is also detected in different cellular compartments, but unlike RAS is not restricted to the plasma membrane and membrane bound cytoplasmic organelles. Among the membrane bound structures, the rough endoplasmic reticulum (rER) is a known site for RNA gene silencing by AGO proteins [14] and AGO2 has been detected in late endosomes [15]

and mitochondria [16] where it associates with different proteins to affect cellular proliferation or differentiation, respectively. Much of the recent literature demonstrates a role for AGO2 within the nucleus where it controls RNA Induced Transcriptional Silencing (RITS) [17-21], DNA methylation [22], pre-mRNA splicing [23] and double stranded break repair [24,25]. Together with silencing activities in the cytoplasmic RISC complexes, these surprising new functions of small RNA bound Argonaute proteins suggest wide-ranging activities within the cell.

AGO2 interacting proteins

In 2005, Dicer [26,27] and TRBP [28] were identified as AGO2 interacting proteins which were later shown to be sufficient for AGO2 mediated RISC activity *in vitro* [29]. An unbiased comprehensive mass spectrometric analysis of tagged AGO2immunoprecipitates, showed a large number of RNA binding proteins that interact with AGO2 [30] in either an RNA dependent or independent manner, suggesting that these proteins can either affect RISC activity/assembly or are components of the mRNP complexes, respectively. A functional interaction between AGO2 and P body component, GW182, helped identify localization of AGO2 to the P-bodies and was demonstrated to be a pre-requisite to microRNA mediated repression [31]. AGO2 interacting proteins with roles/putative functions in every step of RISC function including RISC loading, RISC activation, duplex unwinding, AGO recruitment to mRNA targets, stabilization of AGO-mRNA complexes and others have been identified and reviewed [32]. Yet, RAS has not been detected as an AGO2 interacting partner likely because the workflow did not include analysis of proteins below 25kDa.

AGO proteins bound to both the microRNAs and their binding sites in target transcripts are being identified using Photoactivatable Ribonucleoside-Enhanced Crosslinking and

Immunoprecipitation (PAR-CLIP), a transcriptome-wide crosslinking method for RNA binding proteins that incorporate photoactivatable nucleoside analogs which undergo transition during complementary DNA (cDNA) synthesis and reveal precise binding of the RBP[33]. Global analysis of thousands of such binding sites revealed that AGO proteins bound with equal efficiency to the transcript coding sequences (CDS) and the 3'UTR regions. Using CLIP methodology, arsenite induced stress was also shown to increase AGO2 occupancy of target transcripts (in both the coding and the 3'UTR sequences), accompanied by stronger translation repression [34].

Argonaute 2 in the RAS/MAPK/PI3K pathway

One of the most intriguing aspects of the RAS-AGO2 interaction is the intersection of the RAS/MAPK pathway to AGO2 and its microRNA mediated function (**Figure 5.1**). One of the earliest studies showed that phosphorylation of TRBP, part of the Dicer associated microRNA-generating complex, was activated upon ERK signaling. A coordinated decrease in the tumor suppressor *let-7* microRNA suggested that the signaling mechanism target the microRNA pathway to control biological processes [35]. A more direct link to the MAPK pathway came into focus when EGFR was shown to phosphorylate AGO2 at tyrosine residue 393, reduced AGO2-Dicer interaction and interfered with microRNA maturation only under hypoxic conditions[15].

In a more recent study on oncogene induced senescence, AGO2 demonstrated transcriptional silencing through repression of RB1/E2F-target genes in a *let-7* dependent manner. It is interesting to note that the authors used RAS^{G12V} mutant to induce senescence in these models to establish a tumor suppressor role of AGO2/microRNA axis during senescence[36]. Similarly, a non-receptor type phosphatase, PTP1B, upon inactivation by reactive oxygen species (ROS), dephosphorylates AGO2 Tyrosine 393 residue and counters the effect of oncogenic HRAS to induce senescence in IMR90 cells[37]. Together these studies suggest that AGO2 may

have a vital role in RAS induced senescence through strategic control of the microRNA mediated machinery.

In this chapter, using multiple cell line models, we provide evidence for phenotypic consequences of AGO2 modulation in mutant KRAS driven cellular transformation and a requirement for a direct RAS-AGO2 interaction in this process.

RESULTS

AGO2 positively regulates mutant *KRAS* levels in mutant *KRAS* dependent cancer cells

Next, we set out to analyze functional implications of RAS-AGO2 interaction, particularly in the context of KRAS driven transformation. To this end, we first carried out knockdown of *AGO2* in H358 lung cancer cells that harbor a homozygous *KRAS* mutation and are known to be *KRAS*-dependent[38]. Whereas AGO2 is known to negatively regulate wild-type RAS levels [39], here, *AGO2* knockdown resulted in a remarkable reduction in mutant KRAS protein levels (**Figure 5.2A, left panel**). Conversely, overexpression of *AGO2* in the same cells led to elevated levels of KRAS, implying a positive regulation of mutant KRAS levels by AGO2 in these cells (**Figure 5.2A, right panel**). Consistent with these observations, knockdowns of *AGO2* and/or *KRAS* in H358 cells showed reduced rates of cell proliferation while AGO2 overexpression resulted in increased cell proliferation (**Figure 5.2B**). Furthermore, *AGO2* knockdown reduced the ability of H358 cells to form colonies in colony formation assays (**Figure 5.2C**) and resulted in marked reduction in levels of known mediators of KRAS signaling, including p-Akt, p-mTOR and p-RPS6 based on a Pathscan intracellular signaling array (Cell Signaling) (**Figure 5.2D**). Interestingly, similar *AGO2* depletion experiments (using the same shRNAs as described above) in H460 lung cancer cells that harbor mutant *KRAS* but are known to be *KRAS* independent, did

not affect KRAS levels, cell proliferation, colony formation (**Figure 5.2E**) or intracellular signaling (**Figure 5.2F**). These phenotypic effects upon *AGO2* knockdown in the context of *KRAS* dependency were also observed in pancreatic cancer cell lines where knockdown of either *KRAS* or *AGO2* dramatically reduced cell proliferation in mutant *KRAS*-dependent MIA PaCa-2 cells but not in mutant *KRAS*-independent PANC-1 cells (**Figure 5.2G**). To further explore the dependence of KRAS oncogenic phenotype on AGO2, we tested *AGO2* depleted MIA PaCa-2 cells for their ability to establish xenografts in SCID mice. A dramatic reduction in tumor volume in *AGO2* depleted cells was observed (**Figure 5.2H**). Immunoblot analysis showed that similar to H358 lung cancer cells, knockdown of *AGO2* in the *KRAS* dependent pancreatic MIA PaCa-2 cells also results in reduced levels of KRAS protein (**Figure 5.2H, inset**). These data suggest that *KRAS* dependent cancer cells manifest a coincident dependence on *AGO2* to maintain oncogenic KRAS protein levels. Together, these experiments support a functional role for *AGO2* in potentiating the oncogenic activities of mutant *KRAS*, and led us to further explore mechanistic correlates of the RAS-AGO2 interaction.

KRAS driven NIH3T3 cellular transformation depends on direct AGO2 binding to inhibit functional RISC assembly

To address mechanistic underpinnings of the phenotypic effects associated with the mutant KRAS-AGO2 interaction, we employed the classic experimental model system of NIH3T3 cells to ectopically express human $KRAS^{WT}$ or $KRAS^{G12V}$ [40,41], with or without *AGO2*, and carried out transient foci formation assays. As expected, no foci were observed in cells transfected with $KRAS^{WT}$, as well as in cells with $KRAS^{WT}$±*AGO2*. However, NIH3T3 cells transfected with $KRAS^{G12V}$ generated characteristic foci of transformed cells resulting from loss of contact

inhibition. Remarkably, co-transfection of *KRAS*^{G12V} but not BRAF^{V600E} with AGO2 enhanced the number of foci by approximately five-fold, compared to the vector control (**Figure 5.3A-B**). Consistent with *AGO2* overexpression in H358 cells **(Figure 5.2A)**, immunoblot analysis of NIH3T3 cells overexpressing *AGO2* showed an increase in KRAS protein levels **(Figure 5.3C)**.

Furthermore, to understand the effects of AGO2 in the RAS signaling pathways, we analyzed protein lysates from NIH3T3 cells stably expressing *KRAS*^{G12V}+vector or *KRAS*^{G12V}*+AGO2*, using the Pathscan intracellular signaling arrays. Cells expressing *KRAS*^{G12V}*+AGO2* showed a marked increase in the levels of p-Akt, p-mTOR and p-RPS6 (**Figure 5.3C bottom panel**) suggesting that the increased levels of oncogenic KRASG12V protein signals largely through PI3K activation.

To probe the requirement of mutant KRAS-AGO2 interaction for oncogenic transformation we first performed *in vitro* RAS co-IP assays using mutant KRASG12D and the double mutant KRASG12DY64G which has previously been shown to have limited oncogenic potential[42]. We next engineered a retroviral vector in which we introduced the Y64G substitution in the context of oncogenic *Kras*^{G12V}. Transfecting this *KRAS*^{G12VY64G} double mutant into NIH3T3 cells failed to generate foci (**Figure 5.3D**). As an important corollary to our hypothesis that mutant KRAS-AGO2 interaction leads to elevated mutant KRAS protein levels, the *KRAS*^{G12VY64G} stably expressing cells, in which mutant KRAS fails to engage AGO2 also showed much lower levels of KRAS protein as compared to *KRAS*^{G12V} expressing cells (**Figure 5.3E, top panel**). An independent construct encoding *KRAS*^{G12VY64G} showed similar results in both the foci formation assay and its inability to express high levels of the KRAS protein despite similar levels of KRAS transcripts. Curiously, *KRAS*^{G12VY64G} expression showed activated phospho-Akt and phospho-ERK activation similar to that of *KRAS*^{G12V} expressing cells, suggesting that the switch

II domain may play a critical role in KRAS activation through interactions of Y64 with various effectors and regulators. Yet, despite the increased activated ERK/Akt levels, cells expressing *KRAS*^{G12VY64G} failed to show the characteristic morphology of *KRAS*^{G12V} cells (**Figure 5.3D, bottom panel**). *In vivo* these cells also failed to establish tumors in the xenograft mouse model (**Figure 5.3F**), supporting a critical role for Y64 in the Switch II domain, including its association with AGO2, for transformation.

To more directly explore the potential effect of *KRAS*^{G12V} on functional mRNPs, as implicated by its interaction with AGO2, we exploited a recently described method for intracellular single-molecule, high-resolution localization and counting (iSHiRLoC) of microRNAs [43,44] wherein the mobility of fluorophore labeled *let-7a* microRNAs was tracked following microinjection into NIH3T3 cells. The diffusion coefficient distribution of single particles as a readout of microRNA assembly into mRNPs (**Figure 5.4A**) suggests that in NIH3T3 cells expressing wild-type *RAS*, *let-7a* assembles into both 'fast' (low molecular weight) and 'slow' (high molecular weight) mRNPs representing early and late intermediates of the RNA silencing pathway, respectively. By contrast, in cells expressing mutant *KRAS*^{G12V}, the *let-7a* probe manifested predominantly in fast moving complexes (**Figure 5.4A)** suggesting that the large mRNPs are reduced in the presence of mutant *KRAS*^{G12V}, presumably due to its interaction with AGO2. Importantly, in the NIH3T3 cells stably expressing *KRAS*^{G12VY64G} wherein the mutant KRAS-AGO2 interaction is abrogated, *let-7a* again accumulated in both fast and slow mRNPs (**Figure 5.4A**).

Since AGO proteins, especially AGO2 is known to elevate microRNA levels in general and *let-7* in particular [45], we assessed the levels of let-7 microRNAs in *KRAS*^{G12V} expressing cells and interestingly observed a significant reduction in both *let-7a2* and *let-7f* microRNAs **(Figure**

5.4B). In the same assay, *KRAS*^{G12VY64G} expressing cells, which do not allow mutant KRAS-AGO2 interaction, showed no change in *let-7* levels, providing evidence for a direct role of mutant KRAS in the modulation of microRNA levels in this model. Cognate analysis of the levels of *let-7* target transcripts in these cells, showed an almost one log fold change in the mRNA levels of *HMGA1* and *HMGA2* **(Figure 5.4C)**, known to be post transcriptionally modulated through multiple *let-7* binding sites in their 3'UTR regions [46]. Curiously, we did not observe increased levels of endogenous KRAS or MYCN levels, which are also known to contain *let-7* binding sites in their 3'UTR. Together, our data using the *KRAS*^{G12VY64G} mutant and *let-7,* as an example of AGO2 regulated microRNA, support the conclusion that mutant KRAS, through its direct association with AGO2, attenuates microRNA levels and prevents microRNA mediated gene silencing.

AGO2 interaction is required to maximize oncogenic potential of mutant KRAS

To further underscore the role of AGO2 in *KRAS*^{G12V} driven oncogenesis, we generated NIH3T3 cells with *AGO2* knockout (NIH3T3 *AGO2*-/-) using the CRISPR/Cas9 methodology [47] (**Figure 5.5**). Validation of *AGO2* knockout in NIH3T3 *AGO2*-/- cells was performed at the DNA, RNA and protein levels (**Figure 5.5B-D**). Loss of AGO2 in NIH3T3 cells resulted in lower levels of *let-7* family microRNAs (**Figure 5.5E**), consistent with previous studies demonstrating that a loss of AGO2 results in a reduction of absolute levels of all microRNAs [45]. In NIH3T3 *AGO2*-/- cells, the reduction of *let-7* family microRNA levels resulted in a concomitant increase in target *HMGA1/HMGA2* transcript levels (**Figure 5.5F**).

Despite reduced levels of microRNAs, mutant KRAS expression in the NIH3T3 *AGO2*-/- background showed a markedly reduced ability to generate foci compared to parental NIH3T3

(**Figure 5.6A**). Partial rescue of the ability to establish foci in these cells was achieved by overexpression of *AGO2* or $AGO2^{K98A}$ (which permits RAS interaction) but not the $AGO2^{K112A}$ mutant (which fails to bind RAS). These observations also support the notion that a direct association of oncogenic KRAS and AGO2 is required for mutant KRAS driven transformation. Further, consistent with the data presented thus far, NIH3T3 *AGO2*-/- cells stably expressing $KRAS^{G12V}$ showed reduced expression of mutant KRAS compared to that of NIH3T3 cells stably expressing $KRAS^{G12V}$ (**Figure 5.6B, top panel**). Also consistent with AGO2 overexpression elevating phospho-Akt levels in the presence of activated KRAS (**Figure 5.6B**), loss of AGO2 reduced phospho-Akt signaling by mutant KRAS and a slight increase in phospho-ERK signaling, suggesting that AGO2 may have an essential role in modulating the signaling outputs of activated KRAS in these cells. In addition, NIH3T3 *AGO2*-/- cells stably expressing $KRAS^{G12V}$ did not display the characteristic morphology of NIH3T3 $KRAS^{G12V}$ cells (**Figure 5.6B, bottom panel**). Sucrose density sedimentation analysis of NIH3T3 *AGO2*-/- showed that in contrast to NIH3T3 parental cells, RAS is restricted largely to the first four fractions of the gradient with minimal overlap with AGO1 complexes, indicating that RAS associates with higher molecular weight fractions through its interaction with AGO2 (**Figure 5.6C**). Finally, *in vivo* experiments in a mouse xenograft model showed significantly decreased tumor growth with NIH3T3 AGO2-/- cells expressing $KRAS^{G12V}$ compared to parental NIH3T3 cells expressing $KRAS^{G12V}$, further demonstrating a requirement for AGO2 for KRAS driven transformation (**Figure 5.6D**).

DISCUSSION

Functionally, we demonstrate that the RAS-AGO2 interaction is required for KRAS mediated oncogenesis. Mechanistically, mutant KRAS binding appears to attenuate AGO2 assembly into functional mRNP particles and may directly modulate microRNA levels (as demonstrated by *let-7* microRNA analysis). We also observed that AGO2 may play an important role in the signaling output mediated by mutant KRAS, particularly AKT-mTOR pathway.

Our data also suggests that binding of mutant KRAS to AGO2 inhibits AGO2 function, as seen by reduced *let-7* levels with concomitant increase in target mRNA (*HMGA*) expression. Importantly, experiments using mutants in both KRAS and AGO2 that abrogate binding of the respective partners, shows that the direct binding of mutant KRAS and AGO2 is necessary to elevate mutant KRAS levels and increased phospho-Akt signaling, leading to increased transformation potential (**Figure 5.6A-B**). Since we have used mutant KRAS constructs that do not have 3'UTR regions that bind microRNA, it remains unclear how AGO2 association can elevate mutant KRAS levels. Modulation of various microRNAs (other than *let-7* microRNA, that we describe here) that can bind open reading frames under stress may have a direct or indirect role in this process [34].

Recently, an association of mutant KRAS with the RNA machinery through binding to HNRNPA2B1 was reported[48], which also supports a likely interface of RAS with the RNA processing machinery, including with hub protein AGO2, as observed in our study. While the current study focused on characterization of the KRAS-AGO2 interaction and its role in mutant KRAS mediated transformation, a functional role of this interaction presents an intriguing subject for follow up studies.

The EGFR kinase was recently shown to phosphorylate AGO2 in response to hypoxia leading to inhibition of AGO2-mediated microRNA processing[15,49]. Similarly, the Akt serine threonine kinase was shown to phosphorylate AGO2 to inhibit *AGO2*-mediated mRNA endonucleolytic activity [50]. Interestingly, AGO2 phosphorylation also leads to inhibition of microRNA loading onto RISC complexes in the presence of mutant $HRAS^{G12V}$[51]. The identification of AGO2 as a critical partner of RAS, further provides a direct mechanistic link between RAS oncogenic signaling and RNA silencing. Illumination of such integral effector mechanisms of RAS may inform novel approaches to therapeutically target this frequently mutated cancer pathway.

MATERIALS AND METHODS

shRNA mediated knockdown and cell proliferation assays

H358, H460, MIA PaCa-2 and Panc-1 cells were treated with two independent shRNAs in viral vectors (validated Mission shRNA lentiviral particles, Sigma) targeting *KRAS* (TRCN0000040149, TRCN0000010369, TRCN0000040149) or *AGO2* (TRCN0000007865 and TRCN0000011203). After 5 days, cells were trypsinized and plated in triplicate at 5,000 cells per well in 24-well plates. For NIH3T3 stable lines, cells expressing the indicated plasmids were plated as mentioned earlier. The plates were incubated at 37 °C with 5% CO2. Cells were counted using Coulter counter at the indicated times.

Colony formation assay

Cells were treated with lentiviral particles expressing *AGO2* shRNA sequences in 6 well dishes. To select stably transfected clones, puromycin at 1 µg/ml was added to the cells two days after

transfection and allowed to grow over 10 days. Medium with selection antibiotic was changed every 2 days. Dishes were then stained using crystal violet, washed with water and photographed.

Focus formation assay

Foci formation assays were performed by transfecting/co-transfecting (the indicated constructs) 150,000 early passage NIH3T3 cells in 6 well dishes using Fugene HD (Promega). After two days, cells were trypsinized and plated onto 150 mm dishes containing 5% calf serum. The cells were maintained under low serum conditions and medium was refreshed every two days. After 21 days in culture the plates were stained for foci using crystal violet. Foci were also observed under the microscope to see the altered morphology and were counted manually. Three independent experiments were performed for each condition.

Generation of NIH3T3 stable lines

Early passage NIH3T3 mouse fibroblast cells were plated to 70% confluency and the indicated constructs were transfected using Fugene HD (Promega). Cells transfected with $KRAS^{G12V}$, upon selection with puromycin (1 µg/ul), showed distinct transformed morphology and continued to proliferate as clusters of cells (unlike naïve NIH3T3 cells). The $KRAS^{G12V}$ cells continued to grow in the absence of selection antibiotic and were further transfected with either empty vector (pDEST40) or FLAG-*AGO2* constructs. All the above transfected cells were then selected using G418 (200 µg/ml).

Site directed mutagenesis was performed to generate Y64G mutation in the KRASG12V plasmid, 12544, described earlier. NIH3T3 cells were transfected with this construct, selected using puromycin to generate polyclonal population of cells stably expressing KRASG12VY64G.

Generation of NIH3T3 *AGO2*-/- line

AGO2-knockout NIH3T3 cells were generated by CRISPR-Cas9-mediated genome engineering [47]. Genomic regions in murine *AGO2* between exons 8 and 9, and between exons 11and 12 were targeted for deletion using primers TCCTTGGTTACCCGATCCTGG and AGAGACTATCTGCAACTATGG, respectively (PAM motif underlined). PCR products were cloned into the BbsI site of pX458 (pSpCas9(BB)-2A-GFP; obtained from the laboratory of Feng Zhang via Addgene (Cambridge, MA; plasmid 48138)) according to the cloning protocol provided by the Zhang lab (http://www.genome-engineering.org). Cells were transfected with the vectors using Lipofectamine 3000 (Life Technologies) according to the manufacturer's instructions. 48 hours post-transfection, GFP-positive cells were FACS sorted as a single cell into 96-well plate. After culturing for 3 weeks, cells are distributed into two 24 well plates followed by PCR-based genotyping using primers mentioned above. A clone showing deletion of the targeted region in *AGO2* was used for further analysis. Single-cell sorted cells obtained after transfection of the empty pSpCas9(BB)-2A-GFP construct was used as a negative control. NIH3T3 AGO2-/- cells were also transfected with the KRASG12V plasmid construct to generate stable cell lines after puromycin selection.

Xenograft Models

Five week-old female C.B17/SCID mice were procured from a breeding colony at University of Michigan. Mice were anesthetized using a cocktail of xylazine (80 mg/kg, intraperitoneal) and ketamine (10 mg/kg, intraperitoneal) for chemical restraint. NIH3T3 cells stably expressing *AGO2*, $KRAS^{WT}$, $KRAS^{G12V}$ +vector or $KRAS^{G12V}$ + *AGO2* (0.5 or 1 million cells for each implantation site) were resuspended in 100 μL of 1× PBS with 20% Matrigel (BD Biosciences)

and were implanted subcutaneously into flank region on both sides. Eight mice were included in each experimental group. Tumor growth was recorded every two days by using digital calipers, and tumor volumes were calculated using the formula (π/6) (L × W2), where L = length of tumor and W = width. For the Mia PaCa-2 xenograft model, cells were first treated with either scrambled or *AGO2* shRNA overnight. After 2 days of puromycin selection the cells in each group were injected in 8 mice and the progression of tumor growth was monitored over time. To study oncogenic potential of NIH3T3 $KRAS^{G12VY64G}$ and NIH3T3 *AGO2-/-* cells *in vivo*, subcutaneous implantation of cells on both flanks of mice were performed as before (n=5 mice).

Four to five week old female SCID mice were used for all xenograft studies. Based on power calculation (http://www.biomath.info/power/index.htm), we determined that less than 6 mice per group are sufficient to detect significant differences in tumor volumes between two groups. All mouse experiments were done in a blinded fashion with mice being randomly selected for experiments. The person performing the measurements was blinded to the treatment groups. No animals were excluded in any of the xenograft experiments. All experimental procedures involving mice were approved by the University Committee on Use and Care of Animals at the University of Michigan and conform to their relevant regulatory standards.

Quantitative microRNA and mRNA RT-PCR

For the quantitation of microRNA levels in the NIH3T3 cells transfected with indicated constructs (from both the transient foci assays and stable lines), total RNA was prepared using the miRNeasy kit (Qiagen). MicroRNA RT-qPCR was performed according to the manufacturer's instructions (Applied Biosystems). U6 RNA was used as the endogenous control since its Ct values remained consistent. The vector transfected cells were used as reference.

For quantitation of mRNA transcripts, RNA was extracted from the indicated samples and cDNAs were synthesized using SuperScript III System according to the manufacturer's instructions (Invitrogen). Quantitative RT-PCR was conducted using primers detailed in **Table S4** with SYBR Green Master Mix (Applied Biosystems) on the StepOne Real-Time PCR System (Applied Biosystems). Relative mRNA levels of the transcripts were normalized to the expression of the housekeeping gene *GAPDH* and vector transfected cells were used as reference.

iSHiRLoC analyses

RNA oligonucleotides were purchased from Exiqon and IDT, respectively. RNA oligos were obtained with a 5` phosphate and, for the let-7-a1 guide strand, with a 3` Cy5 modification. All oligos were HPLC purified by the appropriate vendor. Oligonucleotide sequences are as follows,

let-7-a1 guide: P-UGA GGU AGU AGG UUG UAU AGU U-Cy5

let-7-a1-passenger: P-CUA UAC AAU CUA CUG UCU UUC C

RNA oligos were heat-annealed in a 1:1 ratio in 1x PBS, resulting in duplex RNAs, and were frozen for further use. Cells were cultured in DMEM (GIBCO) supplemented with 10% (v/v) fetal calf serum (FCS, Colorado serum) and 1x penicillin-streptomycin (GIBCO) at 37 ^{o}C. 1 - 1.25 x 10^5 cells were seeded onto delta-T dishes (Bioptechs) 4 days prior to microinjection, such that they were ~80% confluent at the time of microinjection. Regular medium was replaced with a minimal medium (HBS), without serum and vitamins, but containing 20 mM HEPES-KOH pH 7.4, 135 mM NaCl, 5 mM KCl, 1 mM $MgCl_2$, 1.8 mM $CaCl_2$ and 5.6 mM glucose immediately before microinjection. After microinjection, cells were incubated in phenol red-free DMEM

containing 2% (v/v) FBS in the presence of a 5% CO_2 atmosphere at 37 ^oC for the indicated amounts of time prior to imaging.

Microinjection was performed with samples containing 1 μM Cy5 labeled let-7-a1 duplexes and 0.05% (w/v) 10 kDa fluorescein dextran (Invitrogen) in PBS**.** Imaging was performed as described [43,44] using a cell-TIRF system based on an Olympus IX81 microscope equipped with a 60x 1.49 NA oil-immersion objective (Olympus), as well as 488 nm (Coherent ©, 100 mW at source, ~38 μW for imaging fluorescein) and 640 nm (Coherent ©, 100 mW at source, 13.5 mW for imaging Cy5) solid-state lasers. A quad-band filter cube consisting of a z405/488/561/640rpc dichroic filter (Chroma) and z405/488/561/640m emission filter (Chroma) was used to filter fluorescence of the appropriate fluorophore from incident light. Emission from individual fluorophores was detected sequentially on an EMCCD camera (Andor Ixon). Particle tracking analysis was performed by using tracks that spanned at least four video frames.

Pathscan Intracellular signaling array analysis

Pathscan intracellular signaling arrays were purchased from Cell Signaling. Indicated cells from the overexpression model or after knockdown were starved overnight and 40-80 μg of lysates generated from these were applied to the arrays. Arrays were processed according to the manufacturer's instructions and developed using chemiluminescent substrates. For the analysis ImageJ software was used and control spots indicated in (**Figure S10A**) were used to normalize the data. The quantitative bar charts shown in the study are for those signaling moelcules that show intensity levels of greater than 50 for each of the duplicate spots in any given treatment of overexpression or knockdown.

REFERENCES

1. Ha, M. & Kim, V.N. Regulation of microRNA biogenesis. *Nat Rev Mol Cell Biol* 15, 509-524 (2014).
2. Hata, A. & Lieberman, J. Dysregulation of microRNA biogenesis and gene silencing in cancer. *Sci Signal* 8, re3 (2015).
3. Fabian, M.R., Sonenberg, N. & Filipowicz, W. Regulation of mRNA translation and stability by microRNAs. *Annu Rev Biochem* 79, 351-379 (2010).
4. Ender, C. & Meister, G. Argonaute proteins at a glance. *J Cell Sci* 123, 1819-1823 (2010).
5. Schurmann, N., Trabuco, L.G., Bender, C., Russell, R.B. & Grimm, D. Molecular dissection of human Argonaute proteins by DNA shuffling. *Nat Struct Mol Biol* 20, 818-826 (2013).
6. Hauptmann, J., *et al.* Turning catalytically inactive human Argonaute proteins into active slicer enzymes. *Nat Struct Mol Biol* 20, 814-817 (2013).
7. Liu, J., Valencia-Sanchez, M.A., Hannon, G.J. & Parker, R. MicroRNA-dependent localization of targeted mRNAs to mammalian P-bodies. *Nat Cell Biol* 7, 719-723 (2005).
8. Leung, A.K., Calabrese, J.M. & Sharp, P.A. Quantitative analysis of Argonaute protein reveals microRNA-dependent localization to stress granules. *Proc Natl Acad Sci U S A* 103, 18125-18130 (2006).
9. Parker, R. & Sheth, U. P bodies and the control of mRNA translation and degradation. *Mol Cell* 25, 635-646 (2007).
10. Zeng, Y., Sankala, H., Zhang, X. & Graves, P.R. Phosphorylation of Argonaute 2 at serine-387 facilitates its localization to processing bodies. *Biochem J* 413, 429-436 (2008).
11. Rudel, S., *et al.* Phosphorylation of human Argonaute proteins affects small RNA binding. *Nucleic Acids Res* 39, 2330-2343 (2011).
12. Qi, H.H., *et al.* Prolyl 4-hydroxylation regulates Argonaute 2 stability. *Nature* 455, 421-424 (2008).
13. Sahin, U., Lapaquette, P., Andrieux, A., Faure, G. & Dejean, A. Sumoylation of human argonaute 2 at lysine-402 regulates its stability. *PLoS One* 9, e102957 (2014).
14. Stalder, L., *et al.* The rough endoplasmatic reticulum is a central nucleation site of siRNA-mediated RNA silencing. *EMBO J* 32, 1115-1127 (2013).
15. Shen, J., *et al.* EGFR modulates microRNA maturation in response to hypoxia through phosphorylation of AGO2. *Nature* 497, 383-387 (2013).
16. Zhang, X., *et al.* MicroRNA directly enhances mitochondrial translation during muscle differentiation. *Cell* 158, 607-619 (2014).
17. Huang, V., *et al.* Ago1 Interacts with RNA polymerase II and binds to the promoters of actively transcribed genes in human cancer cells. *PLoS Genet* 9, e1003821 (2013).
18. Janowski, B.A., *et al.* Involvement of AGO1 and AGO2 in mammalian transcriptional silencing. *Nat Struct Mol Biol* 13, 787-792 (2006).
19. Motamedi, M.R., *et al.* Two RNAi complexes, RITS and RDRC, physically interact and localize to noncoding centromeric RNAs. *Cell* 119, 789-802 (2004).

20. Noma, K., *et al.* RITS acts in cis to promote RNA interference-mediated transcriptional and post-transcriptional silencing. *Nat Genet* 36, 1174-1180 (2004).
21. Verdel, A., *et al.* RNAi-mediated targeting of heterochromatin by the RITS complex. *Science* 303, 672-676 (2004).
22. Qi, Y., *et al.* Distinct catalytic and non-catalytic roles of ARGONAUTE4 in RNA-directed DNA methylation. *Nature* 443, 1008-1012 (2006).
23. Allo, M., *et al.* Control of alternative splicing through siRNA-mediated transcriptional gene silencing. *Nat Struct Mol Biol* 16, 717-724 (2009).
24. Francia, S., *et al.* Site-specific DICER and DROSHA RNA products control the DNA-damage response. *Nature* 488, 231-235 (2012).
25. Wei, W., *et al.* A role for small RNAs in DNA double-strand break repair. *Cell* 149, 101-112 (2012).
26. Gregory, R.I., Chendrimada, T.P., Cooch, N. & Shiekhattar, R. Human RISC couples microRNA biogenesis and posttranscriptional gene silencing. *Cell* 123, 631-640 (2005).
27. Meister, G., *et al.* Identification of novel argonaute-associated proteins. *Curr Biol* 15, 2149-2155 (2005).
28. Chendrimada, T.P., *et al.* TRBP recruits the Dicer complex to Ago2 for microRNA processing and gene silencing. *Nature* 436, 740-744 (2005).
29. MacRae, I.J., Ma, E., Zhou, M., Robinson, C.V. & Doudna, J.A. In vitro reconstitution of the human RISC-loading complex. *Proc Natl Acad Sci U S A* 105, 512-517 (2008).
30. Hock, J., *et al.* Proteomic and functional analysis of Argonaute-containing mRNA-protein complexes in human cells. *EMBO Rep* 8, 1052-1060 (2007).
31. Liu, J., *et al.* A role for the P-body component GW182 in microRNA function. *Nat Cell Biol* 7, 1261-1266 (2005).
32. Meister, G. Argonaute proteins: functional insights and emerging roles. *Nat Rev Genet* 14, 447-459 (2013).
33. Hafner, M., *et al.* Transcriptome-wide identification of RNA-binding protein and microRNA target sites by PAR-CLIP. *Cell* 141, 129-141 (2010).
34. Karginov, F.V. & Hannon, G.J. Remodeling of Ago2-mRNA interactions upon cellular stress reflects miRNA complementarity and correlates with altered translation rates. *Genes Dev* 27, 1624-1632 (2013).
35. Paroo, Z., Ye, X., Chen, S. & Liu, Q. Phosphorylation of the human microRNA-generating complex mediates MAPK/Erk signaling. *Cell* 139, 112-122 (2009).
36. Benhamed, M., Herbig, U., Ye, T., Dejean, A. & Bischof, O. Senescence is an endogenous trigger for microRNA-directed transcriptional gene silencing in human cells. *Nat Cell Biol* 14, 266-275 (2012).
37. Yang, M., *et al.* Dephosphorylation of tyrosine 393 in argonaute 2 by protein tyrosine phosphatase 1B regulates gene silencing in oncogenic RAS-induced senescence. *Mol Cell* 55, 782-790 (2014).
38. Symonds, J.M., *et al.* Protein kinase C delta is a downstream effector of oncogenic K-ras in lung tumors. *Cancer Res* 71, 2087-2097 (2011).
39. Johnson, S.M., *et al.* RAS is regulated by the let-7 microRNA family. *Cell* 120, 635-647 (2005).
40. Qiu, R.G., Chen, J., Kirn, D., McCormick, F. & Symons, M. An essential role for Rac in Ras transformation. *Nature* 374, 457-459 (1995).

41. Shih, C., Padhy, L.C., Murray, M. & Weinberg, R.A. Transforming genes of carcinomas and neuroblastomas introduced into mouse fibroblasts. *Nature* 290, 261-264 (1981).
42. Shieh, A., *et al.* Defective K-Ras oncoproteins overcome impaired effector activation to initiate leukemia in vivo. *Blood* 121, 4884-4893 (2013).
43. Pitchiaya, S., Androsavich, J.R. & Walter, N.G. Intracellular single molecule microscopy reveals two kinetically distinct pathways for microRNA assembly. *EMBO Rep* 13, 709-715 (2012).
44. Pitchiaya, S., Krishnan, V., Custer, T.C. & Walter, N.G. Dissecting non-coding RNA mechanisms in cellulo by Single-molecule High-Resolution Localization and Counting. *Methods* 63, 188-199 (2013).
45. Diederichs, S. & Haber, D.A. Dual role for argonautes in microRNA processing and posttranscriptional regulation of microRNA expression. *Cell* 131, 1097-1108 (2007).
46. Lee, Y.S. & Dutta, A. The tumor suppressor microRNA let-7 represses the HMGA2 oncogene. *Genes Dev* 21, 1025-1030 (2007).
47. Ran, F.A., *et al.* Genome engineering using the CRISPR-Cas9 system. *Nat Protoc* 8, 2281-2308 (2013).
48. Barcelo, C., *et al.* Ribonucleoprotein HNRNPA2B1 Interacts With and Regulates Oncogenic KRAS in Pancreatic Ductal Adenocarcinoma Cells. *Gastroenterology* (2014).
49. McCarthy, N. MicroRNA: lacking in maturity. *Nat Rev Cancer* 13, 377 (2013).
50. Horman, S.R., *et al.* Akt-mediated phosphorylation of argonaute 2 downregulates cleavage and upregulates translational repression of MicroRNA targets. *Mol Cell* 50, 356-367 (2013).
51. Yang, M., *et al.* Dephosphorylation of Tyrosine 393 in Argonaute 2 by Protein Tyrosine Phosphatase 1B Regulates Gene Silencing in Oncogenic RAS-Induced Senescence. *Mol Cell* 55, 782-790 (2014).

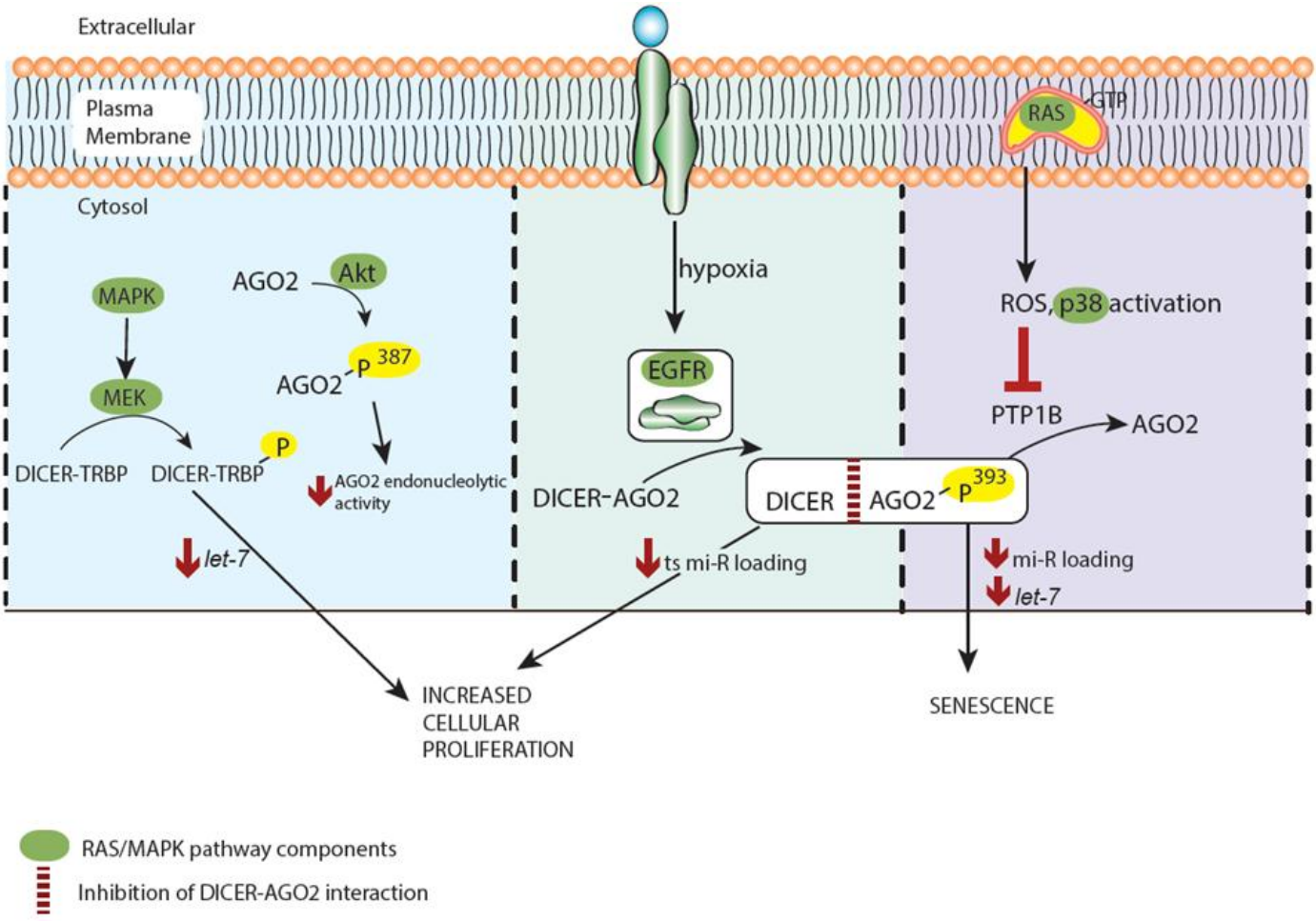

Figure 5.1 Components of the microRNA machinery are modulated by the RAS/MAPK pathway

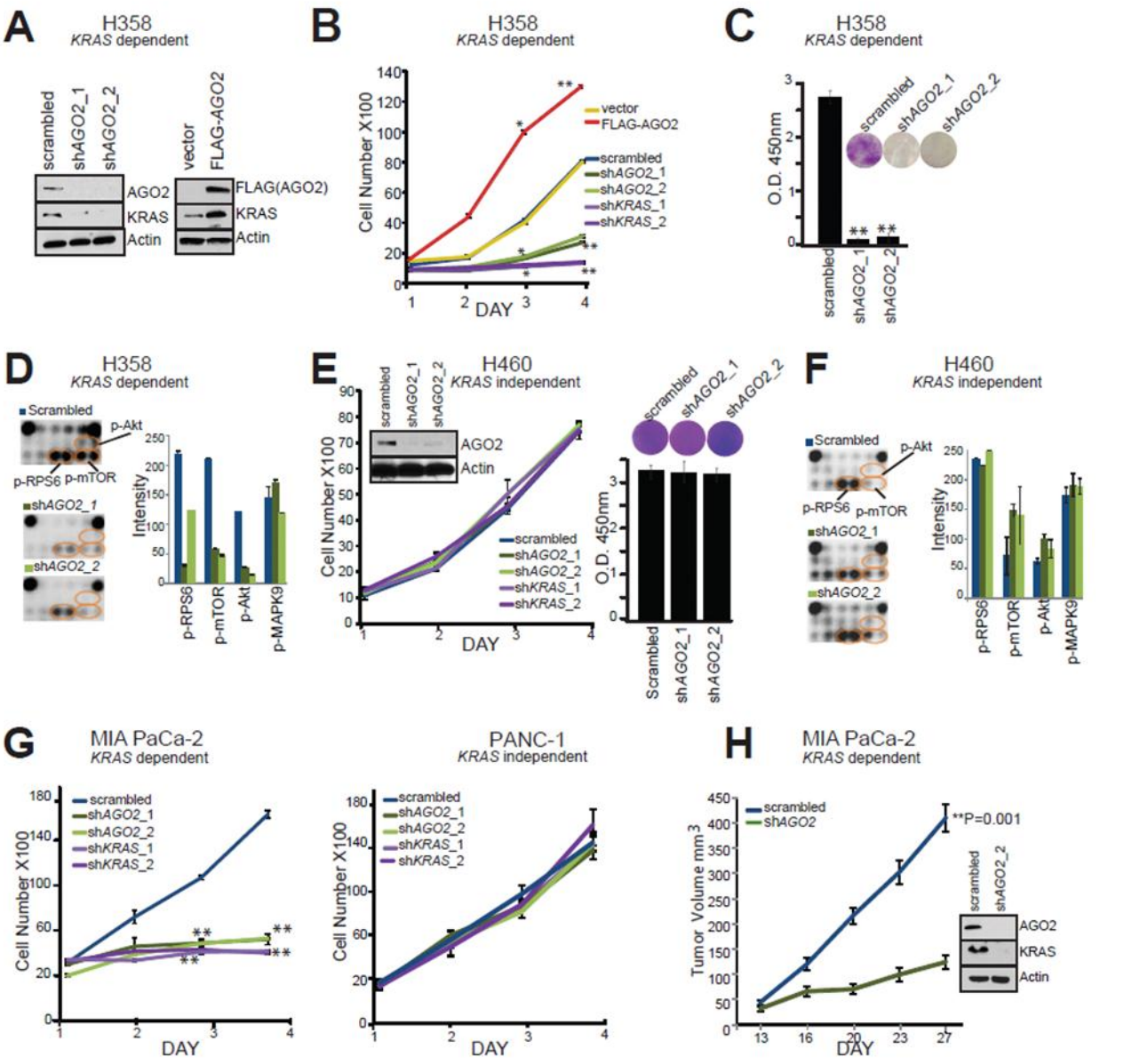

Figure 5.2 *AGO2* enhances mutant *KRAS* dependent growth by elevating KRAS protein expression (A) Immunoblot analysis of AGO2 and KRAS after knockdown or overexpression of *AGO2*. (**B**) Growth curves and (**C**) colony formation assays of mutant *KRAS* dependent H358 lung cancer cells, following either knockdown of *KRAS*/*AGO2* using shRNA or *AGO2* overexpression. Error bars are based on standard error of mean. *($P<0.05$) and **($P<0.005$) denote significant differences in growth at the indicated times compared to either scrambled or vector control. Data obtained from three independent experiments are shown (**D**) Pathscan intracellular signaling arrays probed with lysates from H358 cells following *AGO2* knockdown (**E**) Growth curves (left) and colony formation assays (right) of mutant *KRAS* independent H460 lung cancer cells, following knockdown of *KRAS*/*AGO2*. Data obtained from three independent experiments are shown. Inset, immunoblot analysis of AGO2 and KRAS after *AGO2* knockdown. (**F**) Intracellular signaling array probed with lysates from H460 following *AGO2* knockdown. (**G**) Growth curves of pancreatic cancer cells, MIA PaCa-2 (mutant KRAS dependent) (left) and PANC-1 (mutant KRAS independent) (right) following knockdown of *KRAS* or *AGO2*, as indicated. *($P<0.05$) and **($P<0.005$) denote significant differences in growth at the indicated times compared to scrambled control. Data obtained from three independent experiments are shown (**H**) *In vivo* growth of Mia PaCa-2 cells transiently treated with either scrambled shRNA or shRNA targeting *AGO2* prior to injecting in nude mice. For each group (n=8), one million cells were injected and average tumor volume (in mm^3) was plotted on y-axis and days after injection on the x-axis. Right, immunoblot analysis of AGO2 and RAS following *AGO2* knockdown in Mia PaCa-2 cells. Indicated P-value was calculated using two sided student t-test for the two groups.

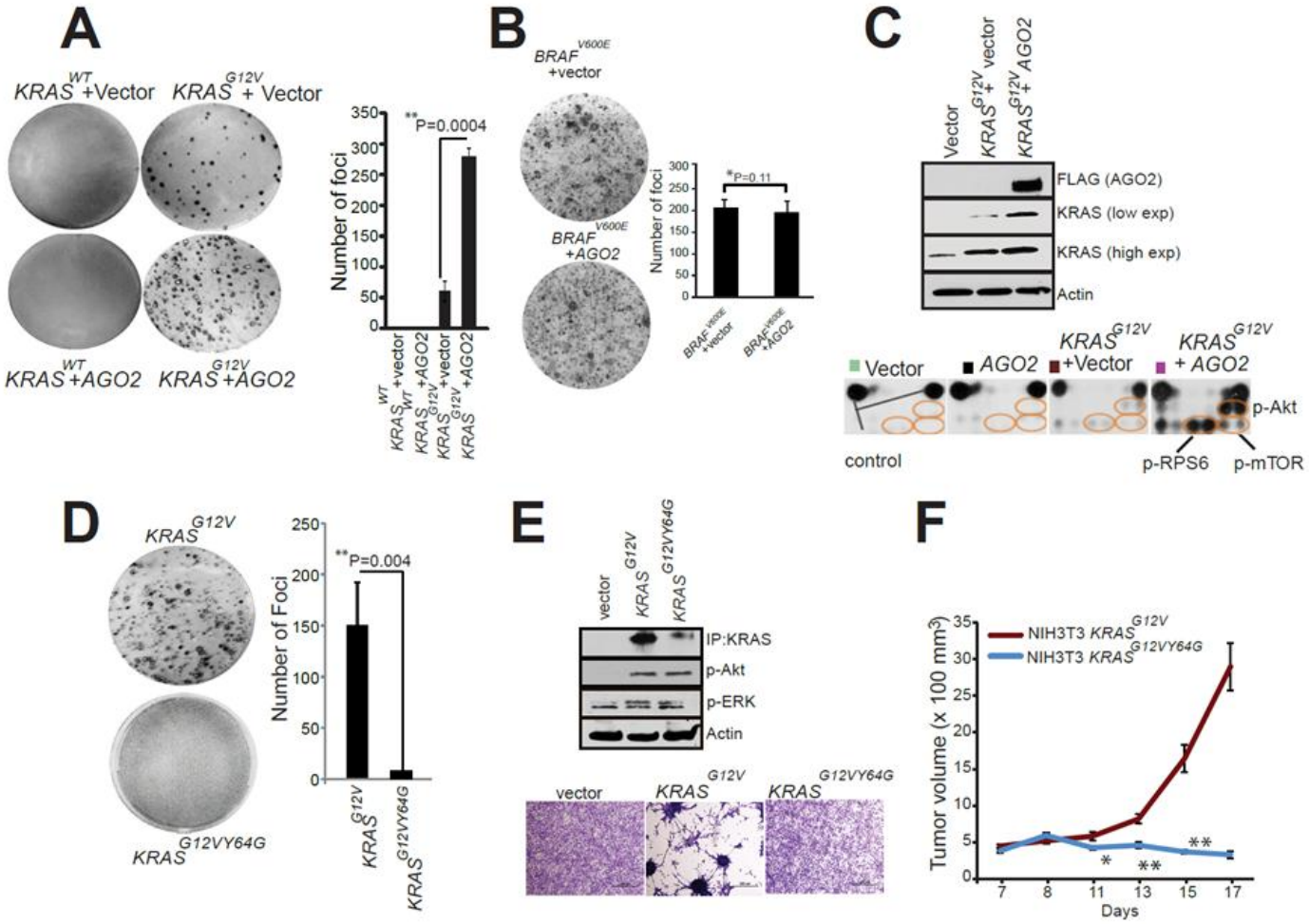

Figure 5.3 Mutant KRAS-AGO2 interaction promotes transformation (**A**) Representative images of foci formation assays using NIH3T3 cells co-transfected with $KRAS^{WT}$ or $KRAS^{G12V}$ and *AGO2* (left panel). Quantitation of foci from two technical replicate experiments (right panel). Foci assays were performed at least three times with similar results. P-value, calculated using two-sided student t-test between the two groups.(**B**) Representative images of foci formation assays using NIH3T3 cells co-transfected with $BRAF^{V600E}$ with or without *AGO2* (left panel). Quantitation of foci from two technical replicate experiments (right panel). Foci assays were performed at least three times with similar results. P-value, calculated using two-sided student t-test between the two groups (**C**) Immunoblot analysis shows increased levels of oncogenic KRAS levels in the presence of AGO2. Lower panel, intracellular signaling arrays probed with lysates from NIH3T3 cells stably expressing vector, *AGO2*, or $KRAS^{G12V}$±*AGO2*. The colored circles mark duplicate spots corresponding to p-AKT (S473), p-RPS6 (S235/236) and p-mTOR (S2448). (**D**) Representative images of foci formation assays using NIH3T3 cells co-transfected with $KRAS^{G12V}$ or $KRAS^{G12VY64G}$. Quantitation of foci from two independent experiments (right). Indicated P-value was calculated using two-sided student t-test. (**E**) KRAS immunoprecipitation (using sc-521 pAb) followed by immunoblot analysis (RAS10 mAb) showing low levels of oncogenic KRAS protein expression in NIH3T3 cells stably expressing $KRAS^{G12VY64G}$, despite similar phospho-Akt activation. Lower panel shows morphology of indicated stable lines grown in 10% serum upon crystal violet staining. **(F**) *In vivo* growth of NIH3T3 cells stably overexpressing $KRAS^{G12V}$ and $KRAS^{G12VY64G}$ in nude mice. For each group (n=8), 500,000 cells were injected and average tumor volume (in mm^3) was plotted on y-axis and days after injection on the x-axis.

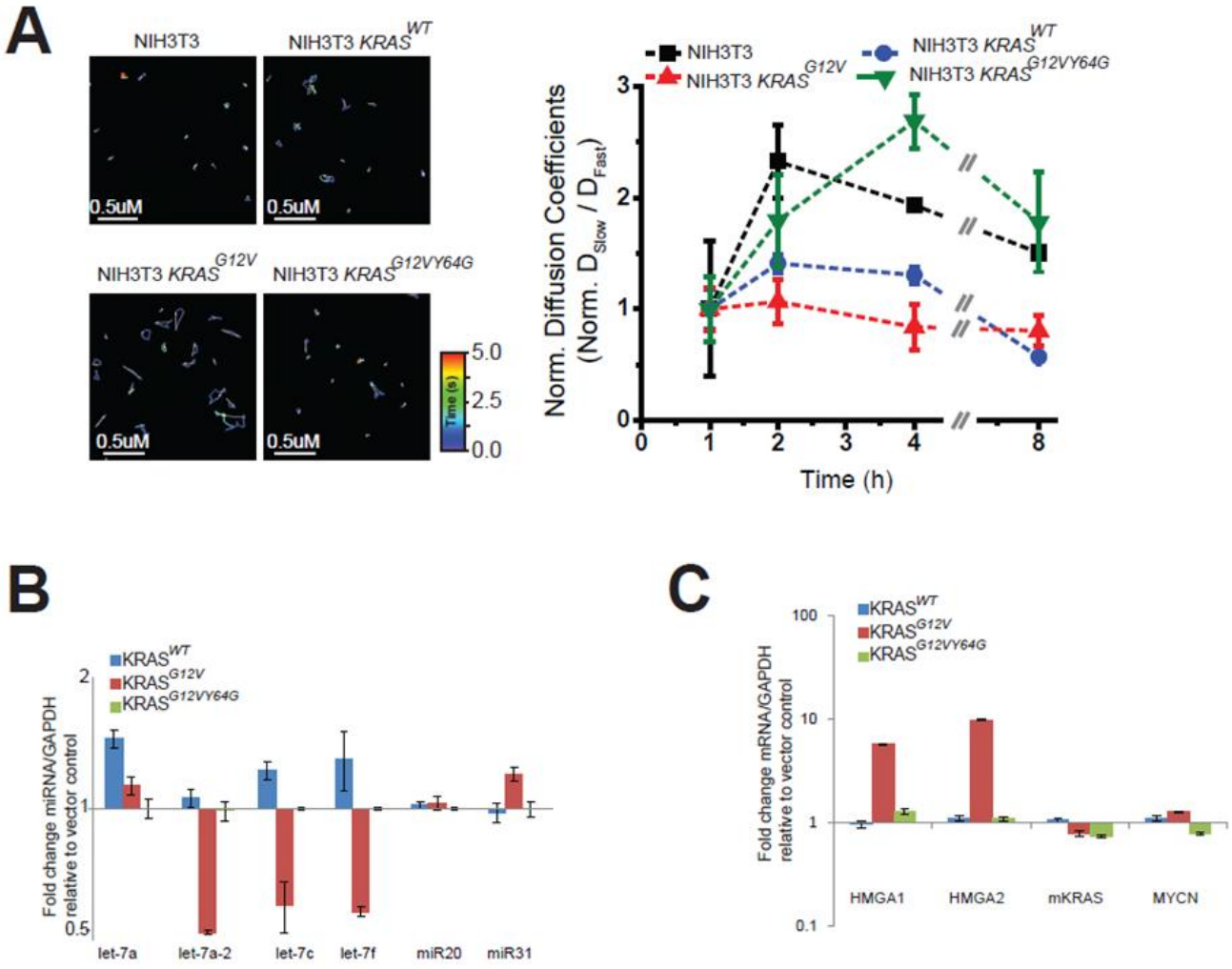

Figure 5.4 *KRAS*^{G12VY64G} fails to limit *let-7a* in small RNP particles. (**A**) Distribution of let-7a-1–Cy5 diffusion coefficients at different time points following microinjection in parental NIH3T3, NIH3T3-*KRAS*^{G12V} and NIH3T3-*KRAS*^{G12V,Y64G} cells, as described earlier. The fast (green) and slow (red) diffusing particles (demarcated by the dotted lines to guide the eye) were defined based on segregation of the two Gaussian distributions 2h after microinjection. Blue shaded region represents the diffusion coefficients lost due to limited time resolution of tracking. Number of particles analyzed is mentioned within each histogram. **(B)** from NIH3T3 cells stably expressing *KRAS*^{WT}, *KRAS*^{G12V} or *KRAS*^{G12VY64G} constructs. U6 RNA and GAPDH mRNA were used as controls to normalize the microRNA and mRNA data respectively and vector transfected cells were used as reference. (**C**) Target genes HMGA1/2, KRAS and MYCN are known to be regulated by *let-7* microRNA. Error bars show standard error of the mean of 4 replicates and asterisks indicate significant log2 fold changes (two sided t-test, P-value less than 0.05) between the indicated conditions compared to vector control.

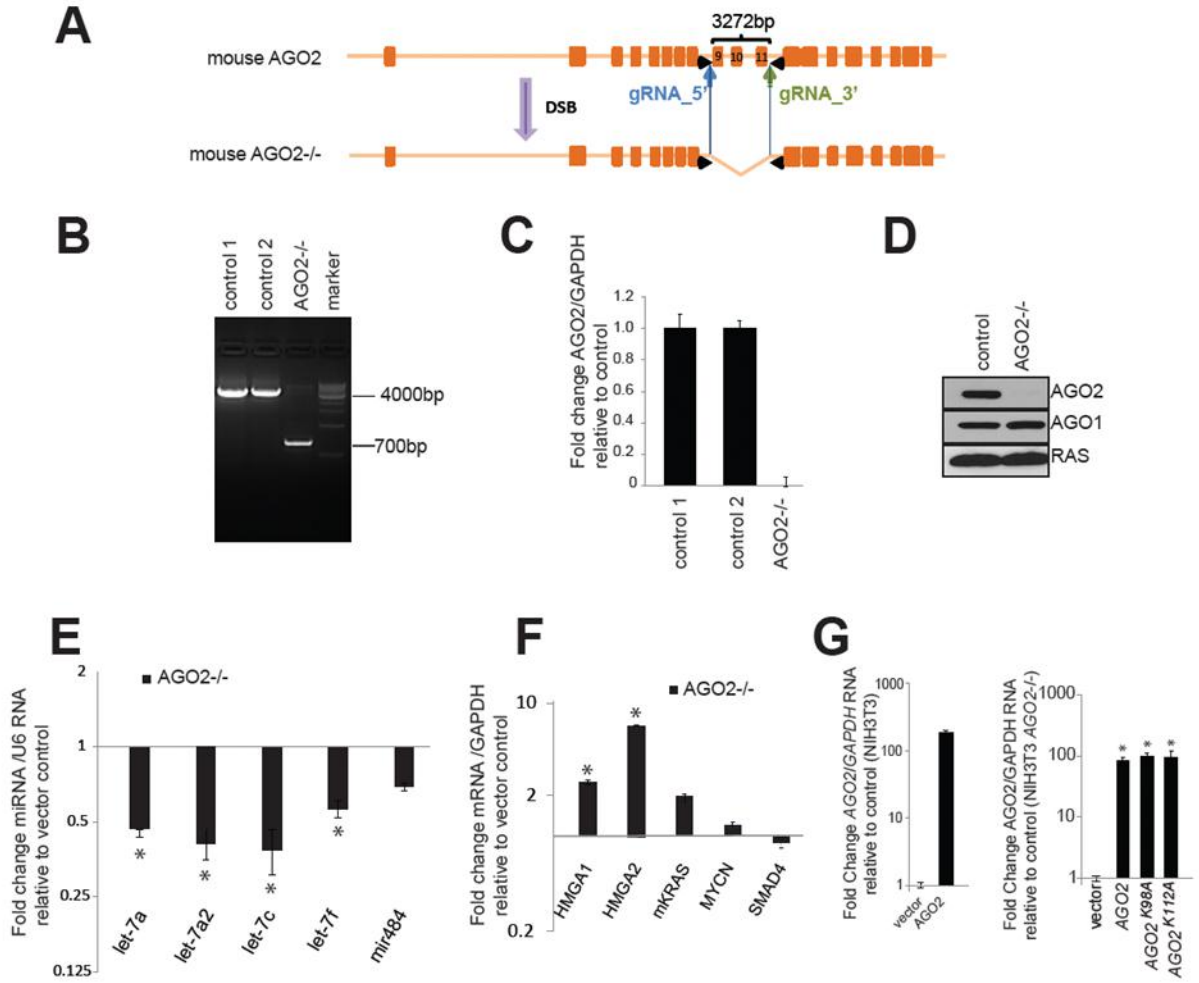

Figure 5.5 Generation and characterization of NIH3T3 *AGO2-/-* cells. (A) Schematic showing the use of the CRISPR/Cas9 methodology to knockout *AGO2* in NIH3T3 cells. Validation of *AGO2* knockout was performed using genomic PCR **(B)**, RT-qPCR **(C)**, and immunoblot analysis **(D)**. qPCR analysis of *let-7* family microRNAs **(E)** and their target genes **(F)** in NIH3T3 *AGO2*-/- cells. Both the microRNA and transcript levels were compared to NIH3T3 cells treated with vector with no guide RNA. Error bars show standard error of the mean of 4 technical replicates and asterisks indicate significant log2 fold changes (two sided t-test, P-value less than 0.05) between the indicated conditions. **(G)** qPCR analysis of *AGO2* transcripts in NIH3T3 (left) and NIH3T3 *AGO2*-/- (right) cells two days after transfection for foci formation assay, demonstrating similar levels of expression of *AGO2* constructs. Error bars show standard error of the mean of 3 technical replicates and asterisks indicate significant log10 fold changes (two sided t-test, P-value less than 0.005) in *AGO2* expression over that of the vector control.

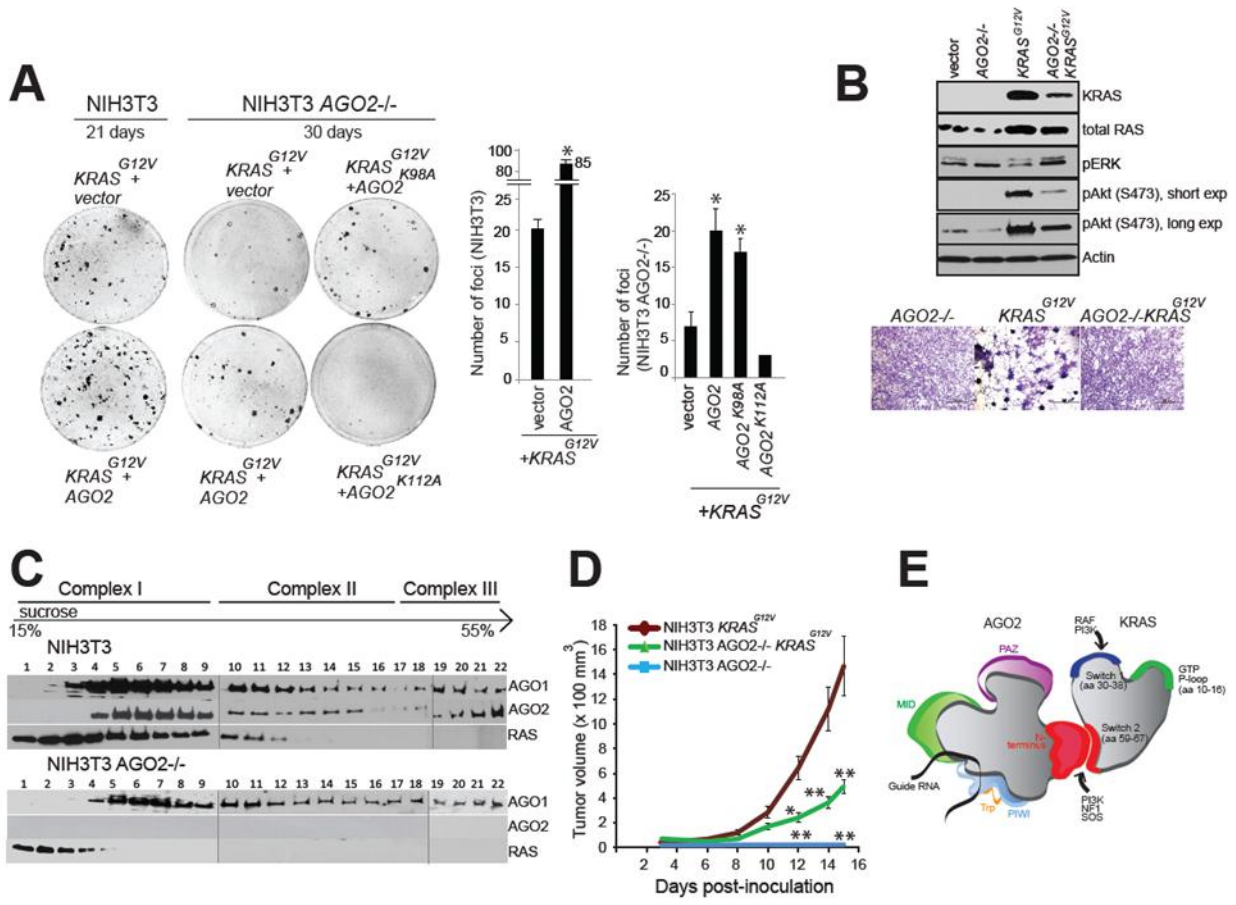

Figure 5.6 AGO2 interaction is required for maximal oncogenic potential of mutant KRAS (**A**) Left, representative images of *KRAS*^{G12V} driven foci in NIH3T3 and NIH3T3 *AGO2-/-* cells upon co-transfection with various *AGO2* constructs. Right, quantitation of foci from two replicate experiments. Error bars show standard error of mean and asterisks indicate P values less than 0.005 for the indicated conditions compared to vector control. (**B**) Upper panel, Immunoblot analysis showing reduced expression of oncogenic KRAS in *KRAS AGO2-/-* stably expressing *KRAS*^{G12V} and the extent of phospho-ERK and phospho-AKT activation in these cells. Lower panel shows crystal violet staining of indicated stable lines grown in 10% serum. (**C**) Sucrose density gradient fractionation of parental NIH3T3, NIH3T3 *KRAS*^{G12V} and NIH3T3 *AGO2-/-* cell lysates followed by immunoblot detection of RAS, AGO1 and AGO2 proteins. (**D**) *In vivo* growth of NIH3T3 or NIH3T3 *AGO2-/-* cells stably expressing *KRAS*^{G12V} in nude mice. For each group (n=8), 500,000 cells were injected and average tumor volume (in mm^3) was plotted on y-axis and days after injection on the x-axis. Error bars are standard error of mean * P<0.05 and ** P<0.005 at the indicated times. (**E**) Schematic representation of the N-terminal domain of AGO2 interacting with the switch II domain in RAS.

Source	Gene	Primer sequence (5'- 3')
Human	AGO2_F	ACCCACCCCACCGAGTTCGAC
Human	AGO2_R	AGTGCGAAGGCCTGCTTGTCC
Human	GAPDH-F	TGTAGTTGAGGTCAATGAAGGG
Human	GAPDH-R	GAGTCCTTCCACGATACCAAAG
Human	AGO2_orf_F	GCACTATCACGTCCTCTGGG
Human	AGO2_orf_R	GGTGTGACACAGCTGGTAGG
Human	KRAS_orf_F	ACACAAAACAGGCTCAGGACT
Human	KRAS_orf_R	AGGCATCATCAACACCCTGT
Human	KRAS_F	TCGACACAGCAGGTCAAGAGGAG
Human	KRAS_R	AGAAAGCCCTCCCCAGTCCTCA
Mouse	MYCN	ACAGAACTGATGCGCTGGAAT
Mouse	MYCN	GGCTGAAGCTTACAGTCCCAA
Mouse	HMGA1_F	CCTCTGGACGGTTGTGTTGT
Mouse	HMGA1_R	TGGGGGAGAGAATACAGGCA
Mouse	HMGA2_F	TGTGCCCTCTGACTTCGTTC
Mouse	HMGA2_R	AGCAAGCCGTCCAAGTACAA
Mouse	KRAS_F	GTTAGCTCCAGTGCCCCAAT
Mouse	KRAS_R	ATTCCCTAGGTCAGCGCAAC

Table 5.1 PCR primers used in this study. orf:open reading frame

CHAPTER 6

DISCUSSION AND FUTURE DIRECTIONS

The physical association of RAS, a signaling hub, with the core component of RNA silencing complex described here, presents exciting new insights for both RAS and AGO2 function, as well as having wider implications not addressed in this thesis. From the discovery of the RAS-AGO2 interaction to its relevance in normal/oncogenic processes, this concluding chapter attempts to connect the intriguing observations made in this study, with broader cellular processes mediated by the two well characterized entities.

Identification of the RAS-AGO2 interaction

It is the unbiased approach of mass spectrometric analysis of endogenous RAS immunoprecipitates that helped identify AGO2 as an interacting partner (**Chapter 4**). Use of a well characterized pan-RAS antibody for immunoprecipitation, used by most labs studying RAS, circumvented issues related to ectopic overexpression RAS, its localization, and potential interference of expression tags in protein-protein interactions; this provided us an opportunity to study RAS interacting proteins in a variety of lung and pancreatic cancer cell line models. Importantly, use of this antibody also excluded some of the canonical RAS interacting proteins that involve Switch I domain, facilitating identification of proteins that bind the Switch II domain.

The only previous report of a physical association of Argonaute with a GTPase is that of a PUF-AGO-eEF1A complex[1] which attenuates translation elongation. Lack of evidence for genetic interaction in knockout mouse models of RAS and AGO2 may likely be due to an essential requirement for both KRAS[2] and AGO2[3] in early development. Previous studies using mass spectrometric analysis of AGO2 interactors have used a 25kda cut-off likely narrowly missing the 21kDa small GTPase[4]. Further, AGO2 antibodies used to demonstrate endogenous RAS co-immunoprecipitation requires the use of increased salt concentration (300mM) during washing of the immunoprecipitates, suggesting that RNA-dependent mRNP complexes bound indirectly to AGO2 may need to be detached before the fraction that binds RAS is uncovered.

Is AGO2 a RAS effector?

The surprising discovery and subsequent validation of RAS and AGO2 peptides in the mass spectrometric analysis in all the cell lines tested, suggested that AGO2 binds RAS in a nucleotide agnostic manner. Indeed, we have demonstrated that both RAS-GDP and RAS-GTP bind AGO2 with equal efficiency, however GTP bound RAS may have distinct effects on AGO2 function, known to be sensitive to magnesium ions[5], which incidentally are also integral to nucleotide exchanges on RAS[6].

Our studies of AGO2 activity in the context of GDP/GTP bound KRAS, suggest that AGO2 function is inhibited when oncogenic KRAS binds AGO2, as evidenced by both reduced *let-7* levels and lack of *let-7* in functional mRNPs (**Figure 5.4**). Since AGO2 is known to stabilize microRNA levels[7], oncogenic RAS associated with AGO2 may result in decreased capacity of microRNAs to bind AGO2 and ultimately result in their degradation.

Considering that AGO2 is central to the RNA silencing machinery and thus controls expression of both proliferative and suppressive messages in the cells, local and compartmentalized effects of oncogenic RAS on AGO2 function may elicit specific proliferative signals. Moreover, the binding of mutant RAS to AGO2 under oncogenic conditions in the cell may also restrict movement of AGO2 to P-bodies that are cytoplasmic hubs of gene silencing, thereby increasing cellular protein translation levels in general. Post translational modifications of AGO2[8,9] that are being identified in different signaling contexts may in turn affect its association with RAS.

Considerable work needs to be performed to delineate and tease out AGO2 mechanisms that are direct and indirect consequences of oncogenic KRAS binding.

Why AGO2?

Although the four mammalian AGO family members have overlapping functions[10], AGO2 binds microRNA most efficiently, stabilizes microRNAs[7], binds to coding regions of the transcripts[11] and is the only AGO protein that has endonucleolytic activity[12]. The AGO proteins differ most in their N-terminal sequences and in AGO2, two motifs in N-domain control the unique endonucleolytic activity of the protein[13,14]. We have also narrowed the region of RAS interaction to a stretch of about 100 amino acids (aa 50-141) in between these two motifs such that RAS binding may change the conformation of AGO2 or simply interfere with the endonucleolytic catalytic center of its PIWI domain. Even more fascinating is that the precise stretch involved in RAS binding has been identified as the 'wedge region'[15] of AGO2 that is involved in removal of the passenger strand of the small RNA duplex, critical for its loading into the RISC. Through

contacts with this unique structural motif of the AGO2 N domain, RAS could have a direct bearing on its microRNA binding and endonucleolytic activity.

Both post translational modifications of KRAS and AGO2 and/or compartment specific protein interactions may provide localized clustering of these proteins for interaction, further suggesting a preference for AGO2 over other clade members of the Argonaute family.

The role of the RAS Switch II domain in AGO2 binding

Both the conserved Switch I and Switch II domains in RAS undergo conformational change upon nucleotide binding. Unlike the RAS-effectors that bind the Switch I domain (RAF, PI3K, RALGDS)[16] or RAS-regulators that bind the Switch II domain in a nucleotide dependent manner (NF1 only binds RAS-GTP, SOS1 only binds RAS-GDP) our studies show that AGO2 binds RAS in a nucleotide agnostic manner.

Considering that KRASY64 is critical for both SOS1 and AGO2 binding, could AGO2 compete with SOS1 for KRAS binding? If so, what would be the consequences of such competition for KRAS signaling and transformation? If not, are there other residues in the Switch II domain that are critical for AGO2 association. Also importantly, does intracellular compartmentalization of KRAS determine preferred binding to AGO2? AGO2-activity based assays will help determine the effects of wild type versus mutant KRAS binding on AGO2 function.

While we observed that expression of oncogenic KRAS but not “oncogenic KRAS with Y64G mutation”, inhibits AGO2 function (reduced *let-7* levels and mRNP complexes), expression of the wild type KRAS protein had no such effect. As mentioned earlier, this suggests that mutant RAS binding through the wedge domain of AGO2, possibly interferes with duplex

unwinding and proper RISC assembly[15]. Whether the structural changes in mutant KRAS caused due to constitutive GTP loading, leads to a direct inhibition of AGO2 function or prevents its shuttling to cellular compartments or simply altersthe profile of its protein/RNA interactions is yet to be determined.

Experiments to elucidate biochemical and functional differences between wild type and mutant KRAS with respect to modulation of AGO2 activity are underway.

Role of AGO2 in mutant KRAS driven cellular transformation

Cellular transformation assays using NIH3T3 mouse fibroblasts, the earliest models to study RAS function, showed that AGO2 potentiates KRAS mediated cellular transformation. Conversely, knockdown of AGO2 using small hairpin RNA silencing molecules also showed a dependency of cellular growth on AGO2 levels in a mutant KRAS dependent manner. While overexpression of AGO2 increases mutant KRAS expression and activates the PI3K/Akt/mTOR pathway, knockdown decreases mutant KRAS levels to reduce signaling.

The oncogenic double mutant used in our study ($KRAS^{G12VY64G}$) was intriguing in many aspects since it had lost oncogenic potential and yet, showed increased activation of the RAS effector pathways. Most relevant and consistent with our understanding of the KRAS-AGO2 interaction, $KRAS^{G12VY64G}$ expressing cells failed to inhibit RISC formation in the iSHirLoC assay and showed no reduction in *let-7* levels, suggesting that failure to bind AGO2 abrogates the ability of oncogenic KRAS to inhibit AGO2 function. Yet expression of $KRAS^{G12VY64G}$, elevates both phospho-Erk and phospho-Akt signaling in cells. While the substitution of Y64 residue in the Switch II domain may have no bearing on the RAF/MEK/Erk pathway, Akt activation through PI3K was predicted to be diminished since PI3K binds KRAS-GTP through

Y64 to elevate phospho-Akt levels. This suggests that indirect mechanisms of Akt/mTOR activation may be responsible for elevated phospho-Akt levels in these cells. Recent work suggests that STAT3 pathway may be more active in the mutant KRAS pancreatic cell context [17] and will need to be explored in these cells.

But the nexus of AGO2 regulating mutant KRAS levels and PI3K pathway was most apparent, when we tested the potential of mutant KRAS to generate tumors in NIH3T3 cells deleted for *AGO2* using CRISPR/Cas9 system. In this scenario, cells lacking *AGO2*, limited both mutant KRAS expression levels and showed reduced activation of phospho-Akt levels, establishing a previously unknown connection between AGO2 and the PI3K pathway.

Can AGO2 be the missing puzzle piece of RAS function?

Despite the vast knowledge of effector function of RAS, the ability to target this function remains limited. Neither inhibitors of downstream RAS effectors, nor inhibitors of RAS membrane targeting mechanisms have yielded benefits to patients with mutant RAS driven tumors. Integrating AGO2 interaction and inhibition of its RNA silencing activities, as one of the functions of mutant KRAS could explain some of the anomalies reported in literature.

Through modulation of the microRNA based machinery, context dependent RAS signaling observed in various models of pancreatic, lung and colon cancer can be explained. Given that microRNA profiles of different cells are distinct, the lack of mutant KRAS specific gene signatures can also be explained through regulation of AGO2 function. Inconsistencies observed in synthetic lethal screens and cell line specific effects also can be attributed to post transcriptional gene silencing mechanisms rather than simple linear effects of RAF/MAPK/ERK or PI3K/Akt/mTOR pathway activation, which are highly conserved and identical in most cells.

Without clear evidence of nuclear reprogramming, the vast number of oncogenic activities of mutant RAS in different models also remains unexplained.

The prevalence of RASopathies suggests that RAS function is compromised during development in these patients. RAS/RAS pathway mutants detected in these patients, show activated RAS-GTP but remain unresponsive to MEK/PI3K inhibition in various models. Activation of RAF/PI3K pathways alone, fails to explain the breadth of the neurological and cytoskeletal deformities observed in these patients.

Differential binding affinities of various RAS mutants to AGO2 or different effects on AGO2 function could also explain how mutant RAS can manipulate the RNA silencing machinery to reprogram cells without direct entry into the nucleus. Given that other regulators like NF1 and SOS1 fail to bind the oncogenic form of RAS (due to conformation change of Switch II region), AGO2 remains the only protein that continues to associate with oncogenic KRAS through its binding to the Switch II domain. In this context, it is intriguing that the new inhibitors of KRAS [18-21] make contacts in the switch II region of KRAS where it is likely that they interfere with AGO2 function.

Exploring RAS-AGO2 interaction in genetic models

The study of functional aspects of the RAS-AGO2 interaction in established genetically engineered lung and pancreatic cancer mouse models of mutant KRAS (crossed with AGO2 conditional lethal mouse models) are still awaited. In parallel, other genetic models like *Saccharomyces cerevisiae*, *Drosophila melanogaster*, *Caenorhabditis elegans*, Arabidopsis need to be explored, retrospectively, as experimental models to trace the evolutionary conservation of the RAS-AGO2 interaction. Here, it is interesting to note that *S. cerevisiae* lacks both the

Argonaute mediated RNA silencing pathway [12] and the PI3K pathway [22], both of which are critical for maximal RAS driven cellular transformation (**Figure 5.6**). Of the 93 small GTPases found in Arabidopsis, RAS homologs are curiously not conserved, limiting the use of both the *S. cerevisiae* and Arabidopsis as genetic models.

While the *C.elegans* genome encodes RAS GTPase similar to the mammalian form, it has 27 Argonaute protein homologs, which largely perform RNA silencing functions with exogenous or endogenous siRNAs involving various Argonautes with or without endonucleolytic activity[23]. It is possible that Argonautes using microRNA based RNA silencing may be involved in RAS mediated signaling. Interestingly a *C.elegans* Argonaute protein CSR-1, homolog of mammalian *AGO1*, was shown to coimmunoprecipitate with translational GTPase, *EEF1A*, to attenuate translation elongation. Both, the interaction and function, was also conserved in mammalian cells, providing the only evidence of a direct interaction between an Argonaute protein and a GTPase[1]. The same Argonaute gene, *csr-1*, was also found to be required in combination with *ksr-1* (kinase suppressor of RAS signaling) providing a genetic evidence for a role for small RNAs and post transcriptional gene silencing in RAS-ERK pathway[24]. Since AGO2 also regulates KRAS levels through small RNA, alternate approaches using binding competent/incompetent rescue mutants will help tease the direct and indirect effects of the RAS-AGO2 interaction.

The Drosophila eye development as a genetic model remains the best model to extrapolate our findings of a direct interaction between mammalian RAS and AGO2. The fruit fly has both the RAS protein, which shares extensive homology to mammalian RAS and has only 4 Argonaute proteins of which *dAGO1* is closely related to human *AGO2* (even retaining one of the residues required for RAS interaction, identified in our study). Elegant studies using *RAS*

mutants that rescue the lethality associated with *RAS* null allele have been performed to demonstrate the role of the RAS/RAF/MEK/ERK pathway in eye development [25]. Yet not all functions of RAS could be restored by effector domain mutants that bind differentially to RAF/PI3K and mechanisms controlling the thresholds of RAS effector pathway were shown to specify distinct cellular responses of the same photoreceptor cells. A direct role for Argonaute and small RNA based silencing machinery in these RAS models can be performed once we demonstrate the interaction between RAS and AGO2 in Drosophila cells.

While probing the interaction to better understand human cancers, the study of evolutionarily primitive model organisms with different RAS-like signaling molecules and silencing mechanisms using different Argonaute proteins will provide insights into the evolutionary underpinnings of the RAS-AGO2 interaction.

REFERENCES

1. Friend, K., *et al.* A conserved PUF-Ago-eEF1A complex attenuates translation elongation. *Nat Struct Mol Biol* **19**, 176-183 (2012).
2. Johnson, L., *et al.* K-ras is an essential gene in the mouse with partial functional overlap with N-ras. *Genes Dev* **11**, 2468-2481 (1997).
3. Lykke-Andersen, K., *et al.* Maternal Argonaute 2 is essential for early mouse development at the maternal-zygotic transition. *Mol Biol Cell* **19**, 4383-4392 (2008).
4. Hock, J., *et al.* Proteomic and functional analysis of Argonaute-containing mRNA-protein complexes in human cells. *EMBO Rep* **8**, 1052-1060 (2007).
5. Schwarz, D.S., Tomari, Y. & Zamore, P.D. The RNA-induced silencing complex is a Mg2+-dependent endonuclease. *Curr Biol* **14**, 787-791 (2004).
6. Rudack, T., Xia, F., Schlitter, J., Kotting, C. & Gerwert, K. The role of magnesium for geometry and charge in GTP hydrolysis, revealed by quantum mechanics/molecular mechanics simulations. *Biophys J* **103**, 293-302 (2012).
7. Diederichs, S. & Haber, D.A. Dual role for argonautes in microRNA processing and posttranscriptional regulation of microRNA expression. *Cell* **131**, 1097-1108 (2007).
8. Yang, M., *et al.* Dephosphorylation of tyrosine 393 in argonaute 2 by protein tyrosine phosphatase 1B regulates gene silencing in oncogenic RAS-induced senescence. *Mol Cell* **55**, 782-790 (2014).
9. Horman, S.R., *et al.* Akt-mediated phosphorylation of argonaute 2 downregulates cleavage and upregulates translational repression of MicroRNA targets. *Mol Cell* **50**, 356-367 (2013).
10. Su, H., Trombly, M.I., Chen, J. & Wang, X. Essential and overlapping functions for mammalian Argonautes in microRNA silencing. *Genes Dev* **23**, 304-317 (2009).
11. Hafner, M., Lianoglou, S., Tuschl, T. & Betel, D. Genome-wide identification of miRNA targets by PAR-CLIP. *Methods* **58**, 94-105 (2012).
12. Ender, C. & Meister, G. Argonaute proteins at a glance. *J Cell Sci* **123**, 1819-1823 (2010).
13. Hauptmann, J., *et al.* Turning catalytically inactive human Argonaute proteins into active slicer enzymes. *Nat Struct Mol Biol* **20**, 814-817 (2013).
14. Kidwell, M.A. & Doudna, J.A. Activating silent Argonautes. *Nat Struct Mol Biol* **20**, 769-771 (2013).
15. Kwak, P.B. & Tomari, Y. The N domain of Argonaute drives duplex unwinding during RISC assembly. *Nat Struct Mol Biol* **19**, 145-151 (2012).
16. Vojtek, A.B., Hollenberg, S.M. & Cooper, J.A. Mammalian Ras interacts directly with the serine/threonine kinase Raf. *Cell* **74**, 205-214 (1993).
17. Corcoran, R.B., *et al.* STAT3 plays a critical role in KRAS-induced pancreatic tumorigenesis. *Cancer Res* **71**, 5020-5029 (2011).
18. Burns, M.C., *et al.* Approach for targeting Ras with small molecules that activate SOS-mediated nucleotide exchange. *Proc Natl Acad Sci U S A* **111**, 3401-3406 (2014).
19. Cox, A.D., Fesik, S.W., Kimmelman, A.C., Luo, J. & Der, C.J. Drugging the undruggable RAS: Mission possible? *Nat Rev Drug Discov* **13**, 828-851 (2014).

20. Sun, Q., *et al.* Discovery of small molecules that bind to K-Ras and inhibit Sos-mediated activation. *Angew Chem Int Ed Engl* **51**, 6140-6143 (2012).
21. Ostrem, J.M., Peters, U., Sos, M.L., Wells, J.A. & Shokat, K.M. K-Ras(G12C) inhibitors allosterically control GTP affinity and effector interactions. *Nature* **503**, 548-551 (2013).
22. Wera, S., Bergsma, J.C. & Thevelein, J.M. Phosphoinositides in yeast: genetically tractable signalling. *FEMS Yeast Res* **1**, 9-13 (2001).
23. Yigit, E., *et al.* Analysis of the C. elegans Argonaute family reveals that distinct Argonautes act sequentially during RNAi. *Cell* **127**, 747-757 (2006).
24. Rocheleau, C.E., *et al.* The Caenorhabditis elegans ekl (enhancer of ksr-1 lethality) genes include putative components of a germline small RNA pathway. *Genetics* **178**, 1431-1443 (2008).
25. Halfar, K., Rommel, C., Stocker, H. & Hafen, E. Ras controls growth, survival and differentiation in the Drosophila eye by different thresholds of MAP kinase activity. *Development* **128**, 1687-1696 (2001).

APPENDIX

Supplementary Information for the individual chapters presented in this thesis can be obtained online at the addresses mentioned below.

CHAPTER 2 CHARACTERIZATION OF *KRAS* REARRANGEMENTS IN METASTATIC PROSTATE CANCER

http://cancerdiscovery.aacrjournals.org/content/1/1/35/suppl/DC1

CHAPTER 3 OUTLIER KINASES IN *KRAS* DEPENDENT CANCER

http://cancerdiscovery.aacrjournals.org/content/3/3/280/suppl/DC1

A number of people have contributed to the research studies presented here and their corresponding manuscripts. Specific contributions of each individual are detailed below.

CHAPTER 2 CHARACTERIZATION OF *KRAS* REARRANGEMENTS IN METASTATIC PROSTATE CANCER

Conception and Design: Xiao-Song Wang, Dhanasekaran S.M., Varambally S and Arul Chinnaiyan.

Methodology: Xiao-Song Wang, Mohan S. Dhanasekaran, Sunita Shankar, Sooryanarayana Varambally

Screening of prostate cancer tissues: Dorothee Pflueger, Anuradha Gopalan, Victor E. Reuter, Mark A. Rubin,

Acquisition of Data: Xiao-Song Wang, Mohan S. Dhanasekaran, Sooryanarayana Varambally, Sunita Shankar, Daniel F. Fries, Bo Han, Irfan A. Asangani, Xuhong Cao, Yong Li, , Rui Wang, Xiaojun Jing, Daniel Robinson, Qi Cao, John R. Prensner

Mass Spectrometric analysis: Anastasia K. Yocum

Xenograft experiments: Ateeq B

FISH analysis: Nallasivam Palanisamy,

Ubiquitination assays and related: Atsuo T. Sasaki, Emily Rose Kahoud and Lewis C. Cantley

Writing, review, and/or revision of the manuscript: Xiao-Song Wang, Dhansekaran S.M., Sunita Shankar, Sooryanarayan Varambally and Arul M. Chinnaiyan.

CHAPTER 3 OUTLIER KINASES IN *KRAS* DEPENDENT CANCER

Conception and design: Dan R. Robinson, Xuhong Cao, Diane M. Simeone, Arul M. Chinnaiyan, Chandan Kumar-Sinha

Development of methodology: Iris Wei, Sunita Shankar , Linda W. Ma , Dan R. Robinson, Yi-Mi Wu, Diane M. Simeone, Chandan Kumar-Sinha

Acquisition of data (provided animals, acquired and managed patients, provided facilities, etc.): Vishal Kothari, Iris Wei, Sunita Shankar, Shanker Kalyana-Sundaram, Lidong Wang, Linda W. Ma, Dan R. Robinson, Xuhong Cao, Diane M. Simeone, Arul M. Chinnaiyan, Chandan Kumar-Sinha

Analysis and interpretation of data (e.g., statistical analysis, biostatistics, computational analysis): Vishal Kothari, Iris Wei, Sunita Shankar, Shanker Kalyana-Sundaram, Lidong Wang, Linda W. Ma, Pankaj Vats, Catherine S. Grasso, Diane M. Simeone, Chandan Kumar-Sinha

Writing, review, and/or revision of the manuscript: Vishal Kothari, Iris Wei, Shanker Kalyana-Sundaram, D.M. Simeone, Arul M. Chinnaiyan, Chandan Kumar-Sinha

Administrative, technical, or material support (i.e., reporting or organizing data, constructing databases): Iris Wei, Sunita Shankar, Shanker Kalyana-Sundaram, Linda W. Ma, Yi-Mi Wu, Diane M. Simeone, Chandan Kumar-Sinha

Study supervision: Diane M. Simeone, Arul M. Chinnaiyan, Chandan Kumar-Sinha

CHAPTERS 4 and 5 MASS SPECTROMETRIC ANALYSIS IDENTIFIES *ARGONAUTE-2* AS A RAS INTERACTING PARTNER and *ARGONAUTE-2* PROMOTES *KRAS* MEDIATED CELLULAR TRANSFORMATION

The study presented in Chapters 4 and 5 have been prepared as a manuscript. It is the combined work of the following authors, with individual contributions detailed.

Conception and Design: Sunita Shankar, Chandan Kumar-Sinha and Arul M. Chinnaiyan

Mass Spectrometric analysis: Anastasia Yocum and Anton Poliakov

Immunoprecipitation/interaction/cell fractionation analysis using cell lysates or recombinant proteins: Sunita Shankar, Harika Gundlapalli, Matthew Shuler

Sucrose density gradient analysis: Rohit Malik, Sunita Shankar

Immunoflourescence analysis: Rohit Malik, Sunita Shankar

Recombinant protein production (collaborators): Krishnapriya Chinnaswamy, Sunita Shankar, Yasmine White, Gideon Bollag, Xiajou Wang, Jeanne Stuckey

Alpha-lisa assay (not included in the study): Ingrid Apel

Generation of NIH3T3 AGO2-/- lines using CRISPR/Cas9: Yasuyuki Hosono

Design and construction of clones used in the study: Sunita Shankar, Vishal Kothari, Mohan S. Dhanasekaran

Cell based assays: Sunita Shankar

Xenograft experiments: Bushra Ateeq, Rachell Stender, June Escara-Wilke, Sunita Shankar

RAS structure and function (collaborators): Ari Firestone, Gideon Bollag and Kevin Shannon

RNA based assays (collaborators): Sethuramasundaram Pitchiaya, Vishalakshi Krishnan, Nils Walter

Transcript and miRNA sequencing analysis: Shanker Kalyana-Sundaram, Mohan S. Dhanasekaran, Xiaojun Jing, Xuhong Cao

Schematic drawings: Robin Kunkel

Writing, review, and/or revision of the manuscript: Sunita Shankar, Gideon Bollag, Kevin Shannon, Nils Walter, Chandan Kumar-Sinha, Arul M. Chinnaiyan